



A POROUS PERMEABLE WALL CONTAINING FERMENTOR FOR IN-SITU EXTRACTIVE RECOVERY OF BIOBUTANOL FROM DILUTE FERMENT LIQUORS

László Kótai^{[a,b]*} and István Gács^[a]

Keywords: Biobutanol, in-situ extractive fermentation, permeable porous wall; fermentor system

A new type of bioreactor containing a porous permeable wall to recover the biobutanol produced in anaerobic ABE fermentation processes is presented. The ferment liquor is contacted with an organic solvent and the butanol in the fermentation liquor distributes between the organic phase and the ferment liquor. The butanol containing solvent located at one side of the permeable wall is in a diffusion equilibrium with a same kind of auxiliary solvent with lower butanol concentration located at the other side of the permeable wall. Due to the concentration difference, butanol diffuses from one side of the wall to the other side. The concentration difference is kept to be constant by continuous removal of the butanol from the auxiliary solvent phase in which the butanol concentration is always lower than in the extractant phase but much higher than the butanol concentration in the ferment liquor phase. In this way, the primary extractant solvent contacting the ferment liquor is only a transmitting media between the ferment liquor and a small volume of the auxiliary solvent separated with the permeable wall. The energy demand of the distillation to remove the butanol from the auxiliary solvent is less than the energy demand of the direct butanol recovery from the ferment liquor or from the extractant phase. The new reactor provides a possibility to develop a continuous fermentation technology, continuous sugar adding and butanol recovery operating far below the toxic limit and inhibition conditions of butanol in the ferment liquor.

Corresponding Author
Fax: +36-23-376-456
E-Mail: kotail@chemres.hu;

[a] Institute of Materials and Environmental Chemistry, Research Centre for Natural Sciences, Hungarian Academy of Sciences, H-1025, Pusztaszeri u. 59-67, Budapest, Hungary;

[b] Deuton-X Ltd., H-2030, Érd, Selmeci u. 89.

Introduction

Biobutanol (n-C₄H₉OH) is the most promising biofuel of the near future. It can be produced by means of the so-called anaerobic ABE (acetone-butanol-ethanol) fermentation not only from food-grade resources like corn, but from various waste materials of the agriculture and of the food production.

Although biobutanol has excellent fuel properties compared to ethanol, its production cost is very high because of its accumulation in the ferment liquor leading to the death of the fermenting enzymes even at low (~2%) concentration. It means that large amount of wastewater formation (98%) occurs and the recovery of the product from the ferment liquor in a usual way (distillation) requires a large amount of energy. Conclusively, the increase of the butanol concentration and the produced butanol/used energy ratio, respectively are the key factors for increasing the feasibility of the production process. Increased productivity can be achieved by the so-called in-situ extractive fermentation in a new type of instrument reported here.

This fermentor separates the formed biobutanol via a special porous permeable wall system. In this paper the construction of the extractive fermentor system is described, and the basic elements of the technology are discussed.

Results and Discussion

General consideration of two-phase extractive fermentation

From the start of the fermentation process, the butanol concentration is allowed to increase up to the toxic limit (C_F^* , kg/kg ferment liquor) in the ferment liquor phase, meanwhile the concentration of the butanol in the extractive solvent (C_E^*) contacted with the ferment liquor can be written as

$$C_E^* = K_B C_F^* \quad (1)$$

where K_B is the distribution coefficient between the ferment liquor and the extractant.

It means that the amount of the butanol formed can be written as

$$\sum X_B = F C_F^* + E C_E^* \quad (2)$$

where F and E are the amounts of the ferment liquor (in kg) and extractive solvent (in kg), respectively. By feeding the same type of auxiliary solvent into the smaller reactor space separated from the fermentor with a permeable composite wall (Fig.1), the concentration difference at $t=0$ time immediately induces a diffusion process which terminates when the concentrations are equalized in the extractant solvents located in the two separated reactor spaces.

If $V_1 > 0$, then C_E definitely less than C_E^* , because the $C_E = C_A$ concentration can be expressed as

$$C_E = \frac{EC_E^*}{E + \rho_1 V_1} \quad (3)$$

where ρ_1 is the density of the organic extractant and V_1 is the volume of the extractant in the separated reactor space. Since the product of $\rho_1 V_1 > 0$, thus $E + \rho_1 V_1 > E$ and

$$C_E < C_E^* \quad (4)$$

When higher volume for V_1 is selected, larger difference between C_E and C_E^* can be reached. Let a given V_1 be the auxiliary solvent volume and the appropriate surface area of the permeable wall between the E and A phases be S_1 . The amount of the butanol from the C_A phase is supplied by diffusion through S_1 surface. In this case,

$$V_1 \frac{dC_A}{dt} \leq E \frac{dC_E}{dt} \quad (5)$$

This process would result continuously decreasing C_A , C_E and C_F values. However, if the rate of the fermentation in the F ferment liquor can supply the amount of butanol removed, then the two key parameters determining the amount of the formed and removed butanol will be the amount of the ferment liquor, F , and the amount of the auxiliary solvent, A , because

$$-V_1 \frac{dC_A}{dt} \leq F \frac{dC_F}{dt} \quad (6)$$

and because the $C_E = C_A$ and $C_F = K_B C_E$ conditions are valid.

These considerations have been taken by neglecting the effect of the back-diffusion of the extractant solvent. Since not only the butanol can move through the porous permeable wall from one side to the other, but the extractant solvent molecules can also diffuse from the lower butanol concentration phase to the higher butanol concentration phase as well. During the design of the reactor this phenomenon has to be taken into consideration.

The construction of the fermentor

The main construction element of the fermentor is a vertical wall which divides the reactor into two non-equal parts. The larger part of the reactor space is used as a common two-phase fermentor in which the ferment liquor (F) and the extractant solvent (E) are located. The extractant (E) is a nonmiscible solvent which does not inhibit the enzymatic processes¹. The same kind of auxiliary solvent (A) used as secondary extractant is located in the smaller separated part (V_1 volume) of the fermentor. The separating wall is divided into two parts. The extractant are generally have lower density than the ferment liquor, thus the extractants are the upper phases. The bottom part of the separating wall is made from a non-permeable material and this part completely prevent the mixing and contacting the ferment liquor and the auxiliary solvent. The upper part of the separating wall is made from a porous permeable composite material², which ensures the diffusion of the butanol

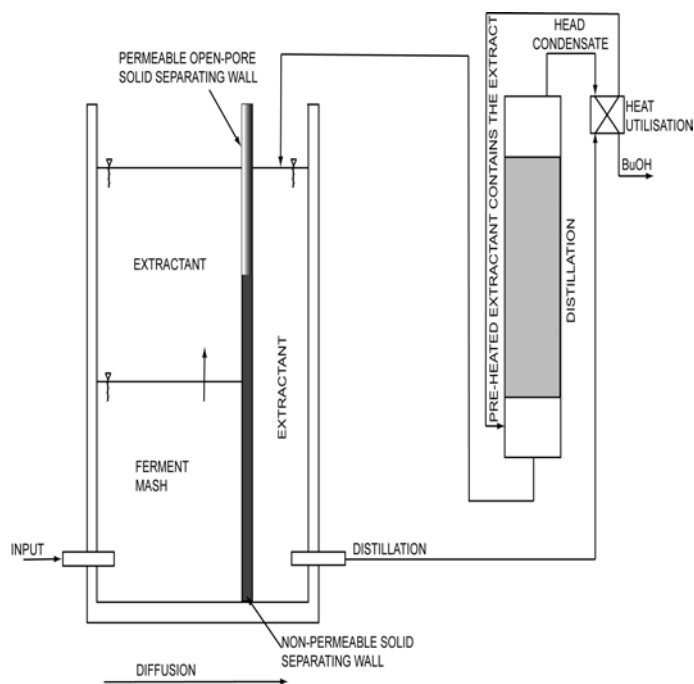


Figure 1. An in-situ two-phase extractive fermentor with porous permeable wall construction

between the extractant solvent and auxiliary solvent by the concentration difference as a driving force. The equilibrium between the ferment liquor and auxiliary solvent is mediated by the extractant phase.

As it can be seen in Fig. 1, the reactor part contains a butanol recovery column attached to the auxiliary solvent tank. This column is a usual distillation column, however, it has a heat utilization system in order to preheat the output of the auxiliary solvent containing butanol and to cool down the recycled butanol-free auxiliary solvent stream.

The temperature and amount of the recycled auxiliary solvent can control the temperature of the ferment liquor via appropriate selection of the thicknesses of the non-porous heat-conducting and the porous heat-insulating parts of the vertical separating wall.

Since the upper porous and the bottom non-porous parts of the separation wall are made from heat-insulating composite material and a heat-conducting metallic material, respectively, it is obvious, that the magnitude of the heat transfer via the porous and non-porous parts is not equal. During the extraction process not only butanol mass transfer but heat transfer also occurs from the ferment liquor to the extractant phase. Two other factors also can decrease the temperature of the ferment liquor without outer heat supplement. Firstly, the optimum temperature of the ferment liquor is around 37 °C in the ABE fermentation³. Thus, without heat supplement the continuous addition of sugar solution at room temperature would decrease the ferment liquor temperature.

Secondly, the amount of the ferment liquor is preferably larger than the amount of the extractant phase, thus the wall surface in contact with the ferment liquor is also larger than the fermentor surface contacting the extractant. Consequently, the heat loss toward the outer environment is larger from the ferment liquor phase. In order to avoid secondary heat transfer from the warmer extractant phase to the ferment liquor phase, namely to the opposite direction of the the heat and mass transfers due to the butanol diffusion from the ferment liquor to the extractant phase, the temperature difference between the two phases has to be minimized.

The temperature of the ferment liquor has to be adjusted to 37°C. In this way the temperature of the extractant should be lower than 37 °C. This condition can easily be adjusted by appropriate selection of the separating wall construction materials with different heat conducting properties and with the thickness of the upper and bottom wall.

Using this type of heat utilization systems the energy balance of the butanol recovery is much more economic than in the case of a simple distillative butanol recovery from dilute (<2%) ferment liquor, especially if the solvent selected has a high distribution coefficient (Table 1) for butanol recovery.

Table 1. Butanol distribution coefficients and heat capacities of solvents used as extractants in butanol recovery at 25 °C

Solvent	K_B value	C_p , J/g.K
Oleyl alcohol	3.5	2.32
Heptanal	13.0	2.15
Oleic acid	3.0	2.80
Hexanol	7.8	2.32
Octanol	6.7	2.34
Ethyl butyrate	2.9	1.96
Water	-	4.18

Taking into consideration the parameters⁴ shown in Table 1, for the selection of an appropriate solvent, the C_A concentration in the quasi-equilibrium state is always much higher than the C_F concentration values. Conclusively, not only the absolute amount of the heated solvent (A) will be less than the absolute amount of the ferment liquor (F), but the relative amount of the heated A to recover one kg of butanol will be less than the heated amount of ferment liquor to recover the same amount of butanol.

Furthermore, the heat capacity values of the organic solvents (see Table 1) are generally only the half to the heat capacity of the water, thus the used thermal energy is much less to heat this mixture up to the boiling point than in case of the aqueous ferment liquor. In the design of the biobutanol production by two-phase extractive fermentation by using porous membrane wall, for an expected productivity the determination of the V_1 volume of the separated reactor space is one of the key parameters.

The ratio of the volume of the two reactor spaces (V_1/V_2) unambiguously determines the required surface area of the wall at a given F/E ratio. The relative amount of the ferment liquor (F) and extractant (E) is determined by the diffusion surface of the wall which has to ensure the same value of the butanol stream (B) from the extractant to the auxiliary solvent which is formed in the ferment liquor and is removed from the auxiliary solvent. If the diffusion rate of the butanol from the E phase to the A phase through the porous wall is equal with the rate of butanol removing from the A phase and the rate of butanol formation in the F phase, supposing that the distribution of the butanol between the E and F phases are faster than its formation rate, then the process is in a quasi equilibrium.

Acknowledgement

We express our thanks to the National Development Agency and MAG Zrt. (Magyar Gazdaságfejlesztési Központ Zrt., 1139 Budapest, Váci út 81-83.) who supplied the “ Biobutanol fuel producing reactor development” project (GOP 1.1.1.-09/1-2009-0069) of Kemobil Co. (Tata, 2890 Agostyáni út 81). The project is supported by the European Union and co-financed by the European Regional Development Fund.

References

- Griffith, W. L.; Compere, A. L.; Googin, J. M. *Dev. Ind. Microbiol. Ser.* **1983**, *24*, 347; Ishii, S., Taya, M., Kobayashi, T., *J. Chem. Eng. Japan.* **1985**, *18*, 125.
- Ernő Tamics, Zsuzsanna Bajnóczki, and Pradeep K. Sharma, *J. Chem. Asia*, **2012**, accepted to publish; Roy, Della M., *Mater. Res. Soc. Symp. Proc.* **1989**, *137*, 179.
- Komarova, L. I., *Mikrobiologiya* **1955**, *24*, 208; Voget, C. E.; Mignone, C. F.; Ertola, R. J., *Biotechnology Lett.*, **1985**, *7*, 607; McNeil, B., Kristiansen, B., *Biotechnol. Lett.*, **1985**, *7*, 499; Oda, M., Yamaguchi, S., *Nippon Nogei Kagaku Kaishi* **1948**, *22*, 3; Lepage, C., Fayolle, F., Hermann, M., Vandecasteele, J. P., *J. Gen. Microbiol.*, **1987**, *133*, 103.
- Dadgar, A. M., Foutch, G. L., *Biotechnol. Bioeng. Symp.*, **1985**, *15*, 611.

Received: 14. 04. 2012, Accepted: 06. 05. 2012.



VARIABLE COMPOSITION OF CHLORINE HYDRATES SYNTHESIZED UNDER VARIOUS CONDITIONS

Györgyi Lakatos,^[a] Pradeep K. Sharma,^[b] Vinita Sharma,^[b] Szabolcs Bálint,^[c]
and Raj N. Mehrotra^[b]

Keywords: Chlorine hydrate, clathrate cage, occupancy, density

The composition of chlorine hydrates synthesised by different reaction routes were determined from experimentally measured density values without isolating the gas hydrate crystals. This method is the simplest and accurate for determining the composition of chlorine hydrates prepared under various conditions. The occupancies of each type of the cavities in the clathrate cage have been calculated.

* Corresponding Authors

Fax: 336-23-376-456

E-Mail: l.gyorgyi@deuton-x.hu

[a] Deuton-X Ltd., H-2030, Érd, Selmeci u. 89

[b] Department of Chemistry, J.N.V. University, Jodhpur,
(Rajasthan) 342005, India

[c] Research Centre for Natural Sciences, Hungarian Academy
of Sciences, H-1025, Budapest, Pusztaszeri u. 59-67

Introduction

Chlorine hydrate is the first gas hydrate discovered by Davy.¹ It is widely used as solid chlorine source in various important products and technological processes such as high energy density batteries, refrigerators, disinfection processes and high pressure chlorination reactions.² The determination of the composition of chlorine hydrate has attracted attention of chemists for long time because of its non-stoichiometric nature and dependence of its composition on the conditions of the preparatory methods.²⁻¹¹ The use of various oxidants as starting materials for the oxidation of hydrochloric acid e.g. hypochlorites or possible new oxidants such as simple or complex permanganates give new perspectives in the preparation of this compound.^{2,11-15} Besides, the composition of the crystals formed depends on the conditions of the methods used for its preparation, a simple and easy method to determine the composition of chlorine hydrate formed without isolation of crystals is required because instability of the crystals during weighing is the main problem in the analysis of the chlorine hydrate.^{9,10}

Results and Discussion

Chlorine hydrate belongs to the type I clathrate hydrates that consist of a 46 membered 3D-network of water molecules including 2 small and 6 large voids. The formula of chlorine hydrate can be written as $(8-x)\text{Cl}_2 \cdot 46\text{H}_2\text{O}$, where x is the number of the unfilled voids in the elementary cell ($Z=1$).³ This formula can also be expressed as $\text{Cl}_2 \cdot n\text{H}_2\text{O}$,

where n is the number of water molecules, termed as hosts, that encage one molecule of the chlorine gas termed as the guest. It theoretically means that the chlorine hydrate, which is richest in chlorine, could be characterized with the formula derived from the maximal filling ratio, namely $\text{Cl}_2 \cdot 5.75\text{H}_2\text{O}$. Since the density can easily be determined experimentally with high accuracy without separating the crystals from the mother liquor^{16,17}, these density values can therefore be used for calculation of the composition of the chlorine hydrates. The general formula of the chlorine hydrate can also be written as $(6\theta_1\text{Cl}_2 + 2\theta_2\text{Cl}_2) \cdot 46\text{H}_2\text{O}$, where θ_1 and θ_2 are the occupancies of the larger and smaller cavities respectively. The density can be expressed as the quotient of the molar mass and the molar volume of each clathrate. The molar mass of the hydrate can be calculated as the sum of the weights of the guest and the water cage, and the molar volume can be expressed by using the known temperature dependent molar volume of the blocks of 46 water molecules of the ice lattice by using the additional term $\Delta V(T, n)$ ¹⁸:

$$V_{\text{clathrate}}^T = V_{\text{ice}}^T + \Delta V(T, n) \quad (1)$$

where T is the absolute temperature in K, and n means the occupancy. The $\Delta V(T, n)$ term can be divided into two parts,

$$\Delta V(T, n) = \Delta V_{n=0} + \Delta V_a(T, n) \quad (2)$$

where $\Delta V_{n=0}$ value is constant and can be taken as 3.0^3 or $3.2 \text{ cm}^3/\text{mol}$ ¹⁹. The value of the additional term, $\Delta V_a(T, n)$ depends on the number of chlorine molecules and includes the effect of the thermal motion on the strength of the host-guest interactions in each type of the cavities^{20,21}. The contribution of the $\Delta V_a(T, n)$ term on the $\Delta V(T, n)$ values, however, proved to be not substantial because the widening of the clathrate hydrate cage reaches roughly 1 % value at the $D_M=5.7 \text{ \AA}$ ²² diameter of the guest molecule, and the D_{Cl_2} is only 5.2 \AA ³. The calculated n_1 values were compared with the n_2 values determined from the known lattice constant 3 and experimental density values (Eqn.(3) and (4)),^{17,18}

$$d_{\text{exp}} = \frac{[(6\theta_1 M_X + 2\theta_2 M_X) + 46M_{H_2O}]}{N_A a^3} \quad (3)$$

where M_{H_2O} is the molar mass of the water, $N_A = 6.0238$, the Avogadro number, and θ_1 and θ_2 are the occupancies.

$$n_1 = \frac{46}{6\theta_1 + 2\theta_2} \quad (4)$$

The use of $\Delta V_{n=0} = 3.1 \text{ cm}^3/\text{mol}$, average value in our calculations, resulted in n_1 and n_2 values that are given in Table 1 for various chlorine hydrates prepared under different conditions. The calculated n_1 and n_2 values are very close to each other. The kinetic factors have great importance because any two samples prepared in the same way but from different charges usually do not provide the same composition before attaining the complete equilibrium state.^{7,10,11} Faraday found that the density of the plate like chlorine hydrate crystals was $d = 1.2$ by a flotation density measurement method.⁶ Since there was continuous gas liberation and the imperceptible bubbles might have adhered to the hydrate surface, therefore the density could be presumed to be less than $d = 1.2 \text{ g/cm}^3$. Thus the composition can be formulated as $\text{Cl}_2 \cdot 7.63\text{H}_2\text{O}$. Roozeboom experimentally determined the density of two samples of crystalline chlorine hydrate to be $d = 1.220$ and 1.237 g/cm^3 .⁹ These values correspond to the $\text{Cl}_2 \cdot 7.28\text{H}_2\text{O}$ and $\text{Cl}_2 \cdot 7.00\text{H}_2\text{O}$ formulas, respectively. This indicated that the water content might have been less than what Roozeboom had observed by direct chemical analysis.⁹ The chlorine hydrate prepared in zinc chloride solutions can be compacted and stabilized with pressure. If the pressure is below 60 atm, the density falls below 1 g/cm^3 , but at 70-80 atm. pressure the value increases to $1.1-1.2 \text{ g/cm}^3$ and becomes 1.23 g/cm^3 above 800 atm. Further increase in the pressure does not result in significant increase in the density value.²³

Table 1. Experimental densities, lattice constants and composition values of the chlorine hydrates at 273.15 K.³

Reference	d, g/cm ³	n_1	n_2	θ_1	θ_2
Faraday ⁶	1.2	7.63	7.58	1.00	0.03
Roozeboom ⁹	1.220 1.237	7.28 7.00	7.23 6.95	1.00 1.00	0.17 0.32
Bjorkman ²³	1.23	7.11	7.07	1.00	0.25
Wilms ⁵	1.239	6.97	6.92	1.00	0.37
Smirnov ²⁵	1.31	6.01	5.98	1.00	0.85
Kislovskii ²⁴	1.37	-	-	-	-

*Density of two samples prepared in different ways were determined

Smirnov and Kleshchunov reported an experimentally determined value of density (1.31 g/cm^3) for the isolated chlorine hydrate which was found to have the formula $\text{Cl}_2 \cdot 6.2\text{H}_2\text{O}$.²⁵ The use of this density value provided the composition of the hydrate to be $\text{Cl}_2 \cdot 6.01\text{H}_2\text{O}$, which is close to the experimentally found value ($n_3=6.2$).²⁵

A density value of 1.37 g/cm^3 was given for a chlorine hydrate formed in capillaries. This value is too large even if a complete occupation ($8\text{Cl}_2 \cdot 46\text{H}_2\text{O}$) is supposed ($d = 1.325 \text{ g/cm}^3$), thus the lattice of the chlorine hydrate should be contracted in the capillaries ($a = 1.192 \text{ \AA}$) or the difference between the molar volumes of the empty clathrate cage and the ice should be diminished from the average 3.1 to $2.5 \text{ cm}^3/\text{mol}$.² No example for this magnitude of contraction among the clathrate hydrates of gases, even at higher pressures than the observed 10-12 atm could be present in the capillaries and the perfect filling of the cavities should cause dilatation rather than contraction. Therefore, the hydrate formed in the capillaries probably does not belong to the clathrate type I but a different type of chlorine hydrate richer in chlorine is rather formed as mentioned by Maumene, and a rhombic polymorph of the chlorine hydrate was also detected by Nordenskjöld.^{2,26,27}

Conclusions

The composition of chlorine hydrates prepared by different reaction routes were determined based on their experimentally measured density values. This method is the simplest and accurate way for the determination of the composition of chlorine hydrates prepared under various conditions because it does not require isolation of the crystals from the solution. The composition of various chlorine hydrates prepared in the last 200 years was re-determined and the values were found between 6.01 and $7.63\text{H}_2\text{O}/\text{chlorine}$ molecule. The results found for the chlorine hydrate prepared in capillaries ($d=1.37 \text{ g/cm}^3$) showed that this chlorine hydrate cannot be type I clathrate hydrate but a new modification or an other type of the chlorine hydrate might be formed within the capillaries.

References

- Davy, H., *Phil. Mag.*, **1811**, 101, 1.
- Kótai, L., Gács, I., Bálint, S., Lakatos, Gy., Mehrotra, R. N. *Trends in Inorganic Chemistry*, **2012**, accepted for publication,
- von Stackelberg, M. Müller, H. R., *Z. Elektrochem*, **1954**, 58, 25.
- Glew, D. N. Rath, N. S. *J. Chem. Phys.*, **1966**, 44, 1710.
- Wilms, D. A. Van Haute, A. A. *Desalination*, **1973**, 12, 379.
- Faraday, M. *Quart. J. Sci.*, **1823**, 15, 81.
- Bouzat, A., Azinieres, L. *Bull. Soc. Chim. Fr.*, **1924**, 35, 545; Cady, G. H. *J. Phys. Chem.*, **1981**, 85, 3225; Cady, G. H. *J. Phys. Chem.*, **1983**, 87, 4437;
- Kótai, L., Bódi, F., Sebestyén, A., Harfouch, S., *Hung. J. Ind. Chem.*, 19(1991), 63; Kótai, L., Nagy, A., Bódi, F., Sebestyén, A., *Hung. J. Ind. Chem.* **1999**, 27, 25;
- Roozeboom, H. W. B. *Rec. Trav. Chim. Pays-Bas*, **1884**, 3, 59.
- Anwar-Ullah, S. *J. Chem. Soc.* **1932**, 1172; Kótai, L., Bálint, S., Gács, I., Lakatos, Gy., Angyal, A., Mehrotra, R. N. *Z. Anorg. Allgem. Chem.*, **2012**, 638, 648.
- Kótai, A. Nagy, A., Bódi, F., Sebestyén, A. *Hung. J. Ind. Chem.* **1999**, 27, 27;

- ¹² Banerji, J., Kótai, L., Banerji, K.K., *Indian J. Chem.* **2009**, *48A*, 797;
- ¹³ Kumar, A., Mishra, P., Kótai, L., Banerji, K. K., *Indian J. Chem.*, **2003**, *42A*, 72; Shukla, R., Kótai, L., Sharma, P. K., Banerji, K.K., *J. Chem. Res.*, **2003**, 184;
- ¹⁴ Kótai, L., Keszler, Á., Pató, J., Holly, S., Banerji, K.K. *Indian J. Chem.* **1999**, *38A*, 966; Kótai, L., Banerji, K.K., *Synth. React. Inorg. Metal. Org. Chem.*, **2001**, *31*, 491; Kótai, L., Horváth, T., Szentmihályi, K., Keszler, Á., *Transit. Met. Chem.*, **2000**, *25*, 293.
- ¹⁵ Kótai, L., Szabó, P., Keszler, Á., *Thermochim. Acta*, **1999**, *338*, 129; Kótai, L., Argay, Gy., Holly, S., Keszler, Á., Pukanszky, B., Banerji, K.K., *Z. Anorg. Allgem. Chem.*, **2001**, *627*, 114; Kótai, L., Kazinczy, B., Keszler, Á., Holly, S., Gács, I., Banerji, K.K., *Z. Naturforsch./B.*, **2001**, *56*, 823;
- ¹⁶ Otake, K., Tsuji, T., Sato, I., Akiya, T., Sato, T., Hongo, M., *Fluid Phase Equil.* **2000**, *171*, 175.
- ¹⁷ Saito, K. Sadanaga, S., *Nihon Shiyo Gakkaishi*, **1964**, *18*, 180.
- ¹⁸ Kótai, L., Bálint, S., Gács, I., Lakatos, Gy., Angyal, A., Mehrotra, R. N. *Z. Anorg. Allgem. Chem.*, **2012**, *638*, 279.
- ¹⁹ Barrer, R. M. Stuart, W. I. *Proc. Roy Soc. London*, **1958**, *243A*, 172
- ²⁰ Tse, J. S. McKinnon, W. R. Marchi, M. *J. Phys. Chem.*, **1987**, *91*, 4188
- ²¹ Ikeda, T., Mae, S., Yamamuro, O., Matsuo, T., Ibberson, R. M. *J. Phys. Chem.* **2000**, *104*, 10623.
- ²² von Stackelberg, M. Jahn, W. Z. *Elektrochem.*, **1954**, *58*, 162.
- ²³ Bjorkman, H. K.; Symons, P. C., 1973, *Ger. Offen.* DE 2313450, 12 pp.
- ²⁴ Kislovskii, L. D., *Dokl. AN SSSR*, **1968**, *183*, 825.
- ²⁵ Smirnov, L. F.; Kleshchunov, E. I., *Kholodil'naya Tekhnika*, **1973**(8), 19
- ²⁶ Nordenskjöld, A. K., Bihang till Kongl. Svenska Vetenskapsakad. handlingar, **1874**, 2.
- ²⁷ Maumene, G., *Bull. Soc. Chim. Fr.*, [2], **1883**, *39*, 397.

Received: 23.04.2012.

Accepted and published online: 31.05.2012.



SOLID PHASE SULPHATIZING OF ZINC FERRITE SPINEL WITH IRON SULPHATES AS AN ENVIRONMENTAL FRIENDLY WAY FOR RECOVERING ZINC

Anurag Saini^[a], László Kótai^[a], István E. Sajó^[a], Imre Miklós Szilágyi^[b], Károly Lázár^[c], Zoltán May^[a], Péter Fazekas^[a], István Gács^[a], Vinita Sharma^[d] and Kalyan K. Banerji^[e]

Keywords: Zinc ferrite; Oxides; Sintering; Sulphatization

The scarcely reactive zinc ferrite can be decomposed in solid phase to water-soluble ZnSO₄ and water-insoluble Fe₂O₃ polymorphs by excess of solid iron(II or III) sulphates at 650°C in 4 h. Since SO₃ forms in situ from the Fe₂(SO₄)₃ as well as anhydrous Fe₂(SO₄)₃ forms in the thermal oxidation of iron(II) sulphate, therefore the gaseous SO₃ is the active sulphatization agent in the reaction of the hydrated iron(II and III) sulphates and the zinc ferrite. The sulphatization process were monitored by XRD, TG/DTA-MS, Mössbauer, Raman and IR-spectroscopy and the changes in reaction's heat and Gibbs energy are reported. The Fe₂O₃ polymorphs formed is worth processing into iron(III) sulphate by sulphuric acid. Since the Fe₂(SO₄)₃ formed in this way can be recycled to the sulphatization process, the only reagent consumed is the sulphuric acid. Therefore, these selective sulphatization reactions can be taken as "iron salts mediated" decompositions of zinc ferrite into ZnSO₄ and Fe₂O₃ by sulphuric acid.

* Corresponding Authors

Fax: +36-23-376-456

E-Mail: kotail@chemres.hu

- [a] Institute of Materials and Environmental Chemistry, Research Centre for Natural Sciences, Hungarian Academy of Sciences, H-1025, Pusztaszeri u. 59-67, Budapest, Hungary; Permanent address: Department of Materials Science and Engineering, Indian Institute of Technology, 208 016 Kalyanpur, Kanpur, India
- [b] Department of Chemistry, University of Helsinki, Helsinki, P.O. Box 55, FI-00014, Finland; Permanent address: Research Group of Technical Analytical Chemistry of the Hungarian Academy of Sciences, Department of Inorganic and Analytical Chemistry, University of Technology and Economics, H-1111, Szent Gellért tér 4, Budapest, Hungary
- [c] Nuclear Analysis Department, Centre for Energy Research, Hungarian Academy of Sciences H-1525, P.O.B. 49, Budapest, Hungary
- [d] J. N. V. University, Department of Chemistry, 342 005, Jodhpur, Rajasthan, India
- [e] National Law University India, Faculty of Science, 342 005 Boranada, Jodhpur, Rajasthan, India

1. Introduction

The scarcely reactive spinel type zinc ferrite, ZnFe₂O₄, is one of the most common wastes from the thermal treatment of various zinc and iron containing industrial wastes¹. Its recycling into the blast furnace technologies is not possible because the elementary zinc formed during its reduction destroys the wall of the blast furnace². Removal of its zinc content, however, is a complicated process due to its low reactivity toward most of the chemicals even under very strict conditions³⁻⁸.

One of the possible reactions is the sulphatization with hot sulphuric acid (100-300°C)^{5,6}. Since concentrated sulphuric acid forms a basic iron sulphate layer on the surface of the ferrite grains which prevents it from the further

dissolution, therefore diluted (15 -60 %) sulphuric acid is generally used in these reactions. But dilute H₂SO₄ is very corrosive and the main disadvantage is that both zinc and iron content of ZnFe₂O₄ are transformed into the appropriate sulphate⁵, and the iron content of the solution can be separated only as slightly soluble Na[Fe₃(SO₄)₂(OH)₆]⁶, which cannot be used in blast furnace technologies due to its sodium and sulphur content. In order to avoid these problems, sulphatization with gaseous reactants, e.g with SO₂ or SO₃ have been developed^{7,8}. ZnFe₂O₄ can be sulphatized by SO₂ gas, especially in the presence of air or oxygen at 500-600 °C with formation of ZnSO₄ and ZnO.2ZnSO₄ and the maximal conversion is roughly 54 % even in the presence of Fe₂O₃ which catalyses⁸ the SO₃ formation.

Since the decomposition of zinc ferrite in SO₂ or in Ar-SO₂ gas mixture without oxygen source could scarcely be observed, the active ingredient in the sulphatization is essentially the gaseous SO₃.⁷ Sulphatization of zinc compounds with ammonium sulphate around its thermal decomposition temperature showed that the in-situ generated SO₃ reacting with the mixture of ZnO and Fe₂O₃ converts ZnO selectively into ZnSO₄. However, the zinc ferrite is completely transformed into a mixture of ZnSO₄ and Fe₂(SO₄)₃^{4,9}.

The partial pressure of SO₃ above the Fe₂(SO₄)₃ is higher than that above the ZnSO₄,¹⁰ thus there is a chance to initiate a selective sulphatization of ZnFe₂O₄ with SO₃ produced in situ from Fe₂(SO₄)₃ to form water-soluble ZnSO₄ and a water-insoluble iron-compound (Fe₂O₃) which is suitable as raw material for blast furnace.

In order to clarify the mechanism of this sulphatization reaction, we studied the reaction of zinc ferrite with hydrated iron(II) and iron(III) sulphates at various temperatures.

2. Experimental Section

The wet hot-dip galvanising sludge obtained directly from Dunaferr Co. (Dunaujváros, Hungary) was dried at 200 °C for 2 h to remove its physically sorbed water content. The zinc was mainly found in the form of basic zinc(II) chloride, $Zn_5(OH)_8Cl_2 \cdot 2H_2O$. The sample was divided into three parts, and they were heated up to 500, 750 and 1000 °C, respectively. XRD analysis of these samples showed that the crystallinity increased with increasing temperature. We have attempted leaching of ZnO from the heat treated samples with treatment with diluted (1:1, v/v) HCl, however, the sample prepared at 500 °C contained highly defectuous ferrite compounds and almost completely dissolved in the aq. HCl. Therefore, an ammoniacal leaching process¹¹ was selected to remove ZnO from $ZnFe_2O_4$. The ZnO could only be removed from the sample prepared at 500 °C in 96 h, the other two samples prepared at higher temperature contained less reactive sintered ZnO particles, thus for complete removal of the ZnO a 2 h treatment with 10 % of acetic acid was consecutively used. The ZnO free samples were heated again at 500, 750 and 1000 °C for 2 h. Zinc ferrite samples (0.5 g in each) were mixed with the sulphatizing agent in an agate mortar (1 equivalent of iron(II) sulphate heptahydrate, 1/3 equivalent of iron(III) sulphate nonahydrate), and the mixtures were kept at 500 °C for 4 h. The Fe_2O_3 and $ZnSO_4$ appeared only in the most reactive spinel containing sample prepared at 500 °C, but the conversion has not been complete. The samples prepared at 750 and 1000 °C did not react with these sulphates at 500 °C. Therefore, the next series of experiments were performed with the samples prepared at higher temperatures, even at 600 °C. In this case, the sample prepared at 750 °C showed the presence of Fe_2O_3 (hematite).

Based on these experiences, all the further experiments were done with the less reactive zinc ferrite samples prepared at 1000 °C, and the sulphatizing temperature was selected to be 650 °C based on the relative thermal stability ranges of zinc and iron sulfates⁹. The less reactive zinc ferrite prepared at 1000 °C was mixed thoroughly in an agate mortar with iron(II) sulphate heptahydrate, iron(III) sulphate nonahydrate or $Al_2(SO_4)_3 \cdot 18H_2O$ at 1:2, 1:5 and 1:12.5 molar ratios and heated at 650 °C for 4 h. The mixture formed was subjected to XRD analysis and Mössbauer investigations.

X-ray powder diffraction measurements were performed by means of a Philips PW-1050 Bragg-Brentano parafocusing goniometer, equipped with a secondary beam graphite monochromator and proportional counter; scans were recorded in step mode by using CuK_{α} radiation at 40 kV and 35 mA tube power. Evaluation of the diffraction patterns have been obtained by full profile fitting techniques.

Raman spectra were measured by a Nicolet 950 FT-Raman spectrometer equipped with a Nd:YAG laser (1064 nm line) for excitation in the 4000-100 cm^{-1} region of Raman shifts in a diffuse reflection mode. IR spectra were recorded in diffuse reflection mode at room temperature in KBr (instrument: Nicolet 205 FT-IR). These vibrational spectroscopic methods were only used for monitoring of sulphate band intensity decreasing and checking the perfectness of sulphate recovering from the end-products.

Mössbauer spectra were obtained at 77 and 300 K in the constant acceleration mode (instrument: KFKI standard spectrometer equipped with a $^{57}Co/Rh$ source).

Thermal studies were performed on a SDT 2960 TA Instruments TG/DTA instrument coupled with a Balzers Thermostat GSD 200 mass spectrometer in air or He flow (130 ml/min) at 10 °C/min heating rate using open platinum crucible. Each studied sample weighed ca. 10 mg.

3. Results and Discussion

3.1. Preparation of zinc ferrite

Zinc ferrite samples were prepared from a sludge consisting of γ - $FeOOH$, ϵ - $Zn(OH)_2$ and $Zn_5(OH)_8Cl_2 \cdot 2H_2O$ ^{1a} by heating it at 500, 750 and 1000 °C for 5 h. These samples contained $ZnFe_2O_4$ and ZnO, which were identified by XRD and leached with 25% NH_4OH ¹¹. Since the sintered ZnO particles formed at higher temperatures could not be completely dissolved in the ammonia solution, an aqueous acetic acid leaching after the ammoniacal treatment was also used that led to pure $ZnFe_2O_4$. The samples prepared in this way were heat treated again at their preparation temperatures, namely at 500, 750 or 1000 °C for 2 h.

3.2. TG-MS studies on the zinc ferrite + hydrated iron(II) and iron(III) sulphate mixtures

In order to determine the optimal temperature ranges for isothermal sulphatization reactions of zinc ferrite with stoichiometric amounts of iron(II) and iron(III) sulphates, TG-MS studies were performed on the mixtures of $ZnFe_2O_4:FeSO_4 \cdot 7H_2O$ and $ZnFe_2O_4:Fe_2(SO_4)_3 \cdot 9H_2O$ mixtures. Since the oxidation processes have key role in the sulphatization process performed with iron(II) sulphate, the iron(II) sulphate heptahydrate – zinc ferrite mixture was studied in inert (He) and oxidative atmosphere (air) as well. The TG-MS curves can be seen on Fig. 1 and 2.

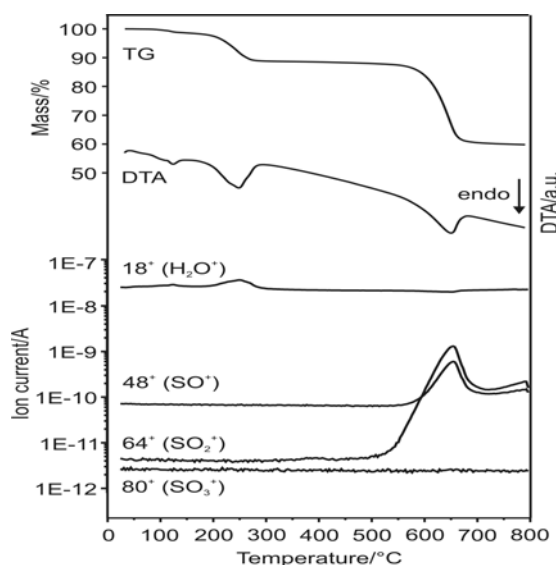


Figure 1. TG/DTA-MS monitoring of the reaction between zinc ferrite and iron(III) sulphate nonahydrate in air

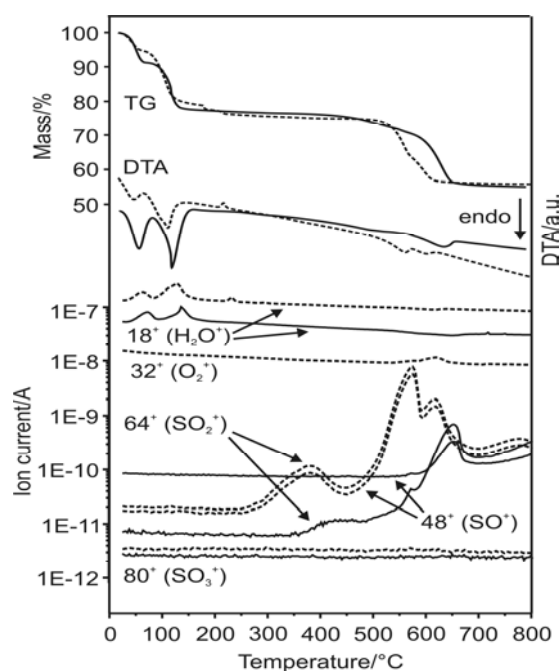


Figure 2. TG/DTA-MS monitoring of the reaction between zinc ferrite and iron(II)sulphate heptahydrate in air (dashed) and under helium (solid).

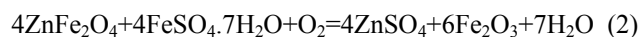
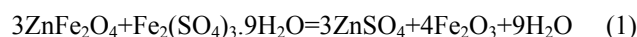
The iron(III) sulphate nonahydrate-zinc ferrite mixture shows two endothermic dewatering steps in the ranges of 100-150 °C and 200-300 °C with losing of one and eight water molecules (1,27 % and 9,80 % mass losses, respectively) from the hydrated iron(III) sulphate. The decomposition of anhydrous sulphate and the consecutive reaction of the formed SO_3 with zinc ferrite take place between 550-700 °C. The decomposition of the anhydrous iron(III) sulphate is endothermic. The SO_3 formed during the decomposition of anhydrous SO_3 either completely reacts with ZnFe_2O_4 or decompose into fragments in the gas phase during the measurement conditions (only SO_2^+ and SO^+ can be observed at $m/z=64$ and 48, the signal of SO_3^+ at $m/z=80$ could not be detected at all).

The iron(II) sulphate heptahydrate loses its water in helium in two main steps between 50-70 or 70-150 °C with elimination of 2.5 and 4.5 moles of water, respectively (8.85 % and 13.59 % mass losses in the two consecutive steps). In air, however, the iron(II) centers of the $\text{FeSO}_4 \cdot \text{H}_2\text{O}$ intermediate are oxidized with formation of $\text{Fe}(\text{OH})\text{SO}_4$ and 0.5 mol of H_2O (a small exothermic peak appears in the DTA curve), and the 0.5 mole of water is eliminated with formation of $\text{Fe}_2\text{O}(\text{SO}_4)_2$. The water elimination steps in air are observed between 50-60 (5.15 %), 60-150 (15.17%) and 180-230 °C (1.1%), which means evolution of 1.5, 4.5 and 1 mol (0.5 +0.5) of water. Small amount of SO_2 could be detected in helium atmosphere between 350 and 550 °C and the main decomposition step occurred between 550 and 700 °C. The SO_2 and its fragmentation products were observed at lower temperature in air but the main decomposition step consists of two overlapping processes due to the stepwise decomposition character of $\text{Fe}_2(\text{SO}_4)_3$ into Fe_2O_3 .

3.3 Sulphatization of zinc ferrite with iron(II) and iron(III) sulphates

Isothermal heat treatment of the solid mixture of the stoichiometric amounts of hydrated iron(II)-sulphate (1:1 molar ratio) or hydrated iron(III)- sulphates (3:1 molar ratio) in air were monitored at 500, 750 and 1000 °C for 4 h. The XRD of the residues showed the same diffraction patterns, which indicated that the same chemical reactions took place, thus only the less reactive zinc ferrite samples prepared at 1000 °C were used in further experiments. The optimal reaction temperature was found to be 650 °C in air for the reactions and large excess (iron sulphate/zinc ferrite ≥ 12.5 molar ratio) of $\text{FeSO}_4 \cdot 7\text{H}_2\text{O}$ and $\text{Fe}_2(\text{SO}_4)_3 \cdot 9\text{H}_2\text{O}$ were required to complete the zinc ferrite decomposition with 4 h reaction time. Similar experiments with aluminium sulphate, which has much less SO_3 tension at the sulphatization temperature¹⁰, proved to be ineffective for the decomposition of zinc ferrite.

The XRD (Figs. 3 and 4) and Mössbauer investigations (Figs. 5 and 6, Table 1) unambiguously show that the only iron containing end products of the reactions are the Fe_2O_3 polymorphs, mainly hematite, $\alpha\text{-Fe}_2\text{O}_3$, thus the reactions can be expressed with the following equations:



The reactions are completed at 650 °C. Since the sulphur distribution is uniform across the iron(II) and iron(III) sulphate samples during their complete decomposition, and the chemical form of sulphur on the surface was proved to be adsorbed SO_3 ¹², the reactions (1) and (2) are probably SO_3 mediated gas-solid phase interactions as observed in sulphatization of red mud with iron(II) and iron(III) sulphates¹³. Therefore the conditions for in-situ generation of SO_3 and the mechanism of SO_3 formation from these iron sulphate compounds are important factors in order to determine the optimal conditions for zinc ferrite decomposition and for the preparation of zinc-free iron containing blast furnace raw materials.

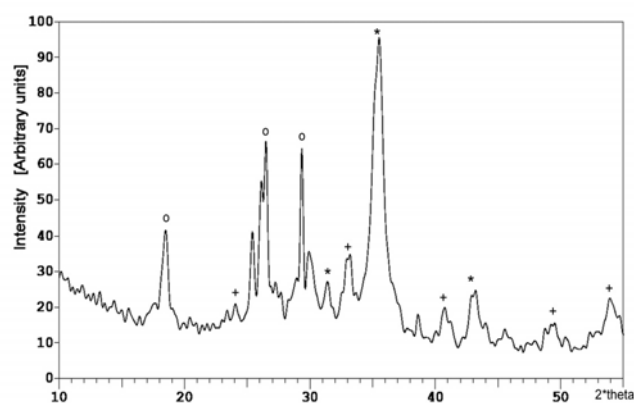


Figure 3. XRD of the $\text{ZnFe}_2\text{O}_4 \cdot \text{FeSO}_4 \cdot 7\text{H}_2\text{O}$ (1:1) mixture after heat treatment at 600 °C for 4 h.

+ $\text{Fe}_2(\text{SO}_4)_3$, * Fe_2O_3 (hematite), o $\text{ZnSO}_4 \cdot \text{H}_2\text{O}$

The formal solid-solid phase “metal-exchange” reaction between the zinc ferrite and hydrated iron(II) sulphate would result in the formation of magnetite as in reaction (3). The reaction (3) is associated with the enthalpy change, $\Delta H = 400.3$ kJ/mol and the Gibbs free energy change, $\Delta G = -183.3$ kJ/mol (all enthalpy and free enthalpy values were calculated with Factsage program package with using the database of this program)



However, the only iron containing reaction product is the hematite, $\alpha\text{-Fe}_2\text{O}_3$. The reaction heat and Gibbs energy change for the reaction given by Eq. (2) are 228.9 kJ/mol and -267.2 kJ/mol respectively, thus thermodynamically the reaction (2) is more favourable than the reaction (3).

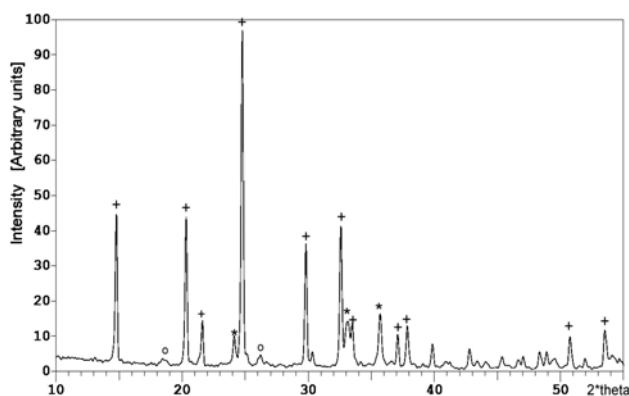
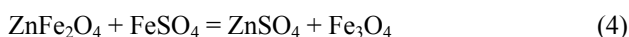


Figure 4. XRD of the $\text{ZnFe}_2\text{O}_4\text{:Fe}_2(\text{SO}_4)_3 \cdot 9\text{H}_2\text{O}$ (3:1) mixture after heat treatment at 600°C for 4 h.

+ - Fe_2O_3 (hematite), * - ZnFe_2O_4 (franklinite), o - ZnSO_4

Furthermore, these reactions are strongly endothermic and take place at high temperature therefore hydrated forms of iron sulphates cannot exist. The formal reaction of the water-free iron(II) sulphate, FeSO_4 can be written as:



The reaction (4) has positive reaction heat and Gibbs free energy values, $\Delta H = 16.1$ kJ/mol and $\Delta G = 11.3$ kJ/mol, respectively. The reaction (5), in which Fe_2O_3 is formed has negative reaction enthalpy, $\Delta H = -105.8$ kJ/mol, and Gibbs energy, $\Delta G = -72.3$ kJ/mol.

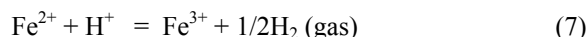


This unambiguously shows that the hydration degree of the iron(II) sulphate is only one among the essential factors, which plays role in the Fe_2O_3 formation and in preventing the magnetite formation. In inert atmosphere the decomposition reaction of freeze-dried iron (II) sulphate¹⁴ can be written as

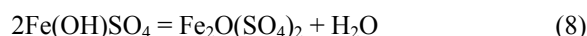


The stepwise dehydration of $\text{FeSO}_4 \cdot 7\text{H}_2\text{O}$, leads to $\text{FeSO}_4 \cdot \text{H}_2\text{O}$ ¹⁵ and the solid-state ^1H NMR of $\text{FeSO}_4 \cdot \text{H}_2\text{O}$ showed the presence of two different kind of protons in 1:1 ratio, thus the formula could be written as $\text{Fe}(\text{OH})\text{SO}_4(\text{H})$ ¹⁶.

Since the OH group is located in the first coordination sphere, and the other proton is located at the sulphate oxygen and therefore acts as a strong acidic centre¹⁶ with the redox equilibrium.



In the absence of oxygen, the reaction (7) is shifted to left because increasing the partial pressure of the hydrogen terminates the oxidation of the iron(II) centres, however, in the presence of oxygen the elementary hydrogen is, probably, catalytically oxidized to water and the equilibrium shifts completely to the right. The consideration of this reaction is therefore an indication that the hydrated iron(II) sulphate is not converted to the anhydrous iron(II) sulphate. $\text{Fe}(\text{OH})\text{SO}_4$ is formed as intermediate that loses a water molecule and gets converted to the detected $\text{Fe}_2\text{O}(\text{SO}_4)_2$ intermediate^{15,17}.



The decomposition products of $\text{Fe}_2\text{O}(\text{SO}_4)_2$, as studied in detail in¹⁵, are Fe_2O_3 and $\text{Fe}_2(\text{SO}_4)_3$, and these compounds were identified in the 1:5 $\text{ZnFe}_2\text{O}_4\text{:FeSO}_4 \cdot 7\text{H}_2\text{O}$ mixture after heating at 600°C for 4 h (Table 1) which is in conformity with XRD (Fig. 3) as well TG-MS results (Fig. 1). Since the intermediate $\text{Fe}_2\text{O}(\text{SO}_4)_2$ formed in the reaction (8) decomposes directly into anhydrous iron(III) sulphate, and the same compound is produced from the hydrated iron(III) sulphates¹⁸, the sulphatization of zinc ferrite can be performed in a similar way by the SO_3 generated along with Fe_2O_3 from the decomposition of anhydrous $\text{Fe}_2(\text{SO}_4)_3$. The reaction of zinc ferrite with SO_3 is expressed by Eq. (9).



The reaction (9) is thermodynamically more favourable ($\Delta H = -223.7$ kJ/mol, $\Delta G = -119.5$ kJ/mol) than the “direct” solid-solid phase interaction between the solid anhydrous iron(II) sulphate and zinc ferrite (reaction 4). The formation of $\text{Fe}_2(\text{SO}_4)_3$ intermediate in the reaction of ZnFe_2O_4 with $\text{FeSO}_4 \cdot 7\text{H}_2\text{O}$ is confirmed by XRD and Mössbauer results (Fig. 3, Fig. 5, Table 1). The assignment of the singlet without quadruple splitting at $\text{IS} = 0.45$ was ambiguous, because this peak was assigned to $\text{Fe}_2\text{O}(\text{SO}_4)_2$ ¹⁹. However, Zboril et al. assigned this peak to $\text{Fe}_2(\text{SO}_4)_3$ ²⁰ and determined a QS value for the compound $\text{Fe}_2\text{O}(\text{SO}_4)_2$.

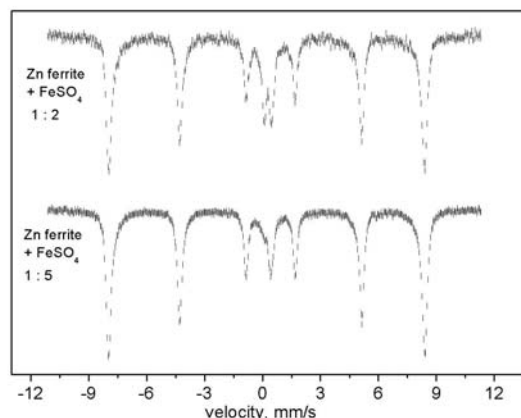


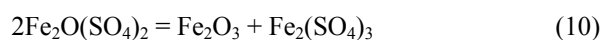
Figure 5. Mössbauer spectrum of the reaction product formed in the reaction of ZnFe_2O_4 and $\text{FeSO}_4 \cdot 7\text{H}_2\text{O}$ in air at 600°C for 4 h.

Table 1. Mössbauer data of the mixtures formed in the reactions of ZnFe₂O₄ with excess iron(II) and iron(III) sulphates at 600 °C for 4 h*

Sulphatizing material	Component	IS	QS	MHF	FWHM	RI
2-fold excess of FeSO ₄ .7H ₂ O	α-Fe ₂ O ₃	0.35	0.20	507	0.29	65
	ε-Fe ₂ O ₃	0.37	-	481	0.53	15
	ZnFe ₂ O ₄	0.31	0.39	-	0.31	19
5-fold excess of FeSO ₄ .7H ₂ O	α-Fe ₂ O ₃	0.35	0.21	508	0.29	76
	ε-Fe ₂ O ₃	0.35	-	483	0.58	12
	ZnFe ₂ O ₄	0.30	0.44	-	0.41	5
	Fe ₂ (SO ₄) ₃	0.45	-	-	0.30	6
2-fold excess of Fe ₂ (SO ₄) ₃ .9H ₂ O	α-Fe ₂ O ₃	0.35	0.20	508	0.26	24
	ε-Fe ₂ O ₃	0.30	-	487	0.65	30
	ZnFe ₂ O ₄	0.33	0.63	-	0.41	14
	Fe ₂ (SO ₄) ₃	0.45	-	-	0.30	31
5-fold excess of Fe ₂ (SO ₄) ₃ .9H ₂ O	α-Fe ₂ O ₃	0.35	0.20	508	0.26	20
	ε-Fe ₂ O ₃	0.31	-	486	0.65	17
	ZnFe ₂ O ₄	0.34	0.69	-	0.41	22
	Fe ₂ (SO ₄) ₃	0.45	-	-	0.30	41

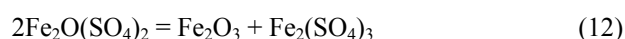
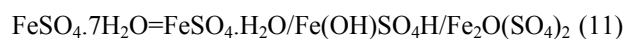
*IS-isomer shift, mm/s; QS-quadruple splitting, mm/s; FWHM-full width of half-maximum, mm/s; RI-relative spectral area, %, MHF-mean hyperfine field, Tesla.

Our XRD studies, however, confirmed the presence of anhydrous Fe₂(SO₄)₃, which could be formed as decomposition intermediate of Fe₂O(SO₄)₂²¹.



The hydrated iron(III) sulphate loses water molecules to form Fe₂(SO₄)₃, which decomposes in air between 500 and 600 °C with the formation of Fe₂O₃ and SO₃¹⁸. The SO₃ evolution contributes to the formation of ZnSO₄ (Eqn. 9) and slows down its dissociation into ZnO.2ZnSO₄⁴.

The sulphatization temperatures with FeSO₄.7H₂O and Fe₂(SO₄)₃ compounds are the same and located in the range of the decomposition of Fe₂O(SO₄)₂ intermediate^{15,18}. The similarities between the results of sulphatization reactions of both iron sulphates indicate that the same SO₃ mediated reaction takes place. The formation of SO₃ from these two iron sulphates during the same conditions can be explained easily with taking into consideration the formation of Fe₂(SO₄)₃ both in the dehydration of Fe₂(SO₄)₃.9H₂O and in the aerial oxidation of FeSO₄.7H₂O.



All iron(II) and iron(III) sulphate hydrates give the same decomposition intermediate in air, Fe₂(SO₄)₃¹⁵.

The X-ray microanalysis of the thermal decomposition process of iron(II) and iron(III) sulphates unambiguously showed that the S/Fe ratio vs. temperature relationship is practically the same¹².

3.4. Industrial significance of the zinc ferrite sulphation with iron(II) and iron(III) sulphates

One of the main advantages of the solid phase sulphatization of zinc ferrite with iron sulphates with the sulphuric acid leaching is that the solid zinc sulphate is

formed and sulphuric acid is not present in the aqueous leachate solution. The only insoluble iron compound formed is Fe₂O₃, which can be removed by simple filtration. The residual water soluble Fe₂(SO₄)₃ can be easily separated by hydrolysis at 185-200°C with precipitation of Fe₂O₃ without Fe(OH)SO₄ formation²². In the presence of sulphuric acid and in the absence of zinc sulphate, however, the main product would be Fe(OH)SO₄^{22,23}. Since the iron contents of the starting materials (ZnFe₂O₄ and iron sulphates) are completely transformed into Fe₂O₃ polymorphs, these polymorphs can be recycled to regenerate iron sulphate or can be used as raw material for blast furnace technologies. In order to regenerate the sulphatization agent, the Fe₂O₃ polymorphs are treated with dilute sulphuric acid at 60 °C to form iron(III) sulphate. Depending on the concentrations, Fe₂(SO₄)₃.6H₂O, Fe₂(SO₄)₃.7H₂O and Fe₂(SO₄)₃.8H₂O can be crystallized out²⁴.

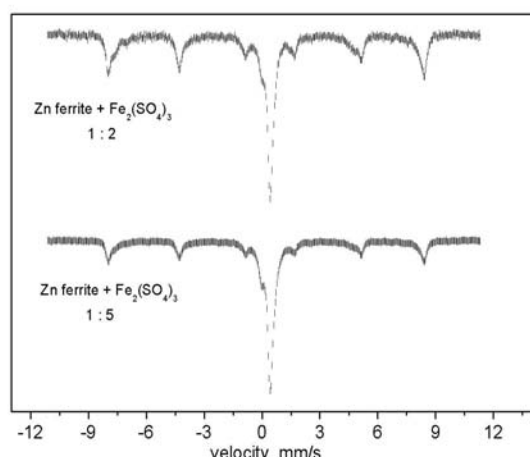
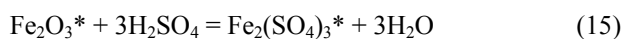


Figure 6. Mössbauer spectrum of the reaction product formed in the reaction of ZnFe_2O_4 and $\text{Fe}_2(\text{SO}_4)_3 \cdot 9\text{H}_2\text{O}$ in air at $600\text{ }^\circ\text{C}$ for 4 h

Both $\text{FeSO}_4 \cdot 7\text{H}_2\text{O}$ and $\text{Fe}_2(\text{SO}_4)_3 \cdot 9\text{H}_2\text{O}$ transform into Fe_2O_3 in their reaction with zinc ferrite, and dissolution of Fe_2O_3 in H_2SO_4 gives iron(III) sulphate compound for which molar sulphatization activity, defined as the number of evolved SO_3 moles per mole of iron(III) sulphate, is 1.5 compared to the value of 1 for $\text{FeSO}_4 \cdot 7\text{H}_2\text{O}$. Formally, the sulphate content of the iron sulphates is completely transformed into zinc sulphate, and the Fe_2O_3 formed from the iron sulphates can be recycled into iron(III) sulphate with sulphuric acid, therefore the only reagent consumed is the sulphuric acid.

Iron sulphates act as a “selective form of sulphuric acid” to decompose zinc ferrite into ZnSO_4 and Fe_2O_3



where Fe_2O_3^* means the iron(III) oxide polymorphs formed from iron sulphates.

4. Conclusions

The scarcely reactive zinc ferrite can completely be decomposed by solid iron(II) or iron(III) sulphates at $650\text{ }^\circ\text{C}$ for 4 h into water-soluble ZnSO_4 and water-insoluble Fe_2O_3 polymorphs. The in situ formation of SO_3 during thermal decomposition of iron(III) sulphate or the thermal oxidation of iron(II) sulphate proved to be the active sulphatization agent. The intermediate, $\text{Fe}_2(\text{SO}_4)_3$, was formed in the decomposition of hydrated iron(III) sulphate as well, thus both iron sulphate compounds give practically the same characteristics of the zinc ferrite sulphatization process. The sulphatization equivalent of iron(III) sulphate is, however, 1.5 times the sulphatization equivalence of iron(II) sulphate. The Fe_2O_3 formed from these compounds can be used to regenerate iron(III) sulphate which is used in the sulphatization process, thus the only reagent used in the sulphatization process is the sulphuric acid. Therefore, the selective sulphatization is an “iron salts mediated” decomposition of zinc ferrite into

ZnSO_4 and Fe_2O_3 by sulphuric acid. This new method is the only known process for transformation of zinc ferrite into sodium-, sulphur- and zinc-free iron raw material for blast furnace technologies in a solvent free simple solid state reaction, including a simple regeneration possibility of the used solid reagents with using the cheapest chemical – sulphuric acid.

5. Acknowledgement

The authors wish to thank Dr. Raj Narain Mehrotra (retired professor of J. N. V. University, Jodhpur) for his valuable help. I. M. S. thanks for a Marie Curie Intra-European Fellowship (PIEF-GA-2009-235655) and a János Bolyai Research Fellowship of the Hungarian Academy of Sciences.

6. References

- 1 a) Kazinczy, B., Kótai, L., Sajó, I. E., Holly, S., Lázár, K., Jakab, E., Gács, I., Szentmihályi, K. *Ind. Eng. Chem. Res.*, **2002**, *41*, 720; Kazinczy, N., Kótai, L., Gács, I., Sajó, I. E., Sreedhar, B., Lázár, K., *Ind. Eng. Chem. Res.*, **2003**, *42*, 318; b) Chen, D., Hou, J., Yao, L.-H., Jin, H.-M., Qian, G. R., Xu, Z. P., *Sep. Sci. Technol.*, **2010**, *75*, 210; Mohai, I., Szépvölgyi, J., Bertóti, I., Mohai, M., Gubicza, J., Ungár, T., *Solid State Ionics*, **2001**, *141-142*, 163.
- 2 Yang, X., Chu, M., Shen, F., Zhang, Z. *Acta Metall. Sinica (English Lett.)*, **2009**, *22*, 454.; Chernov, N. N., Demidenko, T. V., Safina, L. A., Dyshlevich, I. I., Fedorov., B. G., Marder, B. F., Tkach, A. Ya. *Metallurgist*, **1988**, *32*, 349 (*Metallurg*, **1988**(11), 30 (russian edition)).
- 3 Pickles, C. A. *J. Hazard. Mater.*, **2009**, *166*, 1030.; Lee, J. J., Lin, C. I., Chen, H. K. *Metall. Mater. Trans. B.*, **2001**, *32*, 1033.
- 4 Boyanov, B. S. *Thermochim. Acta* **1994**, *240*, 225.
- 5 Snurnikov, A. P., Larin, V. F. *Tsvetn. Metall.* **1969**(6), 33.
- 6 Rastas, J., Fugleberg, S., Bjorkqvist, L. G., Gisler, R.-L. *Erzmetall*, **1979**, *32*, 117.
- 7 Vanyukov, V. A., Vanyukov, A. V., Toropova, T. G. *Izv. Vyssh. Ucheb. Zaved., Tsvetn. Metall.* **1958**(3), 66; Elkina, O. A., Gol'dshtein, D. I., Montil'ov, I. A. *Tr. Ural. Nauch.-Issled. Proekt. Inst. Mednoi Prom.*, **1969**(12), 145.
- 8 Bumazhnov, F. T. *Izv. Vysshikh Ucheb. Zaved. Tsvetn. Metall.* **1972**(6), 56.
- 9 El-Tawil, S. Z., Ibrahim, A. A., Morsi, M. B. *Pyrometall. Symp.*, **1987**, 347. Inst. Min. Metall., London, UK.
- 10 Tagawa, H. *Thermochim. Acta*, **1984**, *80*, 23.
- 11 Kazinczy, B., Kótai, L., Gacs, I., Szentmihályi, K., Sándor, Z., Holly, S., *Hung. J. Ind. Chem.*, **2000**, *28*, 207.
- 12 Siriwardane, R. V., Poston J. A. Jr., Fisher, E. P., Shen, M.-S., Miltz, A. L. *Appl. Surface Sci.*, **1999**, *152*, 219.
- 13 Kótai, L., Sajó, I. E., Gács, I., Papp, K. *Chem. Lett.*, **2006**, *35*, 1278.
- 14 Villard, H. H., Fowler, R. D. *J. Am. Chem. Soc.*, **1932**, *54*, 496.
- 15 Swamy, M. S. R., Prasad, T. P. *J. Therm. Anal.*, **1981**, *20*, 101; Swamy, M. S. R., Prasad, T. P. *J. Therm. Anal.* **1981**, *20*, 107.
- 16 Kleshchev, D. G., Kellerman, L. A., Burmistrov, V. A. *Zh. Prikl. Khim.*, **1986**, *59*, 890.

- ¹⁷ Johnson, D. W. Gallagher, P. K. *J. Phys. Chem.*, **1971**, *75*, 1179; Prasad, T. P. *J. Therm. Anal.* **1986**, *31*, 553.
- ¹⁸ Coombs, P. G. Munir, Z. A. *J. Therm. Anal.*, **1989**, *35*, 967-976.
- ¹⁹ Pelovski, Y. Petkova, V., *J. Therm. Anal.* **1997**, *49*, 1227; Pelovski, Y., Petkova, V., Nikolov, S., *Thermochim. Acta*, **1996**, *274*, 273.
- ²⁰ Zboril, R. Mashlan, M. Petridies, D. Krausova, D. Pikal, P. *Hyperfine Interactions*, **2002**, *139-140*, 437.
- ²¹ Rastas, J. Fugleberg, S. Bjorkqvist, L. G. Gisler, R-L. *Erzmetall*, **1979**, *32*, 117.
- ²² Umetsu., Y. Sasaki, K. Otsuka, K. J. Min. Inst. Met. Jpn (Nihon Kogyo Kaishi)., **1978**, *94*, 175.
- ²³ Shokarev, M. M. Margulis, E. V. Vershinina, F. I. Beisekeeva, L. I. Savchenko, L. A. *Zh. Neorg. Khim.*, 1972, *17*, 2474.
- ²⁴ Novikau, S. G. Sarokin, U. M. Byalou, I. A. Saskavets, V. V. Klyapatski, P. M., *Vestsi Akad. Navuk. Belarus SSR. Ser. Khim. Navuk*, **1990**(3), 3; Novikov, S. G. Rud'ko, P. K. Belov, I. A. Saskovets, V. V. Malyshev, A. A. *Vestsi Akad. Navuk. Belarus SSR. Ser. Khim. Navuk*. **1989**(5), 43.

Received: 12.04.2012;

Accepted and published online: 30.04.2012.



METAL ELEMENTS, ORGANIC AGENTS IN A HERBAL REMEDY, SPECIES *THYMI COMPOSITA*, AND ITS DRUG-CONSTITUENTS

Klára Szentmihályi^{a*}, Zoltán May^a, Mária Then^b, Mária Hajdú^b, Andrea Böszörményi^b, Andrea Balázs^b, Éva Lemberkovics^b, Gabriella Marczal^b, Éva Szóke^b

Keywords: herbal remedy, *Species thymi composita*, respiratory diseases, essential oil, elements

Beside plant drugs the application of herbal mixtures using in several indication fields is very popular in our time. Since these herbal mixtures contain several bioactive agents, their analysis may cause difficulties. Therefore the description of measurements of components and their standardization is generally missing from the Pharmacopoeias. The examined *Species thymi composita* (STC) is highly effective because of its cholagog, carminative, expectorant, anticatarrhal etc. activity. STC is the mixture of *Althaeae radix et folium* (marshmallow leaf and root), *Verbasci flos* (mullein flores), *Liquiritiae radix* (liquorice root) and *Thymi herba* (thyme). The macroscopic and microscopic identification of components, phytochemical characterization have been described, the element composition of the herbal mixture, plant drugs constituents and teas was studied and the *in vitro* element absorption was examined. It has been stated that the STC could be characterized by its mucilage content and volatile oil composition. STC and its tea contain elements as well and the *in vitro* absorption of some of elements showed relatively high amount. The presence of bioactive compounds, volatile oil components, mucilage and elements may be jointly important in the complex effect, although the relatively higher Mg and Zn content in the tea is particularly relevant that acts via signal transduction process.

Corresponding Author
Fax: +36-1-438-1139
E-Mail: szentmihalyi.klara@ttk.mta.hu

- [a] Institute of Materials and Environmental Chemistry, Research Centre for Natural Sciences, Hungarian Academy of Sciences, H-1025, Budapest, Pusztaszeri str. 59-67, Hungary
[b] Institute of Pharmacognosy, Semmelweis University, H-1085, Budapest Üllői road 26, Hungary

1. Introduction

Herbal mixture is one of the best fashionable form of medicinal plant products, firstly in the circle of senior population, considering that medicinal tea contributes to the replacing of liquid in the organism. Beside herbal mixtures putting into circulation by different forms are fundamentally important. The herbal mixtures official in the Formulae Normales VII. (FoNo VII.)¹ and their drug components in the Hungarian Pharmacopoeia VII. (Ph.Hg.VII.)². They are used in numerous indication fields, for example: cholagog, carminative, sedative, laxative, diuretic, antitussive, expectorant and anticatarrhal.

The herbal mixture *Species thymi composita* is official in all (I.-VII.) FoNo prescriptions, although their composition is various and the drug-components –which are directly responsible for the effect- can be found in each composition (Table 1).

The composition of *Species thymi composita* was the richest firstly in FoNo IV. in which 10 dried herbs were applied. Beside the expectorant active *Thymi herba* (thyme

oil), there are *Farfarae folium*, antitussive and antibacterial active *Althaeae folium et radix* (mucilage), *Sambuci flos* (flavonoids), *Verbasci flos* (volatile components, flavonoids and mucilage), antiinflammatory active *Liquiritiae radix*, *Primulae radix* (saponins) and *Papaveris rhoados flos* (alkaloids, anthocyanins), *Pulmonariae herba* (silicic acid)³⁻⁷. The *Species thymi composita* of FoNo V. contains only 7 drugs and in FoNo VI. 6 drug components are only present. The content of water soluble hepatotoxic pyrrolizidine alkaloids justify the omission of *Farfarae folium*⁸. The *Primulae radix* was also omitted from the tea-mixture regarding the *Primula* species would be declared as protected plants. The composition of *Species thymi* official in FoNo VI. and VII. is the same, they consist of 5 drug constituents containing essential oil (tyme), mucilage (marshmallow and mullein), flavonoids (mullein), saponin (liquorice), as active compounds⁹⁻¹⁴.

The aqueous extract (tea) of *Species thymi composita* prepared by prescription of FoNo has very active catarrh- and cough-resolvent and expectorant activities². Coughing is a complex reflex, which purifies the respiratory tracts from the foreign substances and the secretion formed in excess. In case of cold diseases the coughing irritation is caused by the inflammation of the respiratory mucous membrane so the respiratory secretion is produced in extreme scale which is already not removed by the mucociliaric transport². The secretolytic and secretomotoric activity of expectorant remedies decreased the irritation, consequently they have cough-reliever effect. The thyme belongs to the group of expectorants possessing direct effect mechanism¹⁵. The essential oil of thyme is excreted in bronchia and increases the bronchus-secretion.

Table 1. Drug constituents (in weight, g) of species *Thymi composita*

Drug constituents of herbal mixture	FoNo IV. (1958)	FoNo V. (1967)	FoNo VI. (1987)	FoNo VII. (2004)
<i>Thymi herba</i>	4	4	14	14
<i>Farfarae folium</i>	4	-	-	-
<i>Pulmonariae herba</i>	4	-	-	-
<i>Althaeae folium</i>	4	4	10	10
<i>Althaeae radix</i>	4	4	10	10
<i>Sambuci flos</i>	4	4	-	-
<i>Liquiritiae radix</i>	4	4	10	10
<i>Primulae radix</i>	4	4	-	-
<i>Verbasci flos</i>	2	2	6	6
<i>Papaveris rhoados flos</i>	2	-	-	-

Since there is no description for studying the mixture *Species thymi composita* (STC), the aim of our work was the pharmacobotanical and phytochemical evaluation of herbal mixture *Species thymi composita*, official in the last FoNo (VII.) and their drug constituents and aqueous extracts (tea), respectively. Therefore, prominently the contents and composition of essential oils obtained from herbal mixture and drugs were studied. Our main research field was the mineral element analysis of herbal mixture, drugs and their aqueous extracts (teas) as well as the study of element absorption in different circumstances.

2. Experimental

2.1. Plant materials

The following plant drugs were used in the experiment: *Althaeae radix et folium*, root and leaves of marshmallow (*Althaea officinalis* L., *Malvaceae*); *Verbasci flos*, flowers of orange mullein /wooly mullein (*Verbascum phlomoides* L., *Scrophulariaceae*); *Liquiritiae radix*, root of liquorice (*Glycyrrhiza glabra* L., *Fabaceae*); *Thymi herba*, aerial part of common thyme (*Thymus vulgaris* T. *zygis* L., *Lamiaceae*) which was obtained from commercial network (Herbária, Budapest, 2008).

The drug constituents were purchased from trade in cut (scissa) condition. The herbal mixture *Species thymi composita* (STC) was compounded according to the description of FoNo VII.¹

2.2. Extracts

The preparation of aqueous extracts (tea, infusum) of drugs and herbal mixture was the follows: One table spoonful (3-5 g) of herbal mixture is poured off with a cup (300 mL) of hot water and left it to stand for cooling down, then the tea was filtrated (pH=6.2).

The essential oil was obtained by steam distillation, and the determination of essential oil content of herbal mixture and the drugs was carried out by volumetric measuring process according to the Hungarian Pharmacopoeia.¹⁶

2.3. Plant morphology and microscopy

The morphological and microscopical examinations were made on the basis of prescriptions of Hungarian and European Pharmacopoeias (Ph.Hg. VIII., Ph.Eur. 5.)^{16,17}.

2.4. Mucilage content

For characterization of *mucilage content* of marshmallow root and leaf, and the herbal mixture, as well as the swallow value was determined according to Hungarian Pharmacopoeia (Ph.Hg.VIII.)¹⁶.

2.5. Gas chromatographic examinations

The analysis of essential oil composition was made by gas chromatographic (GC) and GC-MS methods: Analysis of composition of essential oils was performed by gas chromatography accomplished with a Fisons 8000 gas chromatograph, equipped with a flame ionisation detector. A Rt- β -DEXm capillary column, 30 m long, 0.25 mm id., 0.25 μ m film thickness was used. Carrier gas was nitrogen at 6.86 mL/min flow rate: 0.2 μ L was injected (5 μ L essential oil in 2 mL chloroform). Splitless injection was made at 10 s, split ratio was 1:50. Temperature of injector and detector was 210 °C and 240 °C, respectively. Oven temperature increased with a rate of 8 °C/min from 60 to 230 °C, with a final isotherm at 230 °C for 5 min. Percentage evaluation of compounds was carried out by area normalization; identification of peaks was made by comparison of retention times of standards and co-addition of standards. All measurement was made at duplicate.

GC-MS was performed with a coupled system Agilent 6890N GC, 5973N mass selective detector, the Chrom Card Server Ver. 1.2 equipped with A HP-5MS capillary column, 30 m long, 0.25 mm id., 0.25 μ m film thickness was used. Carrier gas was helium (pHe was 0.20 MPa), at 1 mL/min flow rate: 1 μ L (10 μ L/mL essential oil in ethanol) was injected at 0.7 mg/mL velocity, splitless-type with an Agilent 7683 autosampler. Temperature of injector was 280 °C, temperature of transfer line was 275 °C. Oven temperature was programmed initially at 60 °C for 3 min, then increased with a rate of 8 °C/min to 200 °C, then kept at 200 °C for 2 min and also increased with a rate of 10 °C/min to 250 °C with a final isotherm at 250 °C for 15 min. MS conditions: ionization energy was 70 eV, mass range was 40-500 mz^{-1} , one analysis/min was made. Identification of peaks was carried out by comparison with MS and retention data of standards, and spectra from the NIST library.

2.6. Element content

For mineral element analysis, an inductively coupled plasma optical emission spectrometry (ICP-OES) was used by the method of Ladó *et al.* with Spectro Genesis instrument after digestion of the samples with nitric acid (5 mL) and hydrogen peroxide (2 mL)¹⁸. Se content was determined by square wave voltammetric method using stripping technique with polarographic analyzer (TraceLab 50) by square wave voltammetric measurement on hanging mercury (working) electrode and in the presence of reference electrode (silver/silver chloride) and counter electrode (platinum)¹⁹.

During the measurement 2 mL sample, 2 mL HCl (1 M) and 2 mL Cu solution (concentration of 5 mg/L) were added to the polarographic cell and the solution was measured.

Table 2. Accuracy of element determination by measurement of Lucerna p-alfalfa reference material standard

	Measured values (mg/kg)	Recovery (%)	Certified values (mg/kg)
Al	325.9±3.6	98.8	330
As	<0.5		0.262
Ba	22.94±0.36	98.0	23.4
Ca	17183±20	98.2	17500
Cd	0.127±0.012	93.4	0.136
Co	0.191±0.017	98.9	0.193
Cr	0.890±0.088	98.8	0.900
Cu	11.27±0.09	96.3	11.70
Fe	321.8±2.1	90.6	355
Hg	<0.3		0.0282
K	17535±16	93.8	18700
Mg	3664±13	104.1	3520
Mn	30.48±0.13	89.1	34.20
Mo	<0.25		0.200
Na	487.6±21.5	102.9	474
Ni	2.87±0.07	112.9	2.54
P	3028±29	99.9	3030
Pb	1.92±0.05	104.3	1.84
Se	0.0501±0.0030	100.2	0.0500
Sr	89.46±0.70	113.6	78.7
V	0.769±0.027	96.1	0.800
Zn	33.51±0.83	100.9	33.2

The accuracy of element determinations was proved by measurements of a certified biological reference material (12-2-03 Lucerna p-alfalfa, Bratislava, Slovakia). The values ranged between 89.1% and 113.6% compared to certified values which show the accuracy of measurements and the well applied digestion method (Table 2). There is no given concentration for Li in the reference material, that's why in case of Li the recovery was determined by the standard addition method where the Li standard was added to one of the samples and measured. The recovery was found to be 95.4%.

2.7. In vitro element absorption

The transfer of elements from tea to the stomach (gastriac acid of pH=1.1; 1 n HCl (94 g), NaCl (0.35 g) and glycocholl (0.5 g) in 1000 mL of water) and from intestine (pH=6.5; Na₂HPO₃ (3.9 g) and KH₂PO₄ (6.1 g) in 1000 mL of water) to plasma (pH=7.5; Na₂HPO₃ (20.5 g) and KH₂PO₄ (2.8 g) in 1 L of water)) was studied on a Sartorius membrane diffusion model at 37 °C²¹. The tea (10 mL) and concentrated tea in buffer solution pH=6.5 (10 mL) was poured into a container supplied with a membrane at the bottom of it. The container was plunged into a larger container. The larger outside container contained 100 mL of buffer solution (pH=1.1 or 7.5). Fractions (10 mL) were

taken from the outside container at the following time periods: 30, 60, 90 and 120 min. The aliquot taken was supplied with buffer solution (10 mL, pH=1.1 or pH=7.5 depending on the experiment). The evaluation was omitted in the case of Na at pH=1.1 and of K, Na, P at pH=7.5 because of the K, Na, P content in buffer solutions.

2.8. Statistical analysis

Most of the results were expressed in mean ± standard deviation.

3. Results

3.1. Morphology

The macromorphological characteristics of scissa drug-constituents could be good recognised in herbal mixture. These diagnostical characteristics of each drug are the follows: the white phloem-fibres of *Althaeae radix*, the yellow-brown root pieces of *Liquiritiae radix*, the tomentose leaf-fractions originating from *Althaeae folium*. The yellowish flow-fractions originating from *Verbasci flos*, and final the mixture can be recognised firstly on the bases of penetration order of thyme (Figure 1).



Figure 1. Species thymi composita

3.2. Micromorphology

In micromorphological point of view the main diagnostical characteristics of STC are the star shaped covering hairs of *Althaeae folium* and the branching covering hairs of *Verbasci flos* (Figure 2).

We can find the eye-tooth shaped and hooked covering hairs and *Labiatae trichomes* (glandular hairs) originating from thyme. The calcium oxalate crystals are also characteristics of mixture: rosettes (cluster shaped crystals) from marshmallow and single crystals in fibres of liquorice *radix*. The phloem fibres of *Althaeae* and *Liquiritiae radix* can be also recognizable in mixture powder (Figure 3).

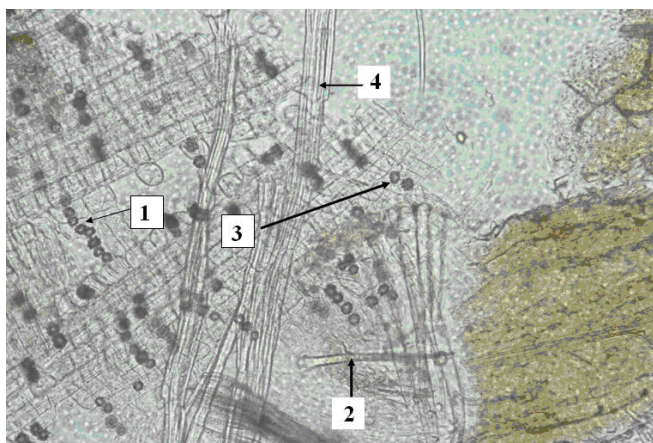


Figure 2. *Species thymi composita* pulvis

1. Liquiritiae radix - fibre containing crystal; 2. *Althaeae folium* - star shaped trichomes, 3. Cluster crystals, 4. *Liquiritiae radix* - fibre bound

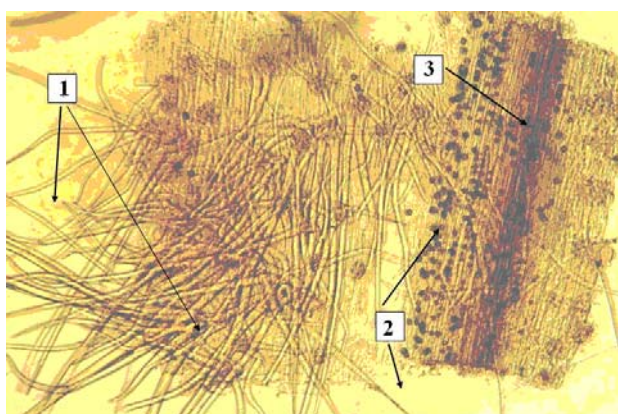


Figure 3. *Althaeae folium* pulvis

Diagnostical characteristic: 1. star shaped covering hairs, 2. cluster crystals; 3. vessels

3.3. Mucilage content

The swallow value of STC is higher than that of *Althaeae radix* and *folium* (Table 3).

3.4. Essential oil content and composition

The contents of essential oil obtained from *Thymi herba*, STC and its infusum are demonstrated in Table 4. The essential oil content of STC is in good agreement with the expectable value, calculated on the basis of essential oil content measured in the thyme leaf. The composition of essential oil obtained from *Thymi herba*, STC and the tea is demonstrated in Table 5 and on the gas chromatograms (Figure 4). In the essential oil of thyme seven characteristic components: β -myrcene, p-cymene, γ -terpinene, linalool, terpinene-4-ol, thymol and carvacrol were identified. These components were detectable in essential oil of the herbal mixture and also in its infusum (tea).

The percentile distribution of the components was similar in oil of thyme and mixture but this rate was changed in the oil of tea: the ratio of polaric phenolic compounds, as tymol and carvacrol increased.

Table 3. Mucilage content

Sample	Swallow value
<i>Species thymi composita</i>	17
<i>Althaeae radix</i>	10
<i>Althaeae folium</i>	7

Table 4. Content of total essential oil

Sample	Oil content (mL/100g)
<i>Species thymi composita</i>	0.36±0.03
<i>Thymi herba</i>	1.3±0.25
Tea of <i>Species thymi composita</i>	0.01±0.001

Table 5. Quantitative characterization of essential oil composition in *Thymi herba*, *Species thymi* mixture and its tea according to gas chromatographic measurements

Components	Percentile distribution (%) of components in essential oil		
	drug	<i>Species thymi composita</i>	
	<i>Thymi herba</i>	herbal mixture	tea
1 β -myrcene	1.0	0.7	0.05
2 p-cymene	22.9	19.0	4.6
3 γ -terpinene	7.9	6.4	2.8
4 linalool	2.00	2.4	4.3
5 terpinene-4-ol	1.6	1.9	1.9
6 thymol	48.2	52.4	66.1
7 carvacrol	4.1	3.7	5.0

3.5. Mineral element composition

The mineral element content of drug components and STC determined by ICP-OES is found in Table 6.

Concentration under the detection limit was obtained for As and Hg in all cases, while for Cd, Co, Li, Pb, Se and V in some cases. At the same time relatively high amount of Li (*Althaeae folium*, *Verbasci flos*, *Thymi herba*), Pb (*Althaeae folium*, *Thymi herba*) and V (*Verbasci flos*) was found compared to the average plant concentrations, which are under 2, 2 and 1 mg/kg, respectively. A slight soil content is shown by the collectively presence of elevated Al (>200 mg/kg), Cr (>1 mg/kg) and Fe (>300 mg/kg) content in *Althaeae folium*, *Verbasci flos*, *Thymi herba* and STC.

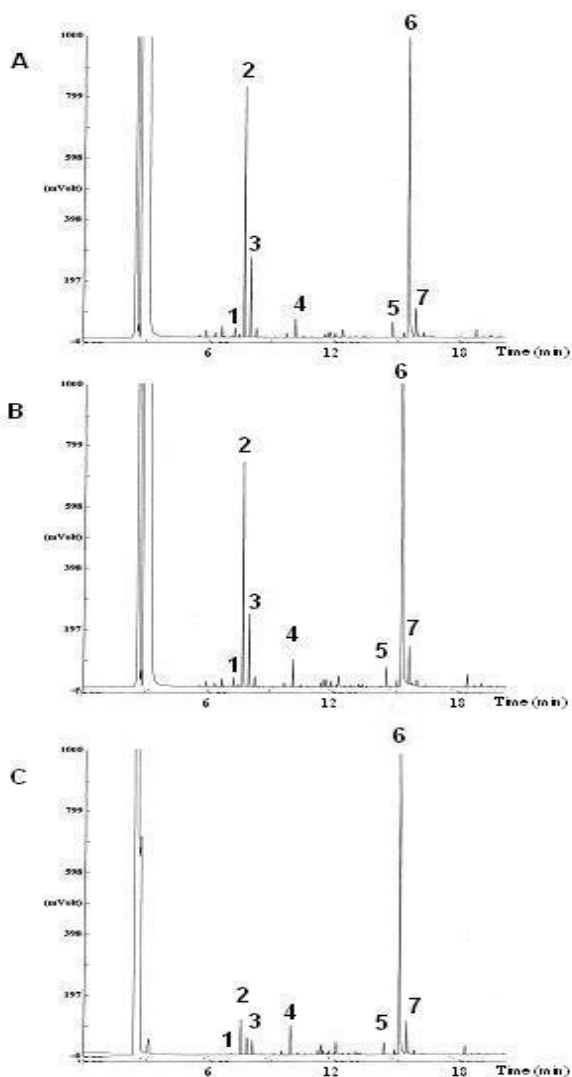


Figure 4. Gas chromatograms of essential oil of *Thymi herba* (A), *Species thymi composita* (B) and tea of *Species thymi composita* (C)

1. β -myrcene; 2. p-cymene; 3. γ -terpinene; 4. linalool; 5. terpinene-4-ol; 6. thymol; 7. carvacrol

Althaeae folium is rich in Ca (>30000 mg/kg), S (>5000 mg/kg) and Sr (>100 mg/kg), *Thymi herba* contains Mo and Ni over average plant concentration (3 and 10 mg/kg, respectively), while Sr concentration of STC is also salient²²⁻²³. All plant materials contain K in relatively low concentration (<20000 mg/kg). The poorest herb in mineral elements is *Liquiritiae radix* in which beside K the concentration of Mn, P, S and Zn also goes under the average plant concentration (<20 mg/kg, <2000 mg/kg, <20 mg/kg, respectively). The mineral element composition of *Althaeae radix* is similar to *Liquiritiae radix*.

The element concentration of most of the toxic and harmful elements in the teas is under the detection limit (Table 7.) which is favourable. According to our previous experiments and papers we can not see any significant concentration in the extracts²⁰⁻²³. The only relevant thing is that the solvability of Ca seems to be higher in STC which could be happened by the synergic effect of organic components in the drug mixture.

3.6. In vitro transfer of elements

The effect of STC may be connected to the organic bioactive agents but the examination of effectiveness and transfer of compounds is rather difficult. The flavonoid content in tea mixture by usual way was unable to determine because of the disturbing effect of mucilage. Therefore, the transfer of flavonoids is also not measurable and the examination of *in vitro* absorption of mucilage does not make sense because of its properties. According to our previous measurements the transfer of essential oils and volatile compounds provides only qualitative results²⁰. Since elements presenting in the extracts may also have favourable effect and they could be well measurable quantitative, the transfer of elements was determined.

Table 8. Amount of elements (μ g) transferred from 100 mL aqueous extract of *Species thymi composita* into buffer solution pH=1.1 and from buffer solution (pH=6.5) with extract of *Species thymi composita* into buffer solution pH=7.5

	30 min.	60 min.	90 min.	120 min.
Into pH=1.1				
Al	20.1	21.1	25.2	26.1
Ba	1.4	2.4	2.6	2.5
Ca	1301	1446	1542	1568
Cu	2.2	2.5	2.6	2.7
Fe	10.1	11.3	11.6	12.1
Mg	447	598	703	727
Mn	2.6	3.3	3.6	3.7
Ni	0.31	0.41	0.42	0.44
P	325	409	456	471
S	394	600	702	714
Sr	7.2	8.1	8.6	8.7
Zn	2.5	26	2.9	3.1
Into pH=7.5				
Al	3.0	3.4	5.2	6.6
Ba	0.4	0.6	0.8	0.9
Ca	391	443	505	618
Cu	1.7	2.0	2.3	2.4
Fe	3.1	3.7	3.9	4.4
Mg	288	446	562	591
Mn	0.8	1.1	1.5	1.6
S	258	405	537	573
Sr	4.2	4.5	5.0	6.0
Zn	0.82	0.89	0.90	0.91

The transfer of elements from tea and buffer solution pH=6.5 of STC into different buffer solutions (pH=1.1 and pH=7.5) was measured in a dialysis system. The result was evaluable for Al, Ba, Ca, Cu, Fe, Mg, Mn, S, Sr and Zn, while the concentration of As, Cd, Co, Cr, Hg, Mo, Pb, Se, V was under the detection limit. The transfer was continuous in all cases (Table 8). Relative high transfer was observed for Al, Ba and Mg in case of buffer solution pH=1.1 (stomach pH), since more than half of the amount in tea passed through the membran (Table 5). The transfer of Ni was obtained to be very low. From buffer solution pH=6.5 (intestine pH) to buffer solution pH=7.5 (plasma pH) the element transfer was found to be of lower rate and the amount of Mg passed from the extract of STC was only relevant with transfer of 591 mg (70% of the initial amount).

Table 6. Element content of drug components and *Species thymi composita* (mg/kg dry weight, n=3)

Elements	<i>Althaeae folium</i>	<i>Althaeae radix</i>	<i>Verbasci flos</i>	<i>Thymi herba</i>	<i>Liquiritiae radix</i>	<i>Species thymi composita</i>
Al	376.6±2.9	83.9±1.54	1168±7	641.7±9.8	47.7±0.3	961.4±20.6
As	<0.5	<0.5	<0.5	<0.5	<0.5	<0.5
Ba	13.35±0.03	7.26±0.21	12.05±0.02	74.67±1.32	13.14±0.11	30.50±0.54
Ca	34044±267	6113±20	6616±31	12687±290	9709±63	17480±346
Cd	0.34±0.02	0.25±0.01	0.09±0.01	0.21±0.01	<0.03	0.14±0.01
Co	<0.015	<0.015	0.56±0.01	<0.015	<0.015	0.33±0.04
Cr	1.28±0.03	0.97±0.04	3.34±0.05	11.51±0.24	0.90±0.03	3.95±0.07
Cu	15.93±0.02	14.47±0.10	14.88±0.09	12.83±0.23	5.90±0.02	17.59±0.31
Fe	404.2±2.5	66.9±0.35	1288±6	563.5±9.4	69.0±0.2	878.5±13.2
Hg	<0.75	<0.75	<0.75	<0.75	<0.75	<0.75
K	17331±79	11343±95	11509±58	15681±255	3946±45	13649±282
Li	5.95±0.46	<0.1	5.98±0.81	4.37±0.46	0.87±0.15	5.86±0.45
Mg	1679±11	1429±8	1758±3	1947±11	1441±11	1833±24
Mn	38.64±0.14	9.70±0.43	46.73±0.23	129.4±2.5	9.19±0.07	54.97±0.99
Mo	2.12±0.30	1.55±0.09	1.57±0.36	12.15±0.43	1.31±0.11	1.92±0.24
Na	883.8±5.01	1006±10	417.1±3	171.2±3.7	436.2±7.2	622.0±15.1
Ni	4.52±0.07	4.63±0.08	7.17±0.09	44.78±0.75	4.29±0.13	6.86±0.14
P	4115±11	3657±23	2946±15	1888±24	1146±8	3220±38
Pb	3.73±0.21	1.29±0.14	1.47±0.06	3.22±0.07	<0.5	1.39±0.07
S	6167±9	3506±7	1454±16	1853±19	876.8±3	3420±17
Se	<0.2	0.364 ±0.086	1.26±0.09	<0.2	<0.2	<0.2
Sr	108.6±0.77	61.29±0.49	35.36±0.27	40.45±0.73	334.5±5.2	146.8±3.4
V	1.01±0.14	<0.05	3.45±0.04	1.24±0.09	0.12±0.01	2.23±0.17
Zn	36.43±1.06	23.19±0.82	26.39±0.23	33.17±1.16	10.14±0.12	26.23±0.62

Table 7. Element content in teas of drug constituents and *Species thymi composita* (µg/100 mL, n=3)

Elements	<i>Althaeae folium</i>	<i>Althaeae radix</i>	<i>Verbasci flos</i>	<i>Thymi herba</i>	<i>Liquiritiae radix</i>	<i>Species thymi composita</i>
Al	0.37±0.04	0.92±0.02	158.0±0.9	30.61±0.93	10.14±0.10	26.98±0.36
As	<0.5	<0.5	<0.5	<0.5	<0.5	<0.5
Ba	0.19±0.01	0.38±0.03	2.02±0.02	10.02±0.04	1.31±0.03	3.94±0.07
Ca	2427±33	949.2±3.6	1901±24	3137±11	514.3±4.3	3706±11
Cd	<0.01	<0.01	0.03±0.01	<0.01	<0.01	<0.01
Co	<0.015	<0.015	0.23±0.01	0.09±0.01	<0.015	0.17±0.02
Cr	0.43±0.02	0.64±0.02	2.06±0.03	2.05±0.02	0.68±0.01	1.86±0.01
Cu	0.69±0.02	2.39±0.05	7.60±0.11	3.35±0.01	3.02±0.02	6.78±0.02
Fe	1.07±0.13	2.52±1.89	175.2±1.9	32.7±0.25	8.48±0.03	30.33±0.09
Hg	<0.75	<0.75	<0.75	<0.75	<0.75	<0.75
K	11847±25	5627±34	8796±48	11109±71	2552±18	9104±34
Li	<0.1	<0.1	<0.1	<0.1	<0.1	<0.1
Mg	576.2±5.5	920.3±4.8	886.0±5.3	992.1±6.6	937.0±2.2	838.3±0.9
Mn	0.79±0.05	0.53±0.16	11.94±0.18	35.70±0.13	2.35±0.02	11.53±0.02
Mo	1.55±0.02	1.17±0.11	1.33±0.11	1.69±0.05	1.16±0.08	1.49±0.08
Na	478.8±0.7	515.8±0.12	398.4±1.97	160.7±1.7	394.7±5.5	459.9±1.0
Ni	4.27±0.07	4.44±0.08	6.02±0.10	9.47±0.03	4.24±0.10	6.19±0.27
P	575.2±5.9	940.4±5.0	2446±30	1279±42	618.5±6.3	1978±14
Pb	<0.05	<0.05	0.58±0.09	0.54±0.02	<0.125	<0.125
S	2655±9	3299±15	976.8±10.6	1181±4	524.5±8.6	2480±11
Se	<0.2	<0.2	0.408±0.052	<0.2	<0.2	<0.2
Sr	7.49±0.35	8.42±0.09	7.12±0.12	6.71±0.52	27.08±0.31	19.09±0.28
V	<0.01	<0.01	<0.01	<0.01	<0.01	<0.01
Zn	0.69±0.08	0.725±0.180	13.72±0.10	8.20±0.38	3.27±0.15	8.22±0.03

4. Discussion and Conclusions

A tea mixture, *Species thymi composita*, known from the FoNo used in respiratory diseases was studied for possible analytical methods (morphological study and composition analyses) and the effectiveness was examined in vitro for elements.

The main macro- and micromorphological characteristics of STC belong to the drug components of mixture, which are well recognizable. The applicable analytical procedures for determination of bioactive agents and compositions were essential oil content and composition by GC and GC-MS, mucilage content, element content by ICP.

According to our analysis of *Thymus vulgaris* oil, the main bioactive compounds are thymol, p-cymene, γ -terpinene, carvacrol and linalool as was found by other authors as well^{24,25}. Its volatile oil components with polyphenolic compounds have relevant antioxidant activities and spasmolytic effect which prove the effectiveness^{26,27}. The mucilage containing *Althaea officinalis* extract has antitussive activity and inhibits the endothelin-1 (ET-1) induced mitogen activated protein kinase (MAPK) activation and calcium mobilization as well as cough caused by ACE drugs^{13,27,28}. Extract of *Verbascum flos* has anti-inflammatory activity²⁹.

Airway inflammation has a key role in the pulmonary and respiratory diseases, as well as in asthma. In these inflammatory processes inflammatory mediators, prostaglandins (PGD2, PGE2), leukotriens and cytokines such as IL-1 β , IL-3, IL-5, IL-6, IL-8, IL-13, TNF- α , form by neutrophils, macrophages, lymphocytes, eosinophils and mast cells³⁰⁻³². At transcriptional level the processes are regulated by NF- κ B. The severity of inflammation is in relation to the elevated activity of NF- κ B.

Prostaglandins (PGs) have a role in cough induced by angiotensin-converting enzyme (ACE) inhibitors³³. Inhibition of PG synthesis by calcium channel blockers can reduce this effect³⁴. Non-steroidal antiinflammatory drugs (NSAID-s) inhibit the biosynthesis of prostaglandins, and the synthesis of iNOS proinflammatory protein as well as proinflammatory cytokines, e.g. *Glycyrrhiza glabra* proved to have antioxidant activity and reduces inflammatory processes, ACE enzyme activity, PGE2 production, as well as LPS (lipopolysaccharide) induced TNF α and IL-1 β , IL-6, mRNA expression^{5,35}.

In PG synthesis reactive oxygen species formed inhibit the function of cyclooxygenase. The inhibition of COX2 is favourable, while of COX1 is contraindicated³⁶. Several nutritional polyphenols and others are COX2 inhibitors and iNOS activators, therefore their uses, e.g. in form of tea, are beneficial³⁷. Mainly the flavonoids in *Althaeae folium*, *Thymi herba* and *Verbasci flos* of STC may participate in this favorable effect.

In living organism transition metal ions (Cu, Fe, Mn, Zn) have a key function in both catalysis of biological oxidation by formation of free radicals and antioxidant

system by scavenging free radicals. The alteration of these element concentrations in the cells significantly modifies the signal transduction processes^{37,38}. Metal ions participate in the activation of NF- κ B, AP-1 and the regulation of I κ B kinases and other redox systems³⁹. Magnesium deficiency may induce transient increase in intracellular Ca level, in which process prooxidant cytokines (IL-1, IL-6, IL-8, TNF- α , - β), different growth factors (EGF- α , TGF- β , NFGF, FGF, PDGF), and interferons (IFN- α , - γ) form. The elevated cytokine production induces genes of reactive oxygen species and produces the following enzymes: NADPH oxidase, xanthine oxidase/dehydrogenase, COX, lipoxygenase, Cyt P450, NO synthase, proteins containing iron, Cu,ZnSOD, MnSOD. At the same time increasing of the intracellular Mg level inhibits the production of prooxidant cytokines by activation of corresponding protein phosphatases⁴⁰. The Mg absorption from the tea of STC seems to be granted, since the initial Ca to Mg concentration ratio was 4 in the tea, the ratio decreased to 2 in gastric acid, while in the plasma the ratio decreased further to 1 (Table 5). Meanwhile the normal plasma Ca to Mg concentration ratio is about 4 or 5, the absorption of tea with ratio of 1 indicates a higher Mg absorption that may affect indirectly against the mentioned proinflammatory process. The favourable effect of oral Mg administration in chronic obstructive pulmonary disease confirms this statement⁴¹. Since Mg as well as Zn have bronchodilatory action and antioxidant flavonoids and Se, Zn, Mn, Cu have relevant effect on respiratory diseases^{41,42}, the presence and absorption of these elements in the tea may prove the effect.

The paper summarized the analytical methods that may use in the analysis of and characterize the tea mixture STC. In the development of favourable effect of STC, which acts via signal transduction process, the presence of bioactive flavonoids, volatile oil components, mucilage and elements may be jointly important.

References

- 1 *Formulae Normales* VII.th Edition (FoNo, VII.). Medicina Könyvkiadó, **2003**.
- 2 *Hungarian Pharmacopoeia* VII.th Edition (Ph.Hg. VII.). Medicina Könyvkiadó, **1992**.
- 3 Nosalova, G., Sutovska, M., Mokry, J., Kardosova, A., Capek, P., Khan, M. T. H., *Minerva Biotechnologica* **2005**, *17*, 141.
- 4 Ozturk, S., Ercisli, S., *Pharm. Biol.* **2007**, *45*, 5.
- 5 Genovese, T., Menegazzi, M., Mazzon, E., Crisafulli, C., Di Paola, R., Dal Bosco, M., Zou, Z., Suzuki, H., Cuzzocrea, S., *SHOCK* **2009**, *31*, 367.
- 6 Iskender, N. Y., Yayli, N., Yildirim, N., Cansu, T. B., Terzioglu, S., *J. Oleo Science* **2009**, *5*, 117.
- 7 Jayaprakasam, B., Doddaga, S., Wang, R., Holmes, D., Goldfarb, J., Li, X. M., *J. Agric. Food Chem.* **2009**, *57*, 820.
- 8 Cao, Y., Colegate, S. M., Edgar, J. A., *Phytochem. Analysis* **2008**, *19*, 526.

- ⁹ Arnal-Schnebelen, B., Hadji-Minaglou, F., Peroteau, J. F., Ribeyre, F., de Billerbeck, V. G., *Int. J. Aromather.* **2004**, *14*, 192.
- ¹⁰ Atti-Santos, A. C., Pansera, M. R., Paroul, N., Atti-Serafini, L., Moyna, P., *J. Essent. Oil Res.* **2004**, *16*, 294.
- ¹¹ Héthelyi, B. É., Stoeva, T., Bernáth, J., *Oil Soap Cosmetics* **2001**, *50*, 239.
- ¹² Horváth, G., Szabó, G. L., Héthelyi, É., Lemberkovics, É., *J. Essent. Oil Res.* **2006**, *18*, 315.
- ¹³ Sutovska, M., Nosalova, G., Franova, S., *Bratislav. Lek. Listy* **2007**, *108*, 93.
- ¹⁴ Me, Y. C., Dong, X. W., Wu, X. M., Yan, X. F., Xie, Q. M., *Int. J. Immunopharmacol.* **2009**, *9*, 194.
- ¹⁵ Babaei, M., Abarghoei, M. E., Ansari, R., Vafaei, A. A., Taherian, A. A., Akhavan, M. M., Toussy, G., Mousavi, S., *Nat. Prod. Res.* **2008**, *22*, 1143.
- ¹⁶ *Hungarian Pharmacopoeia* VIII. Edition (Ph.Hg. VIII). Medicina Könyvkiadó, 2004.
- ¹⁷ *European Pharmacopoeia* 5. Edition (Ph.Eur. 5.), Council of Europe, **2004**.
- ¹⁸ Ladó, K., Then, M., May, Z., Szentmihályi, K., *Acta Aliment. Hung.* **2007**, *36*, 415.
- ¹⁹ May, Z., Ladó, K., Taba, G., Csödö, K., Fekete, T., Biró, E., Szentmihályi, K., *Proceedings of The 12th Symposium on Analytical and Environmental Problems*, **2005** 430.
- ²⁰ Szentmihályi, K., Hajdú, M., Fodor, J., Kótai, L., Blázovics, A., Somogyi, A., Then, M., *Biol Trace Elem. Res.* **2006**, *114*, 143.
- ²¹ Szentmihályi, K., Then, M., *Acta Aliment. Hung.* **2000**, *29*, 43.
- ²² Then, M., Szöllösy, R., Vásárhelyi-Perédi, K., Szentmihályi, K., *Acta Hort.* **2004**, *629*, 123.
- ²³ Szentmihályi, K., Then, M., *Acta Aliment. Hung.* **2007**, *36*, 231.
- ²⁴ Hudaib, M., Aburjai, T., *Flavor Fragrance J.* **2007**, *22*, 322.
- ²⁵ Stoilova, I., Bail, S., Buchbauer, G., Krastanov, A., Stoyanova, A., Schmidt, E., Jirovetz, L., *Nat. Prod. Commun.* **2008**, *3*, 1047.
- ²⁶ Sliwinska, A., Bazytko, A., Strzelecka, H., *Herba Pol.* **2001**, *47*, 56.
- ²⁷ Chizolla, R., Michitsch, H., Franz, C., *J. Agric. Food Chem.* **2008**, *56*, 6897.
- ²⁸ Rouhi, H., Ganji, F., *Pakistan J. Nutr.* **2007**, *6*, 256-8.
- ²⁹ Tatli, I. I., Akkol, E. K., Yesilada, E., Akdemir, Z., *Pharm. Biol.* **2008**, *46*, 781.
- ³⁰ Birring, S. S., Parker, D., Brightling, C. E., Bradding, P., Wardlaw, A. J., Pavord, D., *Am. J. Resp. Crit. Care Med.* **2004**, *169*, 15.
- ³¹ Sastre, B., Fernandez-Nieto, M., Molle, R., Lopez, E. L., *Allergy* **2008**, *63*, 58.
- ³² Blázovics, A., Lugasi, A., Hagymási, K., Szentmihályi, K., Kéry, A., *Phytochemistry and Pharmacology II.*, Editors: Majumdar, D. K., Govil, J. N., Singh, E., SCI TECH Publishing LLC, **2003**. Chapter 8, 107.
- ³³ Ito, K., Ito, K., Sawada, Y., Kamei, J., Misawa, M., Iga, T., *J. Pharmacol. Exp. Ther.* **1995**, *275*, 920.
- ³⁴ Fogari, R., Zoppi, A., Mugellini, A., Preti, P., Banderali, A., Salvetti, A., *Curr. Ther. Res. Clin. Exp.* **1999**, *60*, 121.
- ³⁵ Hong, Y. K., Wu, H. T., Ma, T., Liu, W. J., He, X. J., *Int. J. Biol. Macromol.* **2009**, *4*, 61.
- ³⁶ Dicipinigaitis, P. V., *Pulm. Pharmacol. Ther.* **2001**, *14*, 93.
- ³⁷ Blázovics, A., *Curr. Signal Transduction Ther.* **2007**, *2*, 226.
- ³⁸ Stefanovits-Bányai, É., Szentmihályi, K., Hegedűs, A., Koczka, N., Váli, L., Taba, G., Blázovics, A., *Life Sci.* **2006**, *78*, 1049.
- ³⁹ Kudrin, A. V., *J. Trace Elem. Med. Biol.* **2000**, *14*, 129.
- ⁴⁰ Caddell, J. L., *Am. Soc. Clin. Nutr.* **2007**, *71*, 851.
- ⁴¹ do Amaral, A. F., Rodriguez, A. L., Terra, J., Vannucchi, H., Martinez, J. A. B., *Med. Sci. Monit.* **2008**, *14*, CR524.
- ⁴² Pipinc, I. S., Macan, J., Kanceljak-Macan, B., *Period. Biol.* **2009**, *111*, 41.

Received: 05.05.2012.

Accepted: 10.05.2012.



PHOTOELECTRON SPECTROSCOPIC INVESTIGATION OF THE ELECTRONIC STRUCTURE OF FUROXANS

Gábor Vass^[a], Dániel Dzsotján^[a], Győző G. Lajgut^[a], and Tibor Pasinszki^{[a]*}

Keywords: furoxans, ionization energy, photoelectron spectroscopy, UPS, DFT, ab initio.

Disubstituted furoxans, 1,2,5-oxadiazole-2-oxides ($X_2C_2N_2O_2$, where $X = H, Cl, Br, I, CH_3, NC$), have been investigated in the gas phase by He I and He II UV photoelectron spectroscopy. Ionization potentials have been determined and the electronic structures have been discussed within the frame of molecular orbital theory. The ground-state geometries of the neutral molecules have been obtained from quantum-chemical calculations using the B3LYP/cc-pVTZ method. Photoelectron spectroscopy, supported by quantum-chemical calculations at the SAC-CI/cc-pVTZ level, provides a detailed investigation into the electronic character of the molecules and an analysis of the effect of substitution on the orbitals of the parent furoxan.

* Corresponding Author

Fax: (+36)-1-372-2909

E-Mail: pasinszki@chem.elte.hu

[a] Department of Inorganic Chemistry, Institute of Chemistry, Eötvös Loránd University of Sciences, Budapest, Pázmány Péter sétány 1/A, H-1117, Hungary.

Calculations on the parent furoxan and substituted derivatives indicate that density functional theory using the B3LYP functional can provide a correct description of the furoxan geometry.^{8,13,15,16}

In this paper we report a comprehensive photoelectron spectroscopic study of furoxans ($X_2C_2N_2O_2$, where $X = H, Cl, Br, I, CH_3, NC$) and an investigation of their equilibrium structures using density functional theory. Our previous He I photoelectron spectroscopic studies^{8-11,13} are reinvestigated using higher instrumental resolution and are augmented with He II measurements. The experimental work is assisted by high level SAC-CI *ab initio* calculations.

1. Introduction

Furoxans (1,2,5-oxadiazole 2-oxides) are important compounds in various fields of chemistry, in particular in synthetic organic chemistry¹⁻³ and medicinal chemistry,⁴ due to their unusual structure and reactivity, and biological activity. They are important synthetic precursors and found applications as high energy materials.⁵ A better understanding of the electronic structure of these compounds may help to find further applications.

Although the first furoxan derivative, dibromofuroxan, was synthesized (unknowingly) in the middle of the 19th century, the general structure of furoxans as planar five-membered rings with an exocyclic *N*-oxide group was confirmed only after a century of debate.^{1,2} Furoxans having small substituent groups, such as hydrogen or halogen atoms and cyano or methyl groups, are key to understanding properties and chemistry of all furoxans. The structures of only the parent,⁶ dibromo,⁷ and dicyanofuroxans⁸ were confirmed to date by X-ray crystallography. Vibrational and electronic properties of small furoxans were investigated recently by IR,⁸⁻¹³ Raman,^{8,11,13} and photoelectron spectroscopies.^{8-11,13}

The furoxan moiety, due to its electronegative atoms, usually characterized as electron-rich, and thus its structural description by theoretical methods is challenging. It was pointed out that the description of electronic structures of furoxans were sensitive to dynamical correlation effects¹³⁻¹⁵ and the HF wave function was found to be unstable for the parent furoxan,¹³ therefore early calculations based on HF and MP2 methods must be regarded as artefacts.

2. Experimental section

All furoxan derivatives were synthesized according to known literature methods: the parent furoxan¹⁵ and its dimethyl¹⁷ and dichloro¹⁸ derivatives were synthesized from glyoxime, dimethylglyoxime, and dichloroglyoxime by oxidizing with NO_2 gas, concentrated nitric acid, and anhydrous nitric acid, respectively, dicyanofuroxan¹⁹ from cyanoacetic acid with anhydrous nitric acid, dibromofuroxan²⁰ from oximinoacetic acid with bromine and HgO , diiodofuroxan from silver fulminate with iodine.¹¹ The purity of samples was checked by NMR and IR measurements.

The He I and He II ultraviolet photoelectron spectra (UPS) of gaseous furoxans were recorded using an Atomki ESA-32 photoelectron spectrometer described in detail elsewhere.²¹ Photoelectron spectra were recorded using the constant transmission energy mode of the electron energy analyzer and were calibrated with the $Ar^+(^2P_{3/2,1/2})$ spin-orbit doublet. The resolution of the analyzer was 30 meV in He I measurements (fwhm for the $Ar^+ ^2P_{3/2}$ line). During the He II measurements the resolution of the electron energy analyzer was lowered to 80 meV (fwhm for the $Ar^+ ^2P_{3/2}$ line) in order to gain higher electron count rates.

3. Computational methods

The geometries of the ground state neutral molecules were calculated using the B3LYP method and harmonic vibrational frequencies were obtained to identify them as real minima (zero imaginary frequencies) on the potential energy surfaces. The stability of B3LYP wave functions was checked, and B3LYP wave functions were found to be stable. We note that HF wave functions were found to be unstable (RHF-UHF instability) for all furoxan derivatives and so MPn calculations were rejected in this work. Vertical ionization energies (IEs) were calculated using the Symmetry Adapted Cluster/Configuration Interaction (SAC-CI) method using geometries obtained at the B3LYP level. Calculations were done using the cc-pVTZ basis set on C, H, N, O, Cl, and Br atoms and cc-pVTZ-pp on iodine.²² Only valence electrons were correlated in post-HF calculations. All calculations were performed with the GAUSSIAN-09 quantum chemistry package.²³

4. Results and discussion

4.1. Equilibrium structure of furoxans

Calculated structural data of furoxans are presented in Table 1 and the structure and numbering of atoms are shown in Figure 1. The experimental X-ray structures of parent furoxan, dibromofuroxan, and dicyanofuroxan are also listed in Table 1 for comparison. Although the theoretical equilibrium structure cannot be compared directly with the crystallographic structure due to vibrational averaging and solid-state effects, we expect the differences for rigid molecules like furoxans to be small.

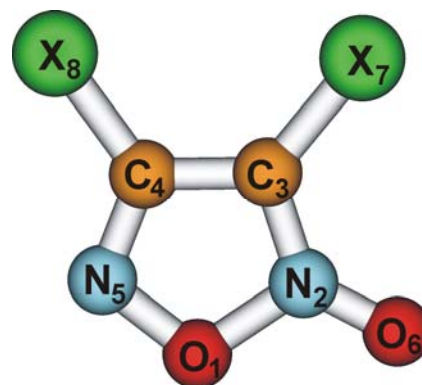


Figure 1. Structure of furoxans and numbering of atoms

According to calculations, all furoxans have a planar structure, not considering methyl group hydrogen atoms, and all molecules have C_s symmetry. Variation in bond lengths and especially in bond angles of the furoxan moiety due to substituent effects is relatively small, the largest is 0.028 Å and 1.9°, respectively. The O_1-N_2 bond is the most sensitive, and its length is increasing with increasing electronegativity of the substituent atoms. This bond is the longest and weakest in all derivatives, suggesting a point of cleavage and ring opening in decomposition processes. Bond orders can be calculated using the Gordy's rule²⁴ and by comparing the calculated bond lengths of furoxans with those of molecules having typical single/double CC, CN, and NO bonds (H_3C-CH_3 (1.527 Å)/ $H_2C=CH_2$ (1.324 Å), H_3C-NH_2 (1.464 Å)/ $H_2C=NH$ (1.263 Å), and H_2N-OH (1.447 Å)/ $HN=O$ (1.198 Å), calculated at the B3LYP/cc-pVTZ level). C–N bonds, nominally double bonds, are between a single and double bonds (bond order 1.6–1.8), and C_3-C_4

Table 1. Calculated^a equilibrium geometry of furoxans ($X_2C_2N_2O_2$)

X=	H	Cl	Br	I	CH ₃	CN
O_1-N_2	1.464 (1.441)	1.458	1.458 (1.438)	1.458	1.445	1.472 (1.454)
N_2-C_3	1.325 (1.302)	1.329	1.329 (1.299)	1.330	1.326	1.340 (1.344)
C_3-C_4	1.408 (1.401)	1.417	1.418 (1.40)	1.422	1.419	1.425 (1.401)
C_4-N_5	1.302 (1.292)	1.297	1.296 (1.25)	1.297	1.305	1.306 (1.300)
N_5-O_1	1.360 (1.379)	1.370	1.371 (1.359)	1.370	1.367	1.346 (1.354)
N_2-O_6	1.210 (1.240)	1.207	1.207 (1.228)	1.208	1.218	1.195 (1.206)
C_3-X_7	1.073 (0.92)	1.693	1.852	2.061	1.486	1.406 (1.423)
C_4-X_8	1.077 (0.97)	1.706	1.868	2.079	1.489	1.420 (1.423)
$C_7-(H' \text{ or } N)$					1.087	1.152 (1.128)
C_7-H''					1.091	
$C_8-(H' \text{ or } N)$					1.088	1.150 (1.134)
C_8-H''					1.091	
$O_1N_2C_3$	105.6 (107.2)	105.6	105.7	106.1	107.0	105.1 (105.4)
$N_2C_3C_4$	107.4 (107.2)	107.1	107.0	106.8	106.7	106.9 (106.8)
$C_3C_4N_5$	111.7 (111.9)	112.1	112.2	111.9	111.1	111.4 (112.1)
$C_4N_5O_1$	107.1 (106.6)	106.5	106.6	107.0	107.5	107.6 (107.2)
$O_1N_2O_6$	118.4 (116.4)	119.2	118.9	118.4	119.0	119.0 (118.2)
$C_4C_3X_7$	132.3 (130)	130.7	131.1	132.0	132.7	130.9 (131.3)
$C_3C_4X_8$	127.9 (128)	125.6	126.1	127.3	127.7	126.7 (126.8)
$C_3C_7(H' \text{ or } N)$					110.5	179.0 (179.0)
C_3C_7H''					110.9	
$C_4C_8(H' \text{ or } N)$					109.5	178.3 (178.0)
C_4C_8H''					111.1	

^a Calculated at the B3LYP/cc-pVTZ level. Bond lengths are in Å and bond angles are in degrees. See Figure 1 for numbering of atoms. Experimental X-ray crystal structures from references [6,7,8] are in parenthesis.

and N₅-O₁ bonds, nominally single bonds, are shorter than a C-C or N-O single bond (bond order 1.4–1.5 and 1.2–1.3, respectively). This tendency to bond order equalization is in agreement with the expected aromaticity of furoxans.¹³ The exocyclic N₂-O₆ bond is short (bond order 1.9–2.0) and may be regarded as a double bond. Its length is decreasing with increasing electronegativity of the substituent atoms connected to the furoxan moiety.

4.2. Photoelectron spectra of furoxans

The He I and He II photoelectron spectra of furoxans are shown in Figures 2 and 3, and experimental and calculated ionization potentials are listed in Table 2. From the calculated IPs, from the comparison of the He I and He II spectra, and from the comparison of the spectra of substituted derivatives, the assignment is relatively straightforward.

A possible starting point to describe the electronic structure of furoxans is to consider the MOs of a five-membered aromatic ring, modified with an exocyclic oxygen atom and two substituent atoms or groups. Three π orbitals, a nitrogen 'lone pair' orbital ($n_{N,ring}$), an oxygen 'lone pair' orbital ($n_{O,ring}$), and two oxygen 'lone pair' orbitals from the exocyclic oxygen atom ($\pi(n_O)$ and $\sigma(n_O)$) can be deduced from the furoxan moiety as low IP MOs. In addition, seven high IP orbitals can be deduced from the ring σ framework, including the terminal 'lone pair' of the exocyclic oxygen atom ($n_{O,term}$). Ionization from some of

these orbitals will produce photoelectron bands in the investigated IP region. In addition to MOs of the furoxan moiety, MOs from the substituent groups are also expected. MOs in general are far from localized, but in order to keep discussion simple we use the notations above. MOs of the parent furoxan are shown in Figure 4.

According to calculations, the first band in spectra between 9 and 11 eV can be unambiguously assigned to the O₆ oxygen $\pi(n_O)$ lone pair with some contribution from the ring. These PE bands show vibrational fine structure with strong adiabatic transition. The band shape indicates a relatively small geometrical change due to ionization from the HOMO. The vibrational fine structure is not entirely resolved, but ionic vibrational frequencies of ground state

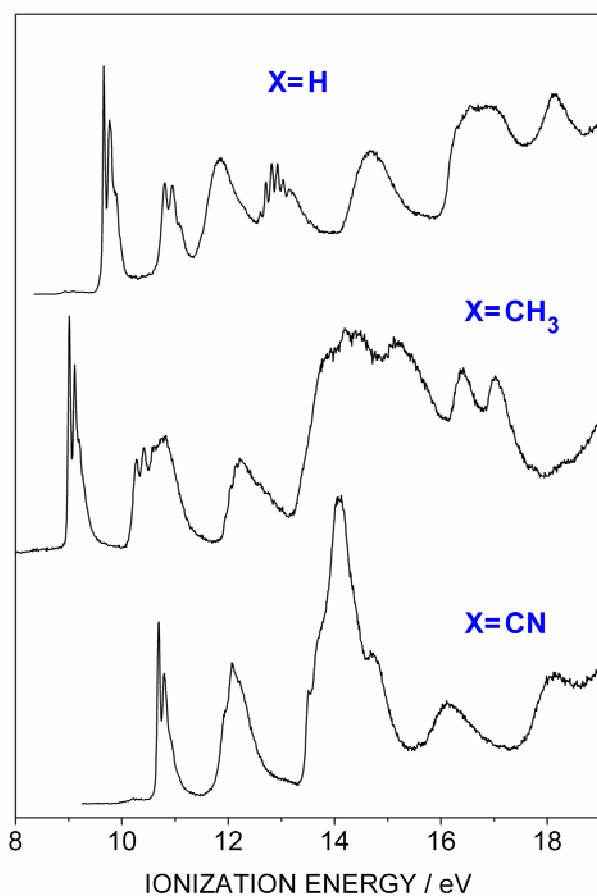


Figure 2. He I photoelectron spectra of the parent (top), dimethyl (middle), and dicyanofuroxan (bottom).

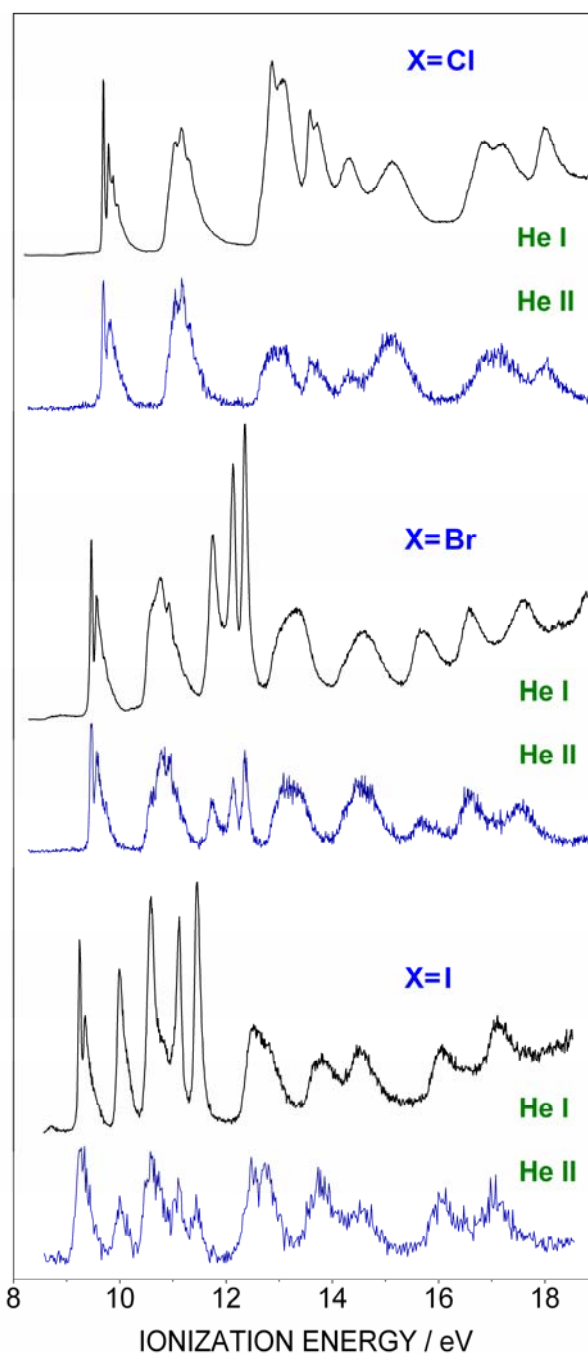


Figure 3. He I and He II photoelectron spectra of the dichloro (top), dibromo (middle), and diiodofuroxan (bottom).

Table 2. Experimental and calculated^a vertical ionization energies of furoxans (X₂C₂N₂O₂)

X= H		Cl		Br		I		CH ₃		CN		orbital character and symmetry
Exp.	Calc.	Exp.	Calc.	Exp.	Calc.	Exp.	Calc.	Exp.	Calc.	Exp.	Calc.	
9.66 ^b	9.27	9.69 ^c	9.35	9.40 ^g	9.22	9.24 ⁱ	8.90	9.01 ^j	8.50	10.69 ^l	10.20	$\pi(n_{O_6})$, a''
							9.99					n_{I_1} , a''
							10.58					n_{I_1} , a'
10.80 ^c	10.55	11.16 ^f	10.93	10.70 ^h	10.69	10.7	10.50	10.27 ^k	9.90	12.08	11.72	$\sigma(n_{O_6})$, a'
		11.16	11.13									$\pi(\text{ring})$, a''
				10.70	10.77	11.12	11.08					n_{Br_1}, n_{I_1} , a''
		12.86	12.87	11.69	11.91	11.45	11.09					$n_{Cl_1}, n_{Br_1}, n_{I_1}$, a'
		13.07	13.13	12.07	12.22							n_{Cl_1}, n_{Br_1} , a'
		13.58	13.53	12.29	12.48							n_{Cl_1}, n_{Br_1} , a''
11.85	11.80			(13.0)	13.77	12.5	12.71	10.80	10.64	12.08	12.15	$\pi(\text{ring})$, a''
						12.9	12.84	12.23	12.06			$\sigma(n_{N,\text{ring}})$, a'
						13.8	13.84					$\sigma(\text{ring}, \text{C-I})$, a'
								13.5	13.30			$\pi(\text{ring})$, a''
									13.70		13.64	CH ₃ , $\pi(\text{cyano})$, a'
									14.37	13.51	14.00	CH ₃ , $\pi(\text{cyano})$, a'
									14.84	14.08	14.14	$n_N(\text{cyano})$
										14.74	14.22	$n_N(\text{cyano})$
									15.22		14.21	CH ₃ , $\pi(\text{cyano})$, a''
12.91 ^d	12.96	14.31	13.75	13.3	13.24						14.42	$\sigma(n_{N,\text{ring}})$, a'
									15.35			CH ₃ , a'
		15.13	15.04					15.5	15.50		15.15	CH ₃ , $\pi(\text{cyano})$, a''
												n_{Cl_1} , a''
14.68	14.24			14.5	14.67	14.5	14.24					$\pi(\text{ring})$, a''
						14.5	14.58					$\sigma(\text{ring}, \text{C-I})$, a'
14.68	14.74	15.13	15.18	14.5	14.67	16.1	16.31	16.41	16.29	16.14	16.52	$\sigma(n_{O_6,\text{ring}})$, a'
16.3	16.46	16.86	17.07	15.65	15.97							C-X, a'
		17.20	17.02	16.53	16.77							$\sigma(\text{ring})$, a'
16.5	17.23											C-H
16.9	17.54		18.09									$\pi(\text{ring})$, a''
18.14	18.47	18.01	18.25	17.54	17.77	17.1	17.40	17.03	17.04	18.1	18.18	$\sigma(n_{O,\text{term}})$, a'
			18.23									$\pi(\text{ring})$, a''
												$\pi(\text{ring})$, a''
												$\pi(\text{ring})$, a''

^a Calculated at the SAC-CI//B3LYP/cc-pVTZ level. ^b Cationic vibrational wavenumbers: 1130±50 and 810±50 cm⁻¹. ^c Cationic vibrational wavenumber: 1210±50 cm⁻¹. ^d Cationic vibrational wavenumber: 810±50 cm⁻¹. ^e Cationic vibrational wavenumber: 800±50 cm⁻¹. ^f Cationic vibrational wavenumber: 1050±100 cm⁻¹. ^g Cationic vibrational wavenumber: 840±50 cm⁻¹. ^h Cationic vibrational wavenumber: 1300±100 cm⁻¹. ⁱ Cationic vibrational wavenumber: 800±50 cm⁻¹. ^j Cationic vibrational wavenumber: 800±50 cm⁻¹. ^k Cationic vibrational wavenumber: 1150±50 cm⁻¹. ^l Cationic vibrational wavenumber: 840±50 cm⁻¹.

cations can be estimated with an accuracy of ca. 50 cm⁻¹ (see Table 2). The second band in all spectra, except that of the iodo derivative, is assigned to the in-plane O₆ oxygen $\sigma(n_{O_6})$ lone pair orbital, mixed some extent with the ring σ orbitals. The two exocyclic oxygen atom lone pair orbitals ($\pi(n_{O_6})$ and $\sigma(n_{O_6})$) are thus separated by 1.1–1.5 eV, which is similar to the ca. 1 eV separation observed in the spectra of simple aromatic N-oxides.²⁵ The third and the fourth bands in the spectrum of parent furoxan at 11.85 and 12.91 eV are unambiguously assigned to the ring highest lying π orbital and nitrogen 'lone pair' orbital ($n_{N,\text{ring}}$), respectively. These PE bands are shifted toward lower IPs upon methyl substitution and can be unambiguously detected in the spectrum of dimethyl-furoxan. The second band in spectra of dichloro, dibromo, and dicyano derivatives, however, is assigned to two MOs, one is the in-plane O₆ oxygen $\sigma(n_{O_6})$ lone pair orbital and the other is a ring π orbital mixed to some extent with the CN group or halogen atoms. In the case of the bromo derivative the bromine lone pair character is dominant. The assignment of the sharp bands in the spectrum of diiodo, dibromo, and dichloro derivatives in the 10–11.5, 11.5–12.5, and 12.5–14 eV region, respectively, is

unambiguous as their relative intensity is strongly reduced in the He II spectra and they clearly originate from lone pair orbitals of halogen atoms. The intense broad feature in the spectrum of dicyano derivative between 13.5–15 eV is a result of the overlapping of seven PE bands assigned to the ionization of six highly localized cyano group based orbitals, four $\pi(\text{cyano})$ and two terminal nitrogen lone pair $n_N(\text{cyano})$, and to the $\sigma(n_{N,\text{ring}})$ orbital. A clear identification to individual orbitals is not possible, but calculation clearly show the clustering of the six cyano based MOs. Similar clustering of the relevant PE bands have been observed in the spectrum of 3,4-dicyano-1,2,5-thiadiazole in the same ionization energy region.²⁶ The assignment of PE bands in the high ionization energy region of spectra is less unambiguous. Our assignment (Table 2) is based on calculations and on comparing spectra of substituted derivatives.

It is interesting to compare the peak positions of PE bands corresponding to molecular orbitals of the furoxan moiety in substituted derivatives. The IE correlation diagram is shown in Figure 4. The dimethyl derivative has

the lowest ionization potential of all furoxans investigated and the dicyano derivative has the highest. Ionization potentials are gradually increasing in the order of $\text{CH}_3 < \text{I} < \text{Br} < \text{Cl} < \text{CN}$ substituted derivatives, which can be explained by the electron donating and electron withdrawing effects of substituent groups. The shift of PE bands due to substituent effects indicates, in general, similar pattern and it is in agreement with the mesomeric and inductive effects of substituents attached to the furoxan moiety.

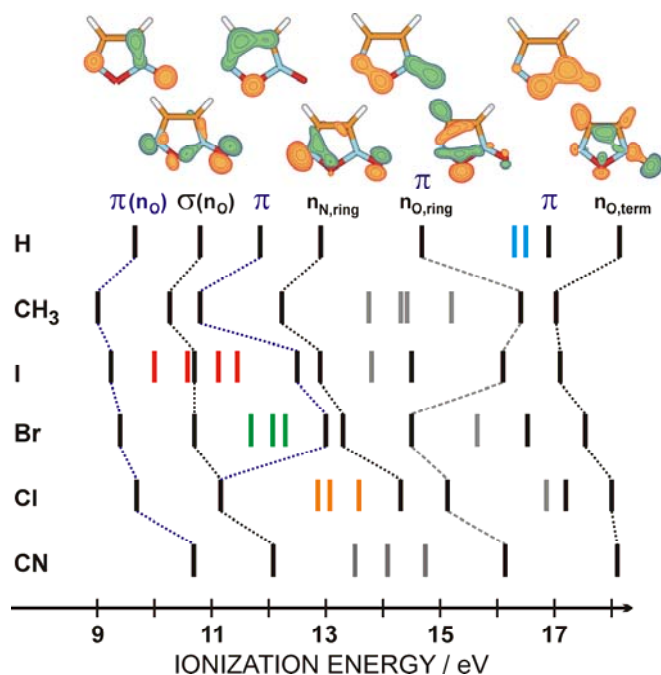


Figure 4. Experimental ionization energy correlation diagram for substituted furoxans and schematics of the corresponding molecular orbitals of the parent furoxan.

5. Conclusion

Structures of simple substituted furoxans have been investigated in the gas phase by photoelectron spectroscopy and by theoretical calculations using B3LYP and SAC-CI methods. According to calculations, furoxans have a planar ring structure with a short exocyclic N–O bond and a long endocyclic N–O bond. Photoelectron spectroscopy has provided information on the valence occupied levels of the neutral molecules and on the fundamental vibrations of the low-lying cationic states. Assessment of the sequence of cationic states has provided an assessment of substituent effects on ionization potentials and electronic structures. HOMOs of all furoxan derivatives have predominant exocyclic oxygen π lone pair character, therefore the lowest energy ionization potentials are assigned to ionizations from the out-of-plane oxygen lone pair orbitals.

Acknowledgments

We thank the Hungarian Scientific Research Fund for a research grant (grant no. OTKA K101164) in support of this work.

References

- Kaufman, J. V. R., Picard, J. F. *Chem. Rev.*, **1959**, 59, 429.
- Gasco, A., Boulton, A. J. *Adv. Heterocycl. Chem.*, **1981**, 29, 251.
- Sheremetev, A. B., Makhova, N. N., Friedrichsen, W. *Adv. Heterocycl. Chem.*, **2001**, 78, 65.
- Cerectto, H., Porcal, W. *Mini-Reviews in Med. Chem.*, **2005**, 5, 57.
- (a) Federoff, B. T. *Encyclopedia of Explosives and Related Items*; Picatinny Arsenal: Dover, NJ, 1962. (b) Oyumi, Y., Brill, T. B. *Combust. Flame*, **1986**, 65, 313. (c) Rice, B. M., Hare J. J. *J. Phys. Chem. A*, **2002**, 106, 1770.
- Godovikova, T. I., Golova, S. P., Strelenko, Y. A., Antipin, M. Yu., Struchkov, Y. T., Khmel'nitskii, L. I. *Mendeleev Commun*, **1994**, 7.
- Pasinszki, T., Westwood, N. P. C. *J. Mol. Struct.*, **1997**, 408/409, 161.
- Pasinszki, T., Ferguson, G., Westwood, N. P. C. *J. Chem. Soc., Perkin Trans. 2*, **1996**, 179.
- Pasinszki, T., Westwood, N. P. C. *J. Phys. Chem.*, **1995**, 99, 6401.
- Pasinszki, T., Westwood, N. P. C. *J. Phys. Chem. A*, **1998**, 102, 4939.
- Pasinszki, T., Krebsz, M., Vass, G. *Chem. Phys. Lett.*, **2010**, 487, 194.
- Havasi, B., Pasinszki, T., Westwood, N. P. C. *J. Phys. Chem. A*, **2005**, 109, 3864.
- Pasinszki, T., Havasi, B., Hajgató, B., Westwood, N. P. C. *J. Phys. Chem. A*, **2009**, 113, 170.
- Rauhut, G., Werner, H.-J. *Phys. Chem. Chem. Phys.*, **2003**, 5, 2001.
- Stevens, J., Schweizer, M., Rauhut, G. *J. Am. Chem. Soc.*, **2001**, 123, 7326.
- Klenke, B., Friedrichsen, W. *J. Mol. Struct. (Theochem)*, **1998**, 451, 263.
- Pasinszki, T., Westwood, N. P. C. *J. Phys. Chem. A*, **2001**, 105, 1244.
- Ungnade, H. E., Kissinger, L. W. *Tetrahedron*, **1963**, 19 (suppl. 1), 143.
- Parker, C. A., Emmons, W. D., Rolewicz, H. A., McCallum, K. S. *Tetrahedron*, **1962**, 17, 79.
- Pasinszki, T., Vass, G., Klapstein, D., Westwood, N. P. C. *J. Phys. Chem. A*, **2012**, 116, 3396.
- Csákvári, B., Nagy, A., Zanathy, L., Szepes, L. *Magy. Kém. Foly.*, **1992**, 98, 415.
- Peterson, K. A., Figgen, D., Goll, E., Stoll, H., Dolg, M. *J. Chem. Phys.*, **2003**, 119, 11113.
- Frisch, M. J. et al. GAUSSIAN 09 (Revision B.01), Gaussian, Inc., Wallingford CT, 2010.
- Gordy, W. *J. Chem. Phys.*, **1947**, 15, 305.
- Maier, J. P., Müller, J.-F. *J. Chem. Soc., Faraday Trans 2*, **1974**, 70, 1991.
- Pasinszki, T., Krebsz, M., Vass, G. *J. Mol. Struct.*, **2010**, 966, 85.

Received: 24.05.2012.

Accepted: 30.05.2012.



COMPARATIVE PHYTOCHEMICAL SCREENING OF PHENOLOIDS IN *LYSIMACHIA* SPECIES

Anita Tóth^[a], Eszter Riethmüller^{[a]*}, Ágnes Alberti^[a], Krisztina Végh^[a] and Ágnes Kéry^[a]

Keywords: *Lysimachia vulgaris*; *Lysimachia nummularia*; *Lysimachia punctata*; phenoloids; antioxidants; RP-HPLC-DAD-ESI-MS/MS

A comparative qualitative and quantitative screening of phenoloids of *Lysimachia vulgaris* L., *Lysimachia nummularia* L. and *Lysimachia punctata* L. is reported for the first time. The total flavonoid, hydroxycinnamic acid, tannin and polyphenol content of these species were examined by spectroscopic methods (Ph. Eur. 5.). The accumulation of various phenoloids in individual organs was investigated as well. The quantitative analytical measurements revealed that the total flavonoid content expressed in hyperoside of *L. vulgaris* was significantly lower than that of *L. nummularia* and *L. punctata*, but its hydroxycinnamic acid content was outstanding. The accumulation of polyphenols and tannins showed to be homogeneous among the samples. The *in vitro* radical scavenging activities of the plant extracts were tested by DPPH and ABTS methods. Our studies proved that *L. nummularia* extract had the most significant activity. The composition of flavonoids in the samples and their *in vitro* antioxidant effect showed that the dominance of myricetin glycosides in *L. nummularia* is closely related to the most significant antioxidant capacity of this sample. In addition to the quantitative accumulation of flavonoids, significant differences have been observed in the composition of their quality as well. The main flavonoids in *L. nummularia* and *L. vulgaris* were identified myricetin- and myricetin-, quercetin, and kaempferol-glycosides, respectively by HPLC-DAD-ESI-MS/MS method.

* Corresponding Authors

Tel./Fax: + 36-1-459-1500/55206; + 36-1-3172979

E-Mail: eszter.riethmuller@gmail.com

[a] Department of Pharmacognosy, Semmelweis University, H-1085, Hungary

Introduction

The members of the *Lysimachia* genus are at the forefront of interests. The various species of the genus are distributed in meadows, but their versions are planted also extensively in gardens. They can commonly be found in the temperate zone in North America, Asia and Europe. Most of the known species are native in China.¹

The phytochemical screenings of Far-East native *Lysimachia* species have started in the last two decades. The chemical studies showed the presence of flavone and flavonol type flavonoids and saponins in these plants. The representatives of the genus include free flavonols and flavone: myricetin, quercetin, kaempferol,^{1,2} isorhamnetin and flavonoid mono-, di- and tri-glycosides. The members of *Lysimachiopsis* and *Nummularia* subgenus have been reported to contain also C-glycosides.²

The polar compounds of the *Lysimachia* genus such as flavonoids have been found to have potent anti-tumor and cytotoxic activity in human leukemia K562 cells.³ Their anti-bacterial and excellent anticholecistic potential, antipyretic effect and the availability to increase bile secretion in acute cholecystitis have been reported as well.⁴ The alcoholic extract of *L. ramosa* herb could give rise to killing of different parasite tapeworm.⁵

Hungarian folk medicine and Traditional Chinese Medicine (TCM) also use the leaves of different *Lysimachia* species. *L. nummularia* L. can be used in rheumatic pains, gingivitis, stomatitis, paradontosis, and purulent skin diseases treatment due to its antibiotic and anti-inflammatory properties. The herb tea is used for gastrointestinal diseases.⁶⁻⁸ The TCM uses the *L. christinae* herb for treatment of retention of urine, painful urination, kidney stones jaundice, anorexia, gallstones. It has diuretic, anti-inflammatory and hepatoprotective properties too. It can be used externally for skin cooling, ulcers, infected wounds, snake bite treatment, reduces swelling and edema.⁹ The *Lysimachia* genus can serve as a good example, helping us to explore the possible links between European folk medicine and Traditional Chinese Medicine.

As the exploration of the European species of the *Lysimachia* genus is incomplete, we aimed their comparing screening. In this paper the first results of the study of the phenolic metabolites of *Lysimachia vulgaris* L., *Lysimachia nummularia* L. and *Lysimachia punctata* L. are summarized.

Materials and methods

Plant material

Samples of *Lysimachia nummularia* L., *Lysimachia vulgaris* L. and *Lysimachia punctata* L. were obtained from Bükk National Park in early and late flowering stage. The samples were dried at room temperature and authenticated in the Department of Pharmacognosy, Semmelweis University, Budapest, where voucher specimen are deposited.

Table 1.: Phytochemical characteristics of *Lysimachia* samples (*average of 3 measurements)

	Total flavonoid* (g/100g, in hyperoside)	Total polyphenol* (g/100g, in pyrogallol)	Tannin* (g/100g)	Hydroxycinnamic acid* (g/100g, in rosmarinic acid)
<i>L. vulgaris</i> L.				
herba	0.55±0.01	3.42±0.15	1.82±0.11	2.43±0.10
leaf	1.14±0.04	3.26±0.18	1.96±0.12	2.45±0.08
stem	0.10±0.02	0.99±0.13	0.32±0.04	0.53±0.04
<i>L. nummularia</i> L.				
herba	1.02±0.02	3.00±0.12	1.95±0.10	1.25±0.03
leaf	1.77±0.05	2.34±0.11	1.26±0.11	1.16±0.07
stem	0.36±0.05	1.77±0.14	0.97±0.10	0.63±0.06
<i>L. punctata</i> L.				
herba	0.87±0.07	4.05±0.13	2.81±0.14	1.78±0.08
leaf	1.32±0.05	3.52±0.14	2.63±0.12	1.69±0.08
stem	0.19±0.03	1.31±0.14	0.99±0.12	0.38±0.02
flower	0.61±0.05	2.98±0.12	1.89±0.12	2.35±0.10

Extraction

Soxhlet extraction was performed in laboratory-scale apparatus according to the guidance of Ph. Eur. 5. Ten g of plant material was extracted with methanol. After filtration, the extract was evaporated under reduced pressure with a rotary evaporator at 60 °C.

Quantitative and qualitative methods

Total phenoloid, tannin, flavonoid and hydroxycinnamic acid content

Contents of polyphenols, tannins, flavonoids and hydroxycinnamic acids were determined in the dried plant samples by applying the methods of Ph. Eur. 5.¹⁰

DPPH (2,2-diphenyl-1-picrylhydrazyl) and ABTS (2,2'-azino-bis-(3-ethylbenzothiazoline-6-sulfonic acid)) method

Antioxidant activities of the *Lysimachia* extracts were determined using DPPH (2,2-diphenyl-1-picrylhydrazyl) and ABTS (2,2'-azino-bis(3-ethylbenzothiazoline-6-sulphonic acid)) as free radicals.¹¹⁻¹³ Ten mg of DPPH (Sigma-Aldrich, Budapest, Hungary) was dissolved in 25.0 mL HPLC grade methanol. Ten mg ABTS (Fluka) was dissolved in 2.6 mL HPLC grade water. To produce ABTS radical cation, stock solution was reacted with 1.72 mg potassium persulfate. Stock solutions were diluted right before measuring by HPLC methanol and spectroscopic ethanol, respectively, so that absorbance of the diluted free radical solutions was approximately 0.900. In their radical forms DPPH and ABTS have absorption maximums at characteristic wavelengths, at 515 nm and 734 nm, respectively. During the reaction with antioxidants, the radicals are converted back to their colorless neutral form. This decolourisation is stoichiometric with respect to the concentration of antioxidant and can be measured spectrophotometrically. During the assay 50 µL of the samples of 5 different concentrations were added to the free radical solutions and the decrease of the absorbance was measured by Hitachi U-2000 spectrophotometer at the characteristic wavelengths for 6 minutes. From the decrease of the absorbance, percentage of inhibition was calculated. The percentages of inhibition were plotted vs. the concentrations.

The concentrations belonging to the 50% inhibition (IC₅₀) were determined by linear regression.

RP-HPLC-DAD-ESI-MS/MS method

Samples were redissolved in super gradient grade methanol (Sigma-Aldrich, Budapest, Hungary), were purified on Supelco SPE Cartridge LC18 (500 mg / 3 mL) and after evaporation, were redissolved in super gradient grade methanol prior to analysis.

For chromatographic separation an Agilent 1200 HPLC system (G1379A degasser, G1312A binary gradient pump, G1329A autosampler, G1316A column thermostat and G1315C diode array detector) was used (Agilent Technologies, Waldbronn, Germany). Samples were separated on a Supelco Ascentis Express C18 column (50 x 3,0 mm, 2,7 µm; Agilent Technologies, Waldbronn, Germany) maintained at 40 °C, injection volume was 10 µL.

MS/MS analyses were performed on an Agilent 6460 triple quadrupole system equipped with an electrospray ionization source (ESI) (Agilent Technologies, Palo Alto, CA). ESI was operated in the positive ion mode, conditions were as follows: temperature: 350 °C, nebulizer pressure: 40 psi (N₂), drying gas flow: 13 L/min (N₂), capillary voltage: 4000 V, fragmentor voltage: 80 V. High purity nitrogen was used as collision gas, collision energy was changed between 10 and 25 eV according to differences in molecule structures. Full mass scan spectra were recorded over a range of 100–1000 m/z. The Masshunter B.01.03 software was used for data acquisition and qualitative analysis.

Results and discussion

Quantitative studies: total flavonoid, polyphenol, tannin and hydroxycinnamic acid content

The total flavonoid content expressed in hyperoside found to be considerably lower in herb of *L. vulgaris* than in herb of *L. nummularia* and *L. punctata* cultivars.

The stem contained much smaller amount of flavonoids than the leaves in the case of all three species, which is important information on the quality of herbal drugs. The higher rate of leaves in the drug is favourable (Table 1.).

More similar accumulations were observed in the total polyphenol and tannin content of the samples. The total polyphenol content was around 3-4%. The highest accumulation was in *L. punctata*, and the lowest in *L. nummularia* herb extract. Tannins' accumulation was also highest in *L. punctata*, while the lowest tannin content was measured in *L. vulgaris*. The accumulation in individual organs was examined as well. The stem contained much less polyphenol and tannin than the leaves in the case of all three species (Table 1.).

The hydroxycinnamic acid content expressed in rosmarinic acid was found to be the highest in the *L. vulgaris*, while the lowest in *L. nummularia*. The *L. punctata* herb's hydroxycinnamic acid content was between. Among the individual organs, the stem contained much less content than the leaves in the case of all three species (Table 1.).

In vitro antioxidant activity assay

Results of the study on *in vitro* DPPH and ABTS antioxidant activity of the samples are summarized in Table 2., indicating also well-known antioxidant compounds' 50% inhibition value (IC_{50}). The *L. nummularia* extract had the highest activity in both systems, which exceeded the antioxidant effect of kaempferol. *L. vulgaris* extract had lower scavenger capacity than the reference materials and than the other two species. The cultivar of *Lysimachia punctata* L. had moderate activity both in DPPH and ABTS tests.

Table 2.: DPPH and ABTS radical-scavenging activities of the *Lysimachia* extracts and the standards

	DPPH IC_{50} (10^{-3} mg/mL)	ABTS IC_{50} (10^{-3} mg/mL)
<i>L. vulgaris</i> L.	35.3±0.3	11.2±0.3
<i>L. nummularia</i> L.	16.3±0.2	3.57±0.2
<i>L. punctata</i> L.	22.8±0.3	6.84±0.2
Gallic acid	2.7±0.1	0.95±0.1
Rutin	7.3±0.1	3.26±0.2
Quercetin	3.4±0.1	1.22±0.1
Kaempferol	19.1±0.2	8.56±0.3

We aimed to find answers for the connection between the flavonoid composition and the bioactivity of the samples, therefore the individual flavonoid compounds were also investigated.

RP-HPLC-DAD-ESI-MS/MS analysis

A new method was improved for the separation of the compounds of the investigated samples, where eluent A was 0.1 % (v/v) TFA - water, eluent B was acetonitrile. The following gradient elution program was applied at a flow rate of 0.9 mL/min; 0 min: 0 % (v/v) B, 10 min: 50 % (v/v) B, 12 min: 100 % (v/v) B. Chromatograms

were acquired at 280 and 340 nm, UV spectra were recorded between 200 and 400 nm. Total ion and UV chromatograms at wavelength of 280 nm and 340 nm were recorded of the methanolic extracts of *L. nummularia* and *L. vulgaris*. In the extract of *L. vulgaris* four, in the extract of *L. nummularia* one flavonoid-type structure was detected. Due to the fact that the MS/MS method is not suitable for accurate identification of the sugar molecules, neither to establish their connection, compounds were tentatively identified based on the structures of the flavonoid aglycones.¹⁴

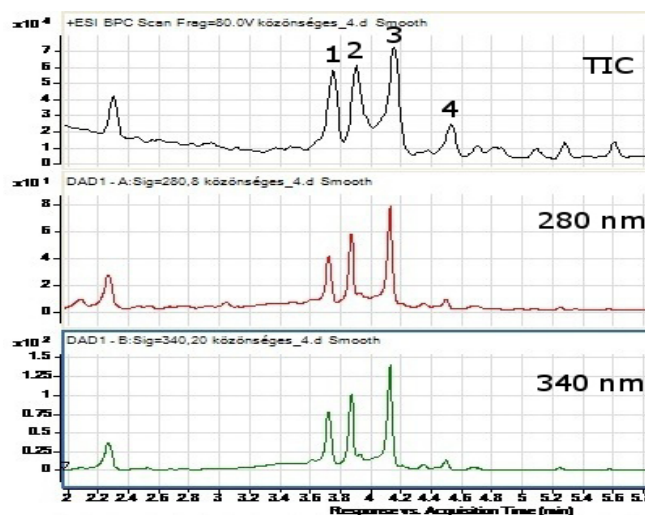


Figure 1. Chromatograms of *Lysimachia vulgaris* L. (total ion, 280 and 340 nm) 1 myricetin-hexosyl-desoxyhexoside, 2 quercetin-hexosyl-di(desoxyhexoside), 3 quercetin-hexosyl-desoxyhexoside /rutin, 4 kaempferol-hexosyl-desoxyhexoside

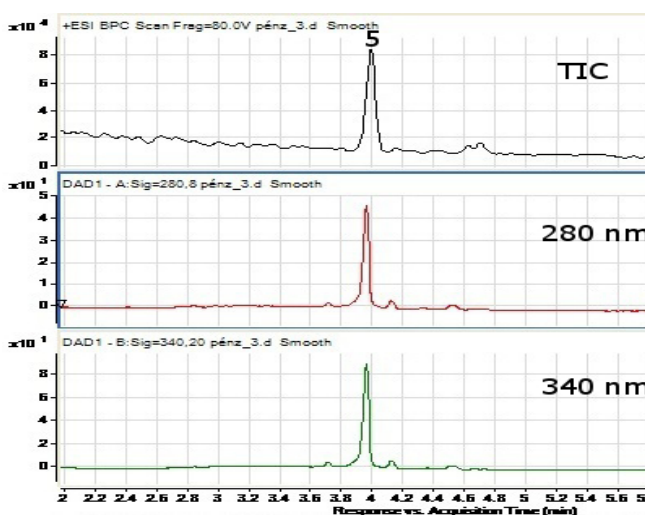


Figure 2. Chromatograms of *Lysimachia nummularia* L. (total ion, 280 and 340 nm) 5 myricetin-rhamnoside

The following compounds were identified in *L. vulgaris*:

Compound 1: Retention time: 3.72 min. The molecule ion $[M+H]^+$ was detected at m/z 627. The mass spectrum exhibited fragments at m/z 319, 217, and 153. The pronounced products correspond to myricetin aglycone, while the loss of 308 amu to desoxyhexose-hexose sugar part. Thus compound 1 characterized as myricetin-hexosyl-desoxyhexoside.

Compound 2: Retention time: 3.87 min. The molecule ion at m/z 757 provided pronounced fragments at m/z 449, 303, 275, and 153. Product ion at m/z 303 determined the type of aglycone to be quercetin, while the neutral loss of 308 amu corresponds to desoxyhexose-hexose, and the neutral loss of 146 amu to desoxyhexose sugar parts. Thus compound 2 was tentatively identified as quercetin-hexosyl-di(desoxyhexoside).

Compound 3: Retention time: 4.12 min. Molecule ion was detected $[M+H]^+$ at m/z 611. Product ion at m/z 303 determined the type of aglycone to be quercetin and the loss of 308 amu pointed to a characteristic sugar part (desoxyhexose-hexose). Therefore compound 3 was characterized as quercetin-hexosyl-desoxyhexoside (rutin).

Compound 4: Retention time: 4.51 min. The compound exhibited molecule ion at m/z 595 and fragments at m/z 287, 165 and 153. The product at m/z 287 indicates kaempferol aglycone, and the neutral loss of 308 amu a desoxyhexosyl-hexosyl group. Thus compound 4 was tentatively identified as kaempferol-hexosyl-desoxyhexoside.

The following compound was identified in *L. nummularia*:

Compound 5: Retention time 3.96 min. Molecule ion $[M+H]^+$ detected at m/z 487 provided fragments at m/z 341, 319 and 153. The pronounced products correspond to myricetin aglycone, while the neutral loss of 146 amu to a desoxyhexose sugar part. Thus compound 5 was characterized as myricetin-desoxyhexoside.

Table 3. Compounds identified in *Lysimachia* samples by RP-HPLC-DAD-ESI-MS/MS

<i>Lysimachia vulgaris</i> L.				
Compound No.	Rt (min.)	$[M+H]^+$ (m/z)	Fragment ions(m/z)	Assumed structure
1	3.72	626	319, 217, 153	Myricetin-hexosyl-desoxyhexoside
2	3.87	757	449, 303, 275, 153	Quercetin-hexosyl-di(desoxyhexoside)
3	4.12	611	465, 303, 257, 165, 153	Quercetin-hexosyl-desoxyhexoside /Rutin
4	4.51	595	287, 165, 153	Kaempferol-hexosyl-desoxyhexoside
<i>Lysimachia nummularia</i> L.				
5	3.96	487	341, 319, 153	Myricetin-rhamnoside

Conclusion

As the phytochemical exploration of European species of *Lysimachia* is incomplete, we aimed their comparative investigation. This study summarizes the first results of the examination of phenolic metabolites of native Hungarian species: *Lysimachia vulgaris* L., *Lysimachia nummularia* L. and *Lysimachia punctata* L. for the first time.

In the DPPH and ABTS *in vitro* antioxidant test systems the extract of *L. nummularia* had the highest activity. The flavonoid content of *L. nummularia* found to be significantly higher than that of *L. vulgaris*. We were looking for answers to relationship between the flavonoid composition and the bioactivity of the samples. Significant differences were found in quantitative accumulation of flavonoids in the different species and their quality as well.

Based on literature data, we tentatively identified the flavonoids of *L. vulgaris* and *L. nummularia* by RP-HPLC-ESI-DAD-MS/MS method for the first time: the dominance of myricetin glycoside in *L. nummularia* is in good accordance with its most significant antioxidant capacity.

References

- Hänsel, R., Keller, K., Rimpler, H., Schneider, G. *Hager's Handbuch der Pharmazeutischen Praxis, Drogen E-O*, Springer-Verlag, Berlin, **1976**, 615.
- Marr, K., Bohm, B., Cooke, C., Gunning, P., *Phytochemistry* **1998**, *49*, 553.
- Liu, Y., Tang, L., Liang, Z., You, B., Yang, S., *J. Ethnopharm.*, **2010**, *131*, 1.
- Yang, X., Wang, B., Zhang, X., Liu, W., Qian, J., Li, W., Deng, J., Singh, G., Su, H., *J. Ethnopharm.*, **2011**, *137*, 57.
- Challam, M., Roy, B., Tandon, V., *Veterinary Parasitol.*, **2010**, *169*, 214.
- Szabó, L. Gy. *Gyógynövények és élelmisznövények A-tól Z-ig – Adatbázis*, Melius Alapítvány, **2010**.
- Makai, A; Házipatika: Pénzlevel lizinka. *Természetgyógyász Magazin Online*, **2005**
- Zelenyák, J., *A gyógynövények hatása és használata*. Stephaneum, Budapest, **1908**, 45 and 108
- Hempen, C.-H., Fischer, T., *A materia medica for chinese medicine plants, minerals and animal products*. Churchill Livingstone elsevier, Oxford, **2009**, 322.
- European Pharmacopoeia V.*, EDQM, **2004**, *2*, 1103 and 2377., **2004**, *1*, 221.
- Re, R., Pellegrini, N., Proggente, A., Pannala, A., Yang, M., Rice-Evans, C., *Free Rad. Biol. Med.*, **2009**, *26*, 1231.
- Arts, M. J., Haenen, G. R., Voss, H. P., Bast, A., *Food Chem. Toxicol.*, **2004**, *42*, 45.
- Brand-Williams, W., Cuvelier, M. E., Berset, C., *Lebensm. Wiss. Technol.*, **1995**, *28*, 25.
- Ma, Y. L., Li, Q. M., Van den Heuvel, H., Claeys, M., *Rapid Comm. Mass Spectr.*, **1997**, *11*, 1357.

Received: 25.05.2012.

Accepted: 30.05.2012.



PHYTOCHEMICAL COMPARISON AND ANALYSIS OF *BERGENIA CRASSIFOLIA* L. (FRITSCH.) AND *BERGENIA CORDIFOLIA* STERNB.

Renáta Árok,^[a] Krisztina Végh,^{[a]*} Ágnes Alberti^[a] and Ágnes Kéry^[a]

Keywords: *Bergenia crassifolia* L. (Fritsch.); *Bergenia cordifolia* Sternb.; Arbutin; Pigmentary disorders; HPLC-UV

Bergenia crassifolia L. (Fritsch.) and *Bergenia cordifolia* Sternb. species of Saxifragaceae are decorative perennial plants. The most characteristic compound with biological activity is arbutin with skin whitening properties. Arbutin from other sources is used in skin pigmentary disorders. The aim of our work was the identification and qualitative analysis of arbutin using HPLC and UV-spectroscopic methods and quantitative determination of arbutin as well as other pharmaceutically interesting compounds: flavonoids, hydroxycinnamic acids, polyphenols and tannins in domestic cultivars, considering the synergism of phytochemical agents in therapeutic effect in skin disorders. The arbutin content was found to be between 4.8 – 9.8 g/100g in the two *Bergenia* species and significant amount of total polyphenol (4.13 – 9.27 g/100g), tannin (3.70 – 6.70 g/100g) and hydroxycinnamic acid (1.80 – 2.42 g/100g) was measured.

* Corresponding Authors

Tel: + 36-1-459-1500/55206

Fax: + 36-1-3172979

E-Mail: krisvvegh@gmail.com

[a] Department of Pharmacognosy, Semmelweis University, H-1085, Hungary

melanocytes.³ *Bergenia* species are cited in literature as being one of the richest in arbutin (15-20%), an important pharmaceutical substance with depigmentation properties.¹ The content of arbutin in vegetative and generative organs of the plant varies in wide limits, being dependent on the method of raw material drying. The plant age is also an important factor affecting arbutin content.¹

Introduction

The species belonging to the genus *Bergenia* are herbaceous, perennial plants mainly distributed in the southeastern regions of Central Asia, northern regions of South Asia and Eastern Asia from Siberia and the Altay Mountains in Russia, South to Northern Mongolia.^{1,2}

Bergenia species contain various biologically active compounds in their roots, leaves, stems and flowers, which can be mainly classified into three categories, including simple phenols/polyphenols, flavonoids and quinines.² The preparations of these plants are used as astringent, anti-inflammatory, bactericidal, haemostatic, immunomodulatory, antiulcer, antihepato-toxic, antifungal, antiarrhythmic preparations. In folk medicine these remedies are used for disinfecting, wound healing, tonic and general strengthening purposes.¹

The most important compound for the phytochemical researches is arbutin. Arbutin inhibits melanin production and decreases tyrosinase activity.³ Tyrosinase is a copper-containing enzyme⁴, also known as polyphenol oxidase (PPO), which catalyses two initial steps in the formation of pigment melanin: hydroxylation of tyrosine and the oxidation of 3,4-dihydroxyphenylalanine.⁵ Overexpression of tyrosinase leads to excessive accumulation of melanin, which causes cutaneous hyperpigmentation including freckles and lentiginosities, melasma and malignant melanoma.³ Observations imply that the depigmenting effect of arbutin may be highly effective in both cell culture and human skin models, making arbutin a useful and safe agent for skin whitening. Tyrosinase inhibitors can be applied in the therapy of this skin disorders, especially in malignant melanoma due to their cytotoxicity in

The aim of this study consisted in phytochemical analysis of two *Bergenia* species: *B. crassifolia* and *B. cordifolia*, acclimated in Hungary. The accumulation of flavonoids, hydroxycinnamic acids, polyphenols and tannins in the leaves and flowers were also studied, considering the synergism of phytochemical agents in therapeutic effect in skin disorders.

Experimental

Plant material

Leaves of *Bergenia crassifolia* L. (Fritsch.) and *Bergenia cordifolia* Sternb. were obtained from the Botanical Garden of Corvinus University and Pesthidegkút. One sample of *B. crassifolia* leaves was collected in Finland. Plant samples were harvested in the early spring, dried at room temperature and were authenticated in the Department of Pharmacognosy, Semmelweis University, Budapest, where voucher specimen are deposited.

Qualitative methods

Identification of arbutin by high-performance liquid chromatography

Bergenia samples (3.0 g) were extracted with 50 mL of 80% methanol in ultrasonic bath. After filtration, the extract was evaporated under reduced pressure with a rotary evaporator at 60 °C and was redissolved in super gradient grade methanol (Sigma-Aldrich, Budapest,

Hungary). Samples were purified on Supelco SPE Cartridge LC18 (500 mg / 3 mL) and after evaporation, were redissolved in super gradient grade methanol prior to analysis. Some samples were extracted with 20 mL of 50% methanol in ultrasonic bath. After filtration 0.3 g basic lead acetate was added and filtrated. The extract was evaporated under reduced pressure with a rotary evaporator at 60 °C and was redissolved in super gradient grade methanol (Sigma-Aldrich, Budapest, Hungary). Samples were purified on Supelco SPE Cartridge LC18 (500 mg / 3 mL) and were redissolved in super gradient grade methanol prior to analysis. One mg/mL arbutin solution was used as a standard. The HPLC analysis was performed with a Jasco system equipped with an ERC-3113 degasser, a Jasco LG-980-02 gradient unit, a PU-980 HPLC pump, a sample injector, and a PU-975 UV-visible detector. Compounds were separated on a 25 cm × 4.6 mm, 5 µm particle, Supelcosil LC-18 column (Sigma-Aldrich). Experiments were performed at 20 °C, the injection volume was 20 µL. Detection was carried out the wavelength of 280 nm and 340 nm. UV-spectra were recorded between 200 and 400 nm.

Quantitative methods

Quantitative determination of arbutin

Herbal drug of 0.40 g was extracted with hot water for 30 min by refluxing on boiling water bath. The extract was filtered into a 250.00 mL volumetric flask and filled up with water. Five mL of the extract was transferred into a separatory funnel and mixed with 45 mL of water, 1 mL of 2% 4-aminoantipyrine, 0.5 mL of diluted NH₄OH and 1 mL of 8% K₃(Fe/CN)₆ solution. After 5 minutes the reaction mixture was extracted with CHCl₃. The organic phases were mixed, filtered through Na₂SO₄ sicc. into a 100.00 mL volumetric flask and filled up with CHCl₃ to 100.00 mL. The absorption was measured at 455 nm. The blank solution was water. The arbutin content of the crude drug was calculated as arbutin (g/100g).

Total flavonoid, total hydroxycinnamic derivative, total phenoloid and tannin content

Total flavonoid, total hydroxycinnamic derivative, total phenoloid and tannin content were determined according to the valid spectroscopic methods of the European Pharmacopoeia.⁶

Results and discussion

The HPLC method of the European Pharmacopoeia was improved. A gradient of acetic acid in water (1.0%, v/v eluent A) and methanol (eluent B) was applied at a flow rate of 1 mL/min; 0-30 min: A: 11%, B: 89% (linear gradient); 30-31. min.: A: 60%, B: 40% (linear gradient); 31– 35. min: A: 100%, B: 0% (isocratic). Arbutin in the samples was identified by standard addition, using authenticated standard. The standard addition measurement was made with 1:1 mixture of sample and standard.

According to the results the analysed *Bergenia* species contain a high level of arbutin and many flavonol glycosides, presumably quercetin glycosides.

The arbutin content of *B. crassifolia* and *B. cordifolia* leaf extracts was identified by the Rf and UV-spectra of authenticated standard using HPLC method. To improve the quality of chromatograms a purification step was also added to eliminate polyphenols from the sample solutions. Arbutin was detectable with retention time of 3.40 minute. The UV-spectra was measured between 200-600 nm, two maximums of the UV-spectra were observed at 235 nm and 291 nm. The presence of arbutin in the samples was confirmed by using standard addition method. The added arbutin was determined by the characteristic Rf. The HPLC-UV chromatograms of arbutin standard and the samples of *B. crassifolia* and *B. cordifolia* are shown in Figure 1-3.

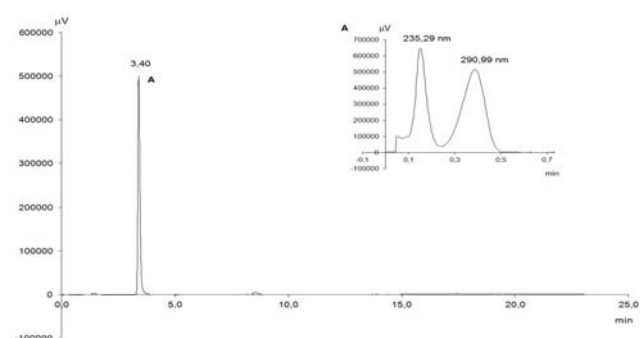


Figure 1. HPLC-UV chromatograms of arbutin standard at 280 nm and UV spectra between 200-600 nm

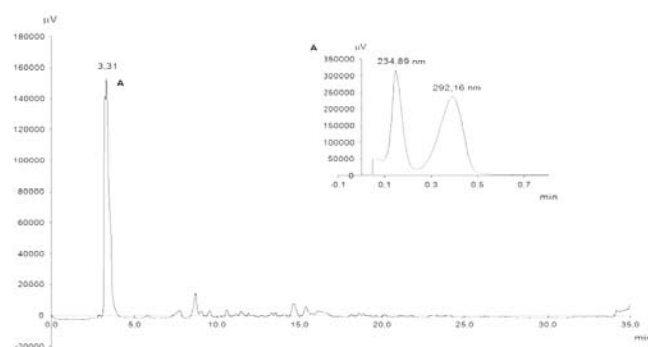


Figure 2. HPLC-UV chromatograms of *Bergenia crassifolia* sample with standard addition

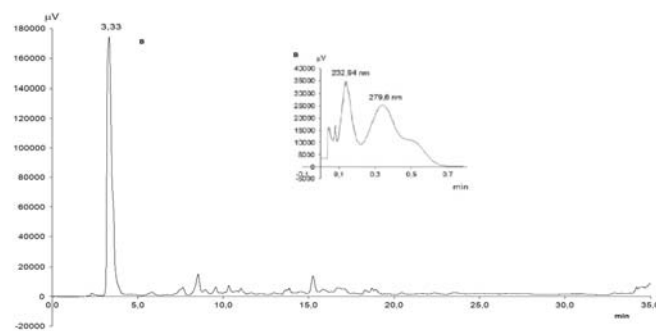


Figure 3. HPLC-UV chromatograms of *Bergenia cordifolia* sample with standard addition

Table 1. Phytochemical characteristics of *Bergenia* samples

Plant sample (<i>Bergenia</i>)		Total flavonoid* (g/100g, in hyperoside)	Total polyphenol* (g/100g, in pyrogallol)	Tannin* (g/100g, in pyrogallol)	Hydroxycinnamic acid* (g/100g, in rosmarinic acid)	Arbutin* (g/100g, in arbutin)
<i>B. crassifolia</i> (Finland)	leaf	0.76±0.05	9.27±0.72	5.01±0.34	2.03±0.11	9.83±0.68
<i>B. crassifolia</i> (Corvinus University)	leaf	0.81±0.04	6.46±0.34	3.70±0.24	2.35±0.23	4.79±0.72
	flower	0.88±0.05	4.35±0.57	3.92±0.19	2.42±0.20	2.08±0.13
<i>B. cordifolia</i> (Pesthidegkút)	leaf	0.65±0.03	8.20±0.41	3.94±0.15	1.95±0.16	9.48±0.74
	flower	0.67±0.03	6.31±0.24	4.23±0.31	1.98±0.09	2.51±0.10
<i>B. cordifolia</i> (Corvinus University)	leaf	0.92±0.06	4.29±0.19	6.50±0.39	1.80±0.12	7.94±0.52
	stem	0.95±0.04	4.13±0.25	6.35±0.52	1.95±0.14	7.94±0.61
	flower	0.87±0.07	4.33±0.41	6.70±0.27	1.98±0.30	2.99±0.18

(* average of 3 determinations)

Total arbutin, flavonoid, polyphenol, tannin and hydroxycinnamic acid content of *Bergenia* samples are summarized in Table 1.

The arbutin content was between 4.8 – 9.8 g/100g. This is lower than the value (17.44 g/100g) was found by Pop et al.¹ and similar than the content (6.96 g/100g) was found by Pozharitskaya et al.⁷ Among the investigated parts of the plants the highest amount of arbutin was detected in the leaves. The leaf of species from Finland contained the largest quantities of arbutin. The samples made of *B. crassifolia* and *B. cordifolia* from Corvinus University could be well compared: *B. cordifolia* shows a higher amount of arbutin (7.94 g/100g) than *B. crassifolia* (4.79 g/100g). Arbutin content in the investigated flowers were 2.08 – 2.99 g/100g (Figure 4.).

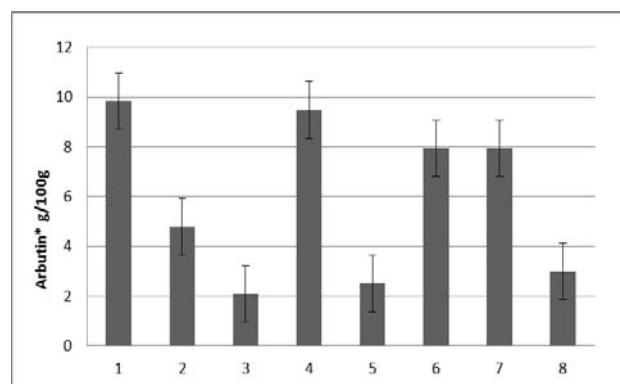


Figure 4.: Total amount of arbutin in *Bergenia* samples (1. *B. crassifolia* (Finland) leaf, 2. *B. crassifolia* (Corvinus University) leaf, 3. *B. crassifolia* (Corvinus University) flower, 4. *B. cordifolia* (Pesthidegkút) leaf, 5. *B. cordifolia* (Pesthidegkút) flower, 6. *B. cordifolia* (Corvinus University) leaf, 7. *B. cordifolia* (Corvinus University) stem, 8. *B. cordifolia* (Corvinus University) flower) (*average of 3 determinations)

The flavonoid, hydroxycinnamic acid, polyphenol and tannin contents are foremost established. The total flavonoid content determined in hyperoside was detectable between 0.65 – 0.95 g/100g. The species from Corvinus University contained the highest amount of flavonoids. The polyphenol and tannin contents were determined in pyrogallol. The content of total polyphenol was 4.13 – 9.27 g/100g, the highest value was 9.27 g/100g in the sample from Finland.

The identified amount of tannin was 3.70 – 6.70 g/100g. In this respect, there was no significant difference between the two species of *Bergenia*. The hydroxycinnamic acid values, determined in rosmarinic acid, were similar, the average content was 2.06 g/100g (Figure 5-6.).

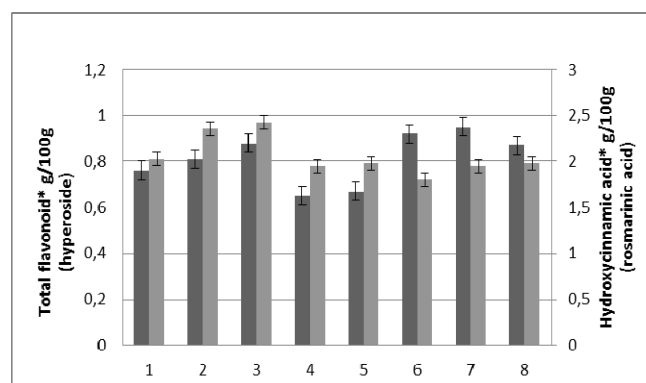


Figure 5. Total amount of flavonoid and total hydroxycinnamic acid content in *Bergenia* samples (1. *B. crassifolia* (Finland) leaf, 2. *B. crassifolia* (Corvinus University) leaf, 3. *B. crassifolia* (Corvinus University) flower, 4. *B. cordifolia* (Pesthidegkút) leaf, 5. *B. cordifolia* (Pesthidegkút) flower, 6. *B. cordifolia* (Corvinus University) leaf, 7. *B. cordifolia* (Corvinus University) stem, 8. *B. cordifolia* (Corvinus University) flower) (*average of 3 determinations)

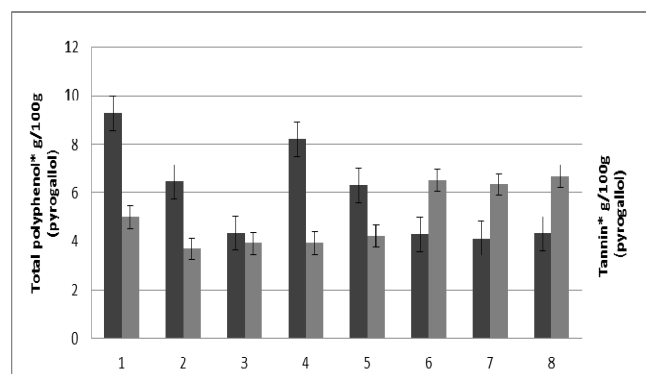


Figure 6. Total amount of polyphenols and tannin in *Bergenia* samples (1. *B. crassifolia* (Finland) leaf, 2. *B. crassifolia* (Corvinus University) leaf, 3. *B. crassifolia* (Corvinus University) flower, 4. *B. cordifolia* (Pesthidegkút) leaf, 5. *B. cordifolia* (Pesthidegkút) flower, 6. *B. cordifolia* (Corvinus University) leaf, 7. *B. cordifolia* (Corvinus University) stem, 8. *B. cordifolia* (Corvinus University) flower) (*average of 3 determinations)

Conclusion

This paper presents a qualitative HPLC method to identify arbutin in two different species of *Bergenia* genus, *Bergenia crassifolia* L. and *Bergenia cordifolia* Sternb. growing in Hungary. In addition content of arbutin and other phenolic compounds (flavonoids, hydroxycinnamic acids, polyphenols and tannins) in the two species was determined and compared for the first time. Due to inhibition of tyrosinase enzyme, which catalyses the rate-limiting step of the melanogenic pathway by arbutin, *Bergenia* species might be suitable for cosmetic and dermatological applications.

Quantitation of other phenolics (flavonoids, hydroxycinnamic acids, polyphenols and tannins) is necessary to complete phytochemical characterization of *Bergenia* samples, since these compounds may also contribute to the pharmacological effect.

References

- ¹ Pop, C., Vlase, L., Tamas, M. *Notulae Botanicae Horti Agrobotanici Cluj-Napoca* **2009**, *37*, 129.
- ² Zhang, Y., Liao, C., Li, J., Liu, X. *J. Med. Plants Res.*, **2011**, *5*, 4396.
- ³ Chakraborty, A. K., Funasaka, Y., Komoto, M., Ichihashi, M. *Pigment Cell Res.* **1998**, *11*, 206.
- ⁴ Decker H., Tuzcek F. *Trends Biochem. Sci.*, **2000**, *25*, 392.
- ⁵ Sánchez-Ferrer, Á., Rodríguez-López, J. N., García-Cánovas, F., García-Carmona, F., *Biochim. Biophys. Acta*, **1995**, *1247*, 1.
- ⁶ *European Pharmacopoeia V.*, EDQM, **2004**, *2*, 1103 and 2377., **2004**, *1*, 221.
- ⁷ Pozharitskaya, O. N., Ivanova, S. A., Shikov A. N., Makarov, V. G., Galambosi, B. *J. Sep. Sci.* **2007**, *30*, 2447.

Received: 24.05.2012.
Accepted: 31.05.2012.



CHARACTERIZATION OF SYNTHETIC VOLTAITE ANALOGUES

István E. Sajó^[a]

Keywords: Inorganic frameworks, experimental mineralogy, mixed valence solids

Recently new NH₄- and Mg-containing minerals of the voltaite group have been discovered. As they were found in minute amounts and are intimately intergrown with their associated minerals, a number of their properties could not be measured and characterized properly. The four pure end members of the solid solution series were synthesized and characterized, that made possible the reliable identification of natural solid solutions within the boundaries of this phase composition range.

* Corresponding Authors

Fax: +36-1-3257554

E-Mail: sajo.istvan@ttk.mta.hu

[a] Institute of Materials and Environmental Chemistry,
Research Center for Natural Sciences Hungarian Academy of
Sciences, Pusztaszeri út 59-67. H-1025 Budapest, Hungary

Introduction

Voltaite, K₂Fe²⁺₅Fe³⁺₃Al[SO₄]₁₂·18H₂O, an inorganic framework structure featuring a large cubic unit cell (space group Fd3c) occurs as a mineral¹. Due to the large unit cell size ($a_0 \sim 27.25$ Å) the structure is not highly sensitive to cationic sizes. Substitution at the K⁺ and Fe³⁺ sites results in a variety of structural analogues with similar cell constants²

The newly discovered ammoniomagnesiovoltaite (NH₄,K)₂(Mg,Fe²⁺)₅Fe³⁺₃Al[SO₄]₁₂·18H₂O³ is a rare mineral intimately intergrown with its associated minerals (eg tschermigite, sabieite, kieserite, etc.). Therefore preparation of phase pure natural specimens was not feasible for the necessary investigations. Having a cubic structure, its unit cell is characterized with a single a_0 cell parameter, resulting in powder diffraction data insufficient for the extraction of two compositional coordinates. Additionally the synthetic analogues were characterized with their IR spectra, density and index of refraction.

Materials and methods

Synthesis: Voltaite analogues were prepared according to Mereiter.⁴ Strongly acidic solution of the appropriate salts was prepared with the molar ratio K₂SO₄ : FeSO₄ : Fe₂(SO₄)₃ : Al₂(SO₄)₃ : H₂SO₄ : H₂O = 0.08 : 0.44 : 0.15 : 0.12 : 1.66 : 40 and evaporated at 80°C for about 2-3 days to the half of its original volume. The well developed crystals were filtered from the mother liquor and immediately rinsed with 10% H₂SO₄ then thoroughly dried. The isomorphous analogues were prepared with the same procedure, replacing K₂SO₄ for (NH₄)₂SO₄ and/or FeSO₄ for MgSO₄, as required. The resulting products were phase pure voltaite analogues, stable at room temperature and atmospheric conditions.

X-ray powder diffraction measurements were done on a Model PW 3710 / PW 1050 Bragg-Brentano diffractometer, using Cu K α radiation ($\lambda=1.541862$ Å), secondary beam graphite monochromator and proportional counter. Synthetic fluorophlogopite mica (NIST SRM 675) and silicon powder (NIST SRM 640) were used as internal two theta standards. Lattice parameters were determined with Le Bail whole pattern decomposition method⁵ using the Fullprof Rietveld⁶ software suite. Infrared spectra were taken on a Thermo Nicolet Avatar 320 FT-IR spectrometer in the 4000–400 cm⁻¹ range using KBr discs. Density values were determined with the sink-float method with a pycnometer and acetone-bromoform mixture. Indices of refraction were determined at 546 nm light wavelength. Theoretical indices of refraction were estimated from the chemical composition and density values for each member using the Gladstone-Dale relationship with the new series of Gladstone-Dale constants (GDCs) as determined by Mandarino and Eggleton.⁷ The experimental and estimated indices of refraction were then compared to see if inconsistencies exist.

Discussion

Mg substitution at the Fe^{II} site results in a decrease of the cell parameter of 0.11Å, while NH₄ substitution of the K increases the cell size about the same amount. As the structure allows the formation of continuous solid solution between the four end members, owing to the opposite effect of the two substituents, a given cell size may represent a range on the two-dimensional composition map. Full substitution at both sites results in a unit cell size close to the un-substituted voltaite, as a consequence of the nearly identical but opposite effect the two substituents (cf. *tab. 1*). The cell constant determined by Gossner and Fell² for K-Mg-voltaite is fairly different from our values (27.42 Å vs. 27.26 Å). However it is not surprising considering the precision of the XRD technique of those times. Mereiter⁴ and Schwarte and Fischer⁸ determined the cell constants from single crystal measurements, that were aimed at structure determination and not for precise lattice parameter measurement. The deviations of their values from ours are well within the error boundaries of the single crystal method.

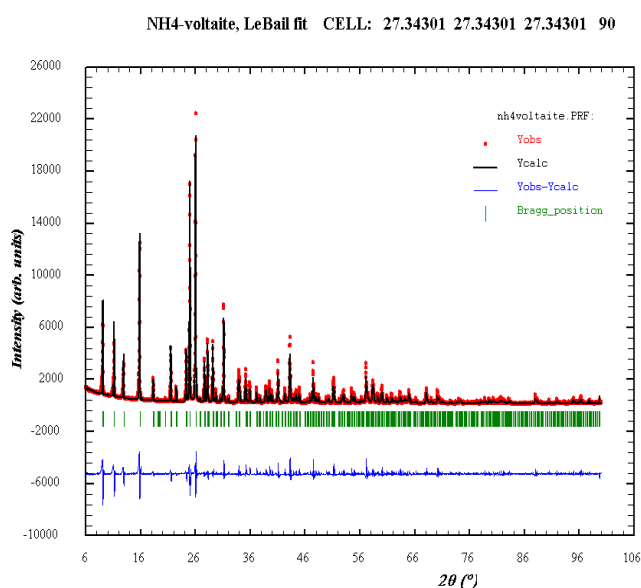
Table 1: Unit cell parameters and physical properties of the synthetic voltaite analogues.

	formula	a_0 [Å]	D_x g/cm ³	D_m g/cm ³	n^* GDC	n exp.	Ref.
Voltaite	$K_2Fe^{2+}_5Fe^{3+}_3Al[SO_4]_{12} \cdot 18H_2O$	27.25	2.664	-	1.5955	-	⁴
Voltaite	$K_2Fe^{2+}_5Fe^{3+}_3Al[SO_4]_{12} \cdot 18H_2O$	27.232	2.669	2.667	1.5955	1.596	this study
Mg-Voltaite	$K_2Mg_5Fe^{3+}_3Al[SO_4]_{12} \cdot 18H_2O$	27.121	2.492	2.495	1.569	1.571	this study
Mg-Voltaite	$K_2Mg_5Fe^{3+}_3Al[SO_4]_{12} \cdot 18H_2O$	27.225	2.464	-	1.569	-	⁸
Ammoniovoltaite	$[NH_4]_2Fe^{2+}_5Fe^{3+}_3Al[SO_4]_{12} \cdot 18H_2O$	27.343	2.582	2.585	1.5975	1.598	this study
Mg-ammoniovoltaite	$[NH_4]_2Mg_5Fe^{3+}_3Al[SO_4]_{12} \cdot 18H_2O$	27.260	2.400	2.395	1.571	1.572	this study
Mg-ammoniovoltaite	$[NH_4]_2Mg_5Fe^{3+}_3Al[SO_4]_{12} \cdot 18H_2O$	27.42	2.357	2.375	1.571	-	²

Calculated densities (D_x) are given for the nominal formula and measured unit cell size. *Estimated indices of refraction (n , GDC) are based on Gladstone-Dale relationship, nominal chemical composition and measured density.

Their FTIR spectra do not show striking differences. Some of the absorption bands exhibit a minor shift corresponding to the difference of the atomic masses of the substituents. The only major difference is the presence of a well defined absorption band at 1428 cm⁻¹ in the NH₄ containing analogues, which is completely missing in the K containing ones. It is suggested, that in the lack of other reliable analytical technique, the relative intensity of the 1428 cm⁻¹ absorption band can be used for the estimation of NH₄ – K substitution ratio.

Fig 1: Whole pattern decomposition of the NH₄-voltaite powder XRD scan.



The measured and calculated densities exhibit a good correlation, referring to that real structures may well correspond to the theoretical formulas. Furthermore, the range of density values is relatively broad (2.40 ~ 2.67 g/cm³) allowing a more sensitive differentiation. The excellent compatibility of the experimental and estimated indices of refraction corroborates the theoretical compositions and gives a further way to navigate in the coordinates of the solid solution map.

References

- ¹Majzlan, J., Alpers, C. N., Koch, C. B., McCleskey, R. B., Myneni, S. C. B., Neil, J. M. *Chem. Geol.*, **2011**, *284*, 296.
- ²Gossner, B., Fell, E., *Ber. Deutsch. Chem. Ges.* **1932**, *65*, 393.
- ³Szakáll, S., Sajó I., Fehér, B., Bigi S., *Can. Mineral.* **2012**, *50*, (in press)
- ⁴Mereiter K. *Tschermaks Mineral. Petrogr. Mitt.*, **1972**, *18*, 185.
- ⁵Le Bail, A., Duroy, H., Fourquet, J. L., *Mater. Res. Bull.* **1988**, *23*, 447.
- ⁶Rodriguez-Carvajal, J., *Reference guide for the computer program Fullprof. Laboratoire Léon Brillouin CEA-CNRS, Saclay, France*, **1996**.
- ⁷Gladstone, J. H., Dale, T. P., *Phil. Trans. Royal Soc. London*, **1863**, *153*, 317; Mandarino, J. A., *Can. Mineral.* **1981**, *19*, 441; **2007**, *45*, 1307; Eggleton, R. A., *Can. Mineral.* **1991**, *29*, 525
- ⁸Schwarte, C., Fischer, W., *Z. Krist.*, **1989**, *186*, 272.

Received: 25.05.2012.

Accepted: 31.05.2012.



DEUTERIUM ISOTOPE SEPARATION IN THE CHEMICAL REACTION OF ALUMINIUM AMALGAM AND WATER

László Kótai^{[a]*}, József Lippart^[a] and István Gács^[a]

Keywords: aluminium amalgam; deuterium-depleted hydrogen; deuterium isotope separation

Deuterium isotope separation process takes place in the reaction of the amalgamated aluminium metal surface and water. The reaction produces hydrogen gas with ~40 ppm deuterium content and the formed aluminium hydroxide gel is enriched in deuterium. The theoretical separation factor is $s=3.9$. Besides the kinetic isotope effect, the key factor in the separation process is the $\text{H}_2\text{O}+\text{HD}=\text{HDO}+\text{H}_2$ exchange reaction. Since only a low amount of amalgam forms on the aluminium surface, the overvoltage difference of the deuterium and the hydrogen on the mercury does not play key role in the process. The main role of the amalgam formation is embodied in the decomposition of the stable oxide layer on the aluminium surface, thus ensuring free metallic surfaces for the reaction with the water.

* Corresponding Authors

Fax: +36-23-376-456

E-Mail: kotai.laszlo@ttk.mta.hu

[a] Institute of Materials and Environmental Chemistry,
Research Centre for Natural Sciences, Hungarian Academy
of Sciences, H-1025, Pusztaszeri. u. 59-67, Budapest,
Hungary

Results and Discussions

The enrichment of the deuterium in natural waters by electrolysis has been known for a long time⁶. The isotope separation factor (s) can be defined as:

$$s = \frac{(H/D)_{gas}}{(H/D)_{liquid}} \quad (1)$$

Introduction

Deuterium-depleted water (DDW) has been a very promising antitumor agent used in human therapy¹. The increasing demand has induced intensive research for new manufacturing methods². Although the reaction of sodium amalgam with water resulted deuterium-depleted hydrogen with ~50 ppm deuterium content³ which can easily be transformed into DDW, the availability of the sodium amalgam is limited (the only source is the mercury cathodic rock salt electrolysis process). Thus, other sources for deuterium-poor hydrogen and DDW respectively, is needed. Dissolution of metallic aluminium in aqueous NaOH and sulphuric acid⁴ has resulted deuterium-depleted hydrogen evolution. Since the reactivity of aluminium toward water can be initiated by amalgamation of its surface with mercury(II) chloride solutions⁵, the reactions of aluminium or aluminium amalgam with water are potential candidates for deuterium poor hydrogen production.

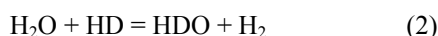
Experimental parts

A metallic aluminium rod (99,99 % aluminium content, ALCOA KÖFÉM, Hungary) was immersed into 20 % aq. NaOH and after washing with water was immediately immersed into an 5 wt. % aq. mercury(II)chloride solution when intensive hydrogen gas evolution and aluminium hydroxide precipitate formation could be observed. The deuterium content of the hydrogen was determined by IR spectroscopy of the water condensed in a liq. trap and obtained by the reaction of the hydrogen gas with CuO at 600°C.

The numerical value of the separation factor is depends on some key factors such as the nature of the electrode materials. The factor is generally higher if the electrode metal has hydrogenating activity⁷ or the metals are alloyed with other metals⁸. The amalgams are a special kind of alloys, and the separation factor in the reaction of sodium amalgam with water is considerably higher⁹ than the separation factor obtained by pure metallic sodium and water¹⁰. The hydrogen and deuterium overvoltage and their differences on metallic mercury are also key factors in the isotope separation processes in the presence of metal amalgams⁹. Although, in the case of amalgams this difference may also be attributed to the presence and effect of metals dissolved in the mercury or the presence of intermetallic compounds as NaHg_x alloys¹¹.

Preparation of hydrogen by the electrolysis of water is a simple reduction of the hydrated proton (deuterium cation)¹². Consequently, reduction of H⁺ and D⁺ cations with electrons originating from chemical reducing agents like metals, the same isotope separation effects can be expected. Since the dissolution rates of metals in deuterated acids are slower than in normal acids¹³, isotope separation can be expected in these reactions. E.g. in case of alkali metals, zink, calcium or aluminium⁴ the deuterium content of the evolved hydrogen gas has decreased. Other factors affecting isotope separation in the electrolytic hydrogen generation can also be occurred.

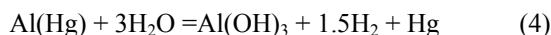
Isotope exchange reaction between the formed deuterium containing hydrogen gas and the water has also occurred:



Using natural water in these processes, no D₂O or D₂ are present due to the low absolute value of deuterium content in the system, so only the HD content has to be taken into consideration. The reaction (3) is an equilibrium reaction, and the equilibrium constant is about 3 at 20 °C¹⁴.

$$K = \frac{[\text{HDO}][\text{H}_2]}{[\text{H}_2\text{O}][\text{HD}]} \quad (3)$$

Aluminium is an amphoteric element and its reaction with 0.1 N sulphuric acid¹⁵ or sodium hydroxide⁴ showed deuterium isotope separation with 2.0 and 4.3 separation factor, respectively. Aluminium does not react directly with water due to the surface oxide layer which prevent the contact with water. Decomposing this layer with mercury(II) chloride which simultaneously amalgamates the aluminium surface, an amalgam covered reactive aluminium layer is formed which easily decomposes the water without adding acids or bases¹⁶:



For water samples containing deuterium at natural abundance level the experimentally found separation factor was proved to be ~3.9 which is slightly higher than the values obtained for sodium amalgams (Table 1).

Table 1.

Isotope separation factors in the reactions of metals and their amalgams with hydrated H⁺(D⁺) ions

Metal	Reactant	s value	Ref.
Na	H ₂ SO ₄	1.2	15
Na	H ₂ O	1.7-2.8	4
Na(Hg)	H ₂ O	3.3-3.5	4,9
Al	H ₂ SO ₄	2.0	15
Al(Hg)	H ₂ O	3.9	Our work
Al	NaOH	4.3	4

Either the pH or the presence of mercury plays important role in the deuterium isotope separation factors. Topley and Eyring have concluded¹⁷ that the separation factors during electrolysis are generally lower in acidic than in alkaline solutions independently from the nature of the electrode metal. The same tendency could be observed in case of alkali metals, calcium and aluminium by Hughes et al.⁴ If the water reacts with sodium, the formed NaOH is a strong base which initiates the deuterium isotope exchange reactions between the water and the HD gas⁹. The main reason for this behaviour is the difference between the activation energies of NaOD and NaOH formation due to the lower zero point energy of the NaOD which leads to the preferred NaOD formation¹⁸.

In case of aluminium hydroxide precipitate¹⁹ there is no considerable concentration of free OH⁻ or OD⁻ ions. It is correlated with the facts that in sulphuric acid solutions the separation factor is much smaller (2.0) than in neutral water (s=3.90). In the presence of NaOH, however, only a slight

increase could be observed since the sodium hydroxide dissolves the aluminium hydroxide precipitate and the free hydroxide ion concentration is controlled by the dissociation equilibria of the formed hydroxyaluminate complexes. Not only the hydroxide ions but other monovalent anions can initiate the isotope separation processes, because using sodium chloride to prevent the passivation of aluminium in sulphuric acid solutions, the presence of sodium chloride increases the deuterium isotope separation factor from 2.0 to 4.0⁴.

References

- Somlyai, G., Kovács, A., Guller, I., Gyöngyi, Z., Krempels, K., Somlyai, I., Szabó, M., Berkényi, T., Molnár, M., *Eur. J. Cancer*, **2010**, *8*, 208.; Cong, F.-S.; Zhang, Y.-R.; Sheng, H.-C.; Ao, Z.-H.; Zhang, S.-Y.; Wang, J.-Y., *Exp. Therap. Med.* **2010**, *1*, 277.; Ioan, S.; Manolescu, N.; Comisel, V.; Tamaian, R.; Titeacu, G., *Bull. Univ. Agric. Sci. and Veter. Med. Cluj-Napoca, Veter. Med.* **2008**, *65*, 443.; Mirica, R. E., *Env. Eng. Manag. J.*, **2010**, *9*, 1543.; Kovacs, A., Guller, I., Krempels, K., Somlyai, I., Janosi, I., Gyongyi, Z., Szabo, I., Ember, I., Somlyai, G., *J. Cancer Therapy* **2011**, *2*, 548.
- Huang, F., Meng, C., *Ind. Eng. Chem. Res.*, **2011**, *50*, 378; Zhang, L.-Y., Kong, Z., Chen, D.-C., *Huaxue Shijie* **2009**, *50*, 748-750, 765.
- Kótai, L., Lippart, J., Gacs, I., Kazinczy, B., Vidra, L., *Ind. Eng. Chem. Res.* **1999**, *38*, 2425. Kótai, L., WO 9633129 A1; HU 2008000528 A1
- Hughes, E. D.; Ingold, C. K.; Wilson, C. L., *Nature (London, United Kingdom)*, **1934**, *133*, 291.; Hughes, E. D., Ingold, C. K., Wilson, C. L., *J. Chem. Soc.*, **1934**, 493;
- Wislicenus, H., Kaufmann, L., *Ber. Deutsch. Chem. Gesell.*, **1895**, *28*, 1323.
- Washburn, E. W., Urey, H. C., *Proc. Natl. Acad. Sci.* **1932**, *18*, 496.
- Reshetnikov, S. M.; Sokol'skaya, A. M.; Sokol'skii, D. V., *Dokl. Akad. Nauk SSSR*, **1966**, *168*, 629.
- Brun, J.; Varberg, Th.; Gundersen, W.; Solli, R. *Forhandlinger - det Kongelige Norske Videnskabers Selskab*, **1956**, *29*, 5.
- Kótai, L., Vidra, L., Kaziczy, B., Gács, I., *Acta Chem. Scand.*, **1999**, *53*, 155.
- Davis, C. O., Johnston, H. L., *J. Am. Chem. Soc.*, **1934**, *56*, 493.
- Inoue, Y., Osugi, A., *J. Electroanal. Soc. Jpn.*, **1952**, *20*, 502; Inoue, Y., Osugi, A., Amawa, T., Asafuji, T., Adachi, K., Takai, A., *J. Electroanal. Soc. Jpn.*, **1952**, *20*, 504.
- Tunold, R., Johansen, B., Jaksic, M., *Adv. Hydrogen Energy*, **1990**, *8*(Hydrogen Energy Prog., Vol. 2), 711.
- Brun, J., *Forhandlinger - det Kongelige Norske Videnskabers Selskab*, **1951**, *24*, 114.; Brun, J. *Acta Chem. Scand.*, **1951**, *5*, 1402.; Bellobono, I. R.; Mazza, F., *J. Phys. Chem.* **1971**, *75*, 2112.
- Bonhoeffer, K. F., Rummel, K. W., *Naturwiss.*, **1934**, *22*, 45.; Farkas, L., Farkas, A., *Trans. Faraday Soc.* **1934**, *30*, 1071; *Proc. Roy. Soc.* **1934**, *146A*, 623.
- Farkas, A., Farkas, L., *Nature*, **1934**, *133*, 139,
- Huang, X.-N; Lu, C.-ju; Huang, Y.-X; Liu, S; Wang, C; Chen, D., *Int. J. Hydrogen Energy*, **2011**, *36*, 15119.
- Topley, B., Eyring, H., *Nature*, **1934**, *133*, 292.
- Horiuti, J., Szabo, A. L., *Nature*, **1934**, *133*, 327.



2ND INTERNATIONAL CONGRESS ON DEUTERIUM DEPLETION

Budapest, Hungary, 17-18 May, 2012.

The 2nd International Congress on Deuterium Depletion was held on 17-18 May 2012 in Budapest, Hungary (www.deuteriumdepletion.com), as a follow-up to the 1st International Symposium on Deuterium Depletion held in Budapest in the spring of 2010. The goal of the organizers was to provide a global and comprehensive update of the newest results and developments in the research of deuterium depletion, and to give the researchers and medical practitioners a new opportunity to get acquainted with this expanding field of science, share their results and experience. Researchers and practitioners from several countries (Hungary, USA, France, Romania, Russia and China) presented 16 lectures on the various biological effects of deuterium depletion in the field of cancer research, diabetes research and anti-aging science.

Deuterium content of natural materials focusing on water: an overview

István Fórizs

Institute for Geological and Geochemical Research,
Research Centre for Astronomy and Earth Sciences,
1112 Budapest, Budaörsi út 45., HUNGARY E-mail:
forizs@geokemia.hu

This paper provides an overview on the deuterium content of materials found in nature, focusing on water as the most important deuterium source for living organisms. Deuterium contents of the water pools on Earth vary from about 90 ppm up to 160 ppm. Deuterium depleted water can primarily be found on the Earth's poles (e.g. Greenland, Antarctica, North Pole ice sheet) in the form of ice, while the water richest in deuterium are of lakes and the oceans.

The deuterium content of the precipitation shows a global pattern: D-content decreases from the Equator to the Earth's Poles and from sea level towards high elevations. The main driver in D-content variations in precipitation is air temperature. As a consequence D-content in precipitations bears prominent seasonal variations; e.g. in Hungary D-content in precipitation varies from cca. 127 ppm in cold winters up to cca. 153 ppm in hot summers.

The D-content of subsurface waters mostly reflect the global pattern of D-content of precipitation with the exceptions of some large scale regional water flow systems, and of ground waters older than 10000 years, which infiltrated during the Ice Age. Lakes that collect water from regions of higher altitude and cooler precipitation contain water, again, with lower deuterium ratios.

Other natural materials: Plants (marine and terrestrial) contain several per cent less deuterium than the water on which these plants grew. The widely used fuels as coal and crude oil are further depleted in deuterium with respect to plants.

Keywords: deuterium, D-content variations, natural materials

Natural mechanisms by which deuterium depletion occurs in specific positions in metabolites

Richard J Robins,^{[a]*} Gérald S Remaud,^[a] and
Isabelle Billault^[a,b]

^[a] Elucidation of Biosynthesis by Isotopic Spectrometry Group, Laboratory CEISAM, University of Nantes–CNRS UMR6230, 2 rue de la Houssinière, BP 92208, F-44322 Nantes, FRANCE, E-mail: richard.robins@univ-nantes.fr,

^[b] Laboratory of Reaction Chemistry and Natural Substances, ICMMO, CNRS UMR8182, Université de Paris-Sud 11, 91405 Orsay, FRANCE

Deuterium is depleted in specific positions in metabolites due to natural processes. This talk will present examples of how this phenomenon can be used to investigate metabolic activities. The information about site-specific deuterium depletion is obtained by using quantitative isotopic ²H NMR spectrometry. In this technique, the ²H NMR spectrum of the molecule of interest is acquired under carefully established quantitative conditions. By reference to a calibrated internal standard, the areas under the peaks in the spectrum can be used to obtain the ²H/¹H ratio at each resolved hydrogen position.

In the first example of the exploitation of this technique, the analysis of the redistribution of hydrogen during the metabolism of glucose by lactic acid bacteria will be developed. It will be shown how, by appropriate slight labelling of specific positions in the glucose to be fermented, the quantitative affiliation between all non-exchangeable positions in the substrate and all positions in the product can be obtained. A linking-factor can be calculated that will indicate whether positions will become enriched or depleted during metabolism. It will be shown how the fermentation of glucose to lactic acid via glycolysis or to lactic acid plus ethanol via the reductive pentose phosphate pathway leads to different isotope patterns in the products.

The second example will present our work on understanding fatty acid metabolism. During the biosynthesis of fatty acids, H atoms can be introduced from acetate, water and NAD(P)H. Thus, the origin of the H, isotope effects during the reduction reactions, and non-enzymatic exchange causes variations in the $^2\text{H}/^1\text{H}$ ratios at the different positions, leading to an alternating enriched/impoverished pattern. This is further altered by the action of desaturases and other enzymes that modify the chain. We have shown that depletion in the residual ^2H at the sites of desaturation is due to the non-equivalence of the $^2\text{H}/^1\text{H}$ ratio in the CH_2 groups that are subjected to desaturase activity.

How such analyses give insight into intramolecular H distributions and their underlying causes will be discussed.

Keywords: deuterium, isotopic ^2H NMR spectrometry, $^2\text{H}/^1\text{H}$ ratio, redistribution of hydrogen

Deuterium depletion □ From tissue culture to human clinical studies

Gábor Somlyai^[a], **Gábor Jancsó**^[b], **György Jákl**^[b], **Miklós Molnár**^[c], **András Kovács**^[d], **Imre Guller**^[d], **Idikó Somlyai**^[a], **Krisztina Krempels**^[a], **Mariann Szabó**^[e], **Tamás Berkényi**^[f], **László Z. Fehér**^[g,h], **László G. Puskás**^[g,h]

^[a]HYD LLC for Cancer Research and Drug Development, Budapest, HUNGARY, E-mail:gsomlyai@hyd.hu,

^[b]Centre for Energy Research, Hungarian Academy of Sciences, Budapest, HUNGARY

^[c]Semmelweis University Medical School, Budapest, HUNGARY,

^[d]Saint John's Hospital, Budapest, HUNGARY,

^[e]Veterinary Clinic, Budapest, HUNGARY,

^[f]Alpha-Vet Veterinary Hospital, Székesfehérvár, Hungary,

^[g]Avidin Ltd, Szeged, HUNGARY,

^[h]Biological Research Center of the Hungarian Academy of Sciences, Laboratory of Functional Genomics, Szeged, HUNGARY

The growth-altering role of naturally occurring deuterium (D) in living organisms has been examined using deuterium-depleted water (DDW) (25-105 ppm D) and compared with that of natural deuterium containing water in control cultures (150 ppm). DDW significantly decreased the growth rate of L₉₂₉ fibroblasts, HT-29 colon, A4, MDA and MCF-7 breast, PC-3 prostate, as well as M19 melanoma cells. This growth-inhibiting effect was more pronounced when the D-concentration of growth medium was gradually decreased in 3 to 5 steps. In order to reveal the molecular background of the inhibitory effect of deuterium depletion

the expression of different genes was investigated. It was found that deuterium depletion inhibited COX-2 expression and there were positive correlations among the degree of growth retardation, COX-2 gene expression and D-concentrations. DDW also influenced the expression of genes encoding different kinases using nanocapillary quantitative real-time PCR analysis. Phosphatidylinositol 3-kinase and hexokinase-2 expressions were stimulated by DDW, whereas glutathione peroxidase 2 and peroxiredoxin 1, which play key roles in regulating electron transport, were suppressed.

Mammary tumors in 81 dogs and 14 cats showed a response rate above 70%; yet, in more than 50% of the animals a complete recovery was achieved in response to DDW treatment. Similar efficacies were observed in 43 dogs and 3 cats bearing rectal tumors. Local treatment with an injectable DDW preparation regressed tumors, which otherwise were resistant to oral DDW administration. Microscopic evaluation of the tumors verified that DDW injection caused a disappearance of tumor cell infiltration, demarcation and a consequent rejection of invasive tumors, while DDW injections were harmless for healthy tissues in the surroundings of tumor sites.

A four-month double blind, phase II, placebo controlled human clinical trial was conducted in 44 prostate cancer patients. Prostate size during the 4-month DDW administration period showed a net decrease of 160.3 cm³ but only that of 54 cm³ in the control group. Two patients (9.1%) died in the treated and 9 patients (40.9%) in the placebo group, which is consistent with a decrease in mortality in the treated group (Fisher's Exact Test, p=0.034).

Beside the phase II clinical trial in prostate cancer, a human data base was created from 1992 involving all patients who had been subjected to DDW administration. This data base includes 1,450 patients who consumed DDW for longer than 90 days (654 male and 796 female patients), between October 1992 and March 2012. The cumulative time from diagnosis to the end of the follow-up period was 5,601 years; the cumulative time of DDW administration was 1,964 years. The median age of the investigated population was 55 years. The distribution of the main tumor types among the examined patients was almost identical to the data of the National Cancer Registry (Hungary). Median survival time (MST) was 9.5 years in the entire cohort of 1,450 patients, of which 1,320 patients started consuming DDW with detectable tumor(s), with 130 patients already in remission. Four hundred ten (410) patients died (one in every 12.1 years) out of 1,320 patients within 4,980 years covering the cumulative time from diagnosis to the end of the follow-up period. The MST of the 1,320 patients was 8.3 years. The cumulative follow-up period of 130 patients starting DDW consumption in remission was 615 years. Cohort statistical evaluations show that 8 patients (i.e.: one in every 76.8 years) died, which strongly suggests that integrating D-depletion into conventional therapies may prevent relapses of cancer with a complete recovery in some patients.

It is suggested that cells are readily able to regulate their D/H ratios, while its changes trigger distinct molecular processes. One possibility to modify intracellular D/H ratios is the activation of the H⁺-transport system, which preferentially eliminates H⁺, resulting in increased D/H ratios within cells.

Altered D/H ratios strongly regulate the expression of distinct genes and the activity of enzymes having key roles in cell cycle regulation and also regulate various molecular mechanisms. We contemplate that naturally occurring D is a key element of a still obscure sub-molecular growth-regulatory system (SMRS).

Keywords: deuterium, deuterium depletion, deuterium-depleted water, cell cycle regulation, gene expression, Phase II clinical trial

Biological effects of deuterium content variation in water

V. I. Lobyshev and A. A. Kirkina

Physics Department, M.V. Lomonosov Moscow State University, 119992 Moscow, RUSSIA, E-mail: lobyshev@yandex.ru

The aim of the work is to study the nature of biological effects of deuterium depleted and slightly deuterium enriched water on living cell. It was shown in our previous works that increasing of deuterium to 500 ppm resulted in twice hydrolytic activity of the membrane specimens of Na,K-ATPase and Ca-ATPase, increasing of hydroid regeneration velocity [1-3]. On contrary this activation effect was not obtained on Na,K-ATPase at temperature lower than temperature of lipid phase transition and on Na,K-ATPase from muscles. The results obtained proved that this anomalous effect of deuterium is not consistent with biochemical reactions themselves (primary kinetic isotope effect), but occurred due to the cooperative ternary complex of water-protein-lipid.

Natural fractionation of deuterium occurs during phase transitions vapor-liquid-ice. The experiments carried out on the SP-22 North Pole drifting station show that both depleting and increasing deuterium content around the isotopic content of the ancient ocean leads to the increasing of single-cell algae grown inside the ice mass [4-5]. In [6] one can see both activation of small and inhibition of large concentration of deuterium on the growth of bacteria.

The experiments with Na,K-ATPase from nasal salt glands of a duck were followed recently with the depleted light water of various deuterium concentration. Hydrolytic activity of the samples containing 4, 24 and 150 ppm is obtained to have 181 ± 9 , 158 ± 12 and 179 ± 10 arbitrary units, respectively. The result shows that depleted water containing 4 ppm of deuterium does not differ from the ordinary water, but 24 ppm depleted water leads to the inhibition of Na,K-ATPase activity.

The experiments with fertilized roe of loach *Misgurnus fossilis* show that the number of live embryos after six days of incubation is twice higher in depleted water with 2, 9 ppm of deuterium in comparison to ordinary water. The dying dynamics of non-fertilized roe does not depend on isotopic content of deuterium.

Our preliminary experimental result on motility of human sperm cells indicates that in light water (4 ppm) motility is 40% higher during five hours of the registration. However

the effect depends on the initial properties of a sperm sample. The results obtained clearly shows that deuterium content variation in water including deep deuterium depletion produce various nonlinear isotopic effect on key processes in a cell as enzyme action of Na,K-ATPase, regeneration, motility, fertilizing effectiveness and embryo developing. It should be noted that in any case concentration dependence is needed to find an optimal condition for the best result. Sometimes small variation of deuterium in frame of natural fractionation on the Earth may be the most effective. Due to the fact that heavy isotope of hydrogen tends to be accumulated in an organism, deuterium depleted water seems to be preferable in practical use.

We are thankful to the "Light water" Russian company which gives us an opportunity to study isotopic effects in wide concentration range of deuterium and for light water samples which are used in the experiments.

Keywords: deuterium, deuterium-depleted water, natural fractionation, DDW, Na,K-ATPase, Ca-ATPase, nonlinear isotopic effect

Physiological effects of drinking water enriched with $^1\text{H}_2^{16}\text{O}$

T. N. Burdeynaya^[a], A. S. Chernopyatko^[a], and N. A. Fudin^[b]

^[a]ZAO "Light water", Moscow, RUSSIA, E-mail: burdeynaya@lightwater.com

^[b]P.K. Anokhin Institute of Normal Physiology of Russian Academy of Medical Science, Moscow, RUSSIA

The quality and purity of drinking water are determinative factors for life quality and human health. In natural water the residual concentration of isotopomer molecules, containing the heavy isotopes ^2H , ^{17}O , ^{18}O , can amount to 2.97 g/l. Light and heavy water isotopomers differ appreciably in their physical properties such as boiling point, freezing point, and density.

Molecules containing heavy isotopes in the mammalian organism can lead to changes in normal biochemical processes and to a decrease of functional resources of the organism.

In our studies, water enriched with $^1\text{H}_2^{16}\text{O}$ was used, which is the main ingredient of the commercial product AquaSLAP™. Such water was produced by the company ZAO "Light water". The level of the light isotopomer was 99.757 % (D/H= 90 ppm), which corresponds closely with water of the Antarctic, the one with the least concentration of heavy water isotopomers in Nature.

The goal of the work was to reveal biological effects of water enriched with $^1\text{H}_2^{16}\text{O}$ on quantitative blood chemistry values and physical challenges in 20 volunteers (healthy persons aged 18-34 years). At the P. K. Anokhin Institute of Normal Physiology, subjects were tested for their psychological and vegetative statuses, lung function and gas

exchange, general health and physical performance, while blood tests were conducted to assess clinical and biochemical parameters, immunological and hormonal statuses, as well as antioxidant activities).

Results of the 28 days intake period of light water revealed in every subject an improvement in health and reduced anxiety with improved psychological response.

The positive influence of drinking light water on blood chemistries included a significant reduction of glucose, cholesterol, erythrocyte sedimentation rates, leukocyte counts and cortisol (stress hormone) levels, while also revealed an increase in antioxidant capacities.

Volunteers who consumed 1 liter of light water per day improved their hemodynamic parameters (i.e.: increased stroke volume and cardiac output, decreased total peripheral vascular resistance), which had a positive impact on overall physical performance and aerobic metabolism during an exercise.

These findings evidence the significance of light water to increase energy resources even in a healthy cohort, while decreasing risks of psycho-emotional stress, which is known to pose a negative influence on blood biochemistries that often lead to psychosomatic diseases and shorten life.

Keywords: deuterium, heavy isotopes, isotopomer molecules

Comparative study concerning deuterium depletion in two laboratory animal species

Ioan Ștefănescu^[a], Cristian Mladin^[b], Radu Tamaian^[a], Victor Feurdean^[c] and Gheorghe Tițescu^[a]

^[a]National Institute for Research and Development for Cryogenic and Isotopic Technologies, I.C.I.T. Ramnicu Valcea, 4th Uzinei Street, P. O. Râureni Box 7, RO-240050 Râmnicu Vâlcea, VL, ROMANIA, corresponding author: radu.tamaian@icsi.ro

^[b]S.C. Mecro System S.R.L., 100P Timișoara Avenue, RO-061334 Bucharest, ROMANIA

^[c]National Institute for Research and Development of Isotopic and Molecular Technologies, 65-103rd Donath Street, P.O. Box 700, RO-400293 Cluj-Napoca, CJ, ROMANIA

Deuterium depletion is a cutting-edge tool used especially in cancer research and oncotherapy, diabetes and anti-aging studies. The aim of this paper was to investigate comparatively how a deuterium-depleting agent (deuterium depleted water) lowers the isotopic concentration of deuterium, acquired via bioaccumulation processes, in Wistar rats and Swiss mice. Control animals were

maintained on standard food and drinking water, while experimental rats and mice were maintained on standard food and deuterium depleted water (produced at ICIT, according patent WO/2006/028400 "Process and installation for obtaining the deuterium depleted water"). The water extracted from biological samples of the sacrificed animals was analyzed by mass-spectrometry. Results showed that deuterium depleted water efficiently decreased deuterium isotopic content at systemic level in both species. It can be stated that the grade of deuterium depletion was directly dependent on two extrinsic factors: deuterium concentration of the depleting agent, and duration of administration. Moreover, deuterium depletion seems to depend on genotype, at both species and individual level, and on behavioral influences by each specimen.

Keywords: deuterium, deuterium depletion, deuterium-depleted water, mass spectrometry

Tracer substrate-based metabolic profiling, phenotypic phase plane and regression matrix analyses of pancreatic cancer cells under deuterium depleted growth environment

Laszlo G. Boros^[a] and Gábor Somlyai^[b]

^[a]University of California, SiDMAP LLC., Los Angeles, USA, E-mail: LBoros@sidmap.com

^[b]HYD LLC. for Cancer Research & Drug Development, Budapest, HUNGARY

The current state of metabolomics art involves the increasing use of stable ¹³C isotope tracers in medicine. Main advantages of ¹³C tracer-based metabolomics include functional, real time and phenotype related surrogate markers of cell function, drug response, and to determine drug efficacy for flux control in the metabolic network. This presentation covers important milestones in ¹³C tracer substrate based metabolomics, its business projections for medical research, as well as significant new applications for deuterium depletion. Phenotypic phase plane analyses and regression matrices of the ¹³C stable isotope labeled metabolome, especially its energy yielding products, intermediary metabolites, and cell membrane/nucleic acid components in cultured tumor cells, already indicate a major System response to deuterium depletion primed by limited reductive synthesis.

One prominent effect of deuterium depletion is to inhibit fatty synthesis, chain elongation and desaturation. These anabolic reactions utilize acetyl-CoA, as well as hydrogen of water for new fatty acid pools. Fatty acids then are used for new membrane formation in the rapidly proliferating cell. The complex structure and molecular organization of the mammalian fatty acid synthase offer remarkable opportunities with altered morphology and flux handling properties [*Nature Chemical Biology* 2, 232-234 (2006)].

Thus, fatty acid synthase (FAS; EC 3.2.1.85) is an attractive novel drug development target site in oncology where major pharmaceutical companies have already positioned themselves. For example, GSK837149A by GlaxoSmithKline controls the β -ketoacyl reductase subunit of human fatty acid synthase [FEBS Journal 275 (2008) 1556–1567] with potential clinical candidacy. This is also the site where hydrogen/deuterium ratios readily affect enzyme reactivity as well as reaction elasticity.

Besides affecting reductive (proton dependent) synthesis, our previous ^{13}C glucose experiments indicate that there is a deuterium-dependent decrease in *de novo* fatty acid ^{13}C net labeling in multiple tumor cells, with a decreased contribution of glucose-deriving acetyl-CoA to newly formed palmitate and sterols. This indicates an important role for limiting malonyl-CoA's carbon skeleton trafficking towards the consecutive acyl chain-elongating reductive synthesis steps within the FAS complex. Therefore, it is evident that reactivity and elasticity are also limited for ^{13}C -acetyl-CoA trafficking towards several membrane-bound newly formed lipids by DDW administration. This is consistent, on one hand, with a limited role of the Copenhagen model for malonyl-CoA processing (decarboxylation) but, on the other, that of an alternate, activated water and deuterium-dependent rate limiting mechanism [Biochemistry, Vol. 41, No. 35, 2002]. As the decarboxylation reaction is initiated by the attack of an activated water molecule, or hydroxide, on the malonyl C-3 target, the significant mass difference between deuterium and hydrogen readily alters reaction kinetics for acetyl-CoA trafficking, with a major impact on fatty acid synthesis and cell proliferation, as one of DDW's growth limiting mechanisms with pharmaceutical appropriateness.

Keywords: deuterium, deuterium depletion, ^{13}C isotope tracers, metabolomics, phenotypic phase plane analyses, tumor cells, fatty acid synthesis

Effects of deuterium depleted water alone and in combination of known chemotherapeutic agents on different tumor cells

Lajos István Nagy,^[a] Gabriella Fábíán,^[b] and László G. Puskás^[a,b]

^[a]Avidin Ltd. Szeged, HUNGARY, E-mail: lajos@avidinbiotech.com

^[b]Avicor Ltd. Szeged, HUNGARY

Consumption of deuterium depleted water can be used as a supplement for anti-cancer treatments and could also serve as a tumor prevention strategy. The anticancer effects of the optimal concentration of deuterium in water, the duration of treatment, the gradient decrease of deuterium content and

the possible synergistic effects of deuterium depleted water with known chemotherapeutic agents were analyzed on different tumor cell lines by using a real-time cell analysis method, Excelligence.

The Excelligence RTCA SP (Acea-Roche) is a microelectronic cell sensor method, where microelectrodes are integrated in the bottom of a microtiter plate (96-well E-plate) and measures adhesion and proliferation. The real-time measurement can detect changes continuously, which means that the system can give information at any stages of the experiment. Real-Time Cell Analyzer (RTCA) DP is a novel cell migration and invasion assay system that uses the Boyden Chamber principle but does not involve any fixation, labelling or counting of the cells. The core of the system is the CIM-Plate device, composed of an upper chamber and a lower chamber. The upper chamber has 16 wells that are sealed at the bottom with a micro-pore-containing polycarbonate or polyester membrane. The membrane contains microelectronic sensor arrays that are integrated on its bottom surface. Migration of cells will occur through these electrodes, which changes impedance, and will increase cell index.

In the present paper we report the effects of different concentrations of deuterium depleted water (155 ppm, 135 ppm, 125 ppm, 115 ppm, 105 ppm, 85 ppm, 65 ppm, 40 ppm) on the proliferation of HT199 melanoma, A549 lung cancer and MCF7 breast cancer cells. In addition we studied the synergetic effect of deuterium depleted water with known chemotherapeutic agents, namely etoposide, taxol, doxorubicin and cisplatin.

Deuterium depletion interfered with cell proliferation at the concentration of 105 ppm. The 40 ppm concentration showed the most significant effects in A549 and MCF7 cultures, while the proliferation of HT199 cells was most efficiently controlled by the 65 ppm preparation. During the combined treatment modalities deuterium depleted water enhanced the growth controlling effects of anti-cancer drugs. Combining 450 nM doxorubicin with 85 ppm deuterium depleted water decreased cell proliferation, yet combining 85 ppm deuterium depleted water with 900 nM doxorubicin induced cell death in all cultures. The 85 ppm deuterium depleted water significantly increased the effect of 65 μM cisplatin in A549 and HT199 cultures.

In conclusion, deuterium depletion inhibits tumor cell proliferation and decreases their migration. Furthermore, in combination with known anti-cancer drugs deuterium depletion had a synergistic effects. Based on these results deuterium depletion therapy could be used alone as well as in combination with different chemotherapeutic treatment protocols in the clinics. Further studies are needed to confirm the effects of combination therapy in animal experiments as well as in human clinical trials.

Keywords: deuterium, deuterium-depleted water, real-time cell analyzer, cell proliferation, cell migration, cancer cell lines, chemotherapeutic agents

Effects of deuterium depletion on proliferation and apoptosis in cultured murine haemopoietic cells

Gábor Laskay^[a], Gábor Somlyai^[b] and György Jákl^[c]

^[a]Department of Plant Biology, University of Szeged, Szeged, HUNGARY, E-mail: glaskay@bio.u-szeged.hu

^[b]HYD LLC for Cancer Research and Drug Development, Budapest, HUNGARY,

^[c]Centre for Energy Research, Hungarian Academy of Sciences, Budapest, HUNGARY

The purpose of the study was to investigate the effects of deuterium depletion (DD) on proliferation and apoptosis in a murine cell model system. The murine haemopoietic cells (cell line FDCP-Mix clone A4) used in this study require the growth factor Interleukin-3 (IL-3) for survival and proliferation. In the absence of IL-3 these cells not only undergo cell cycle arrest at the G₁/S checkpoint but also enter apoptosis. Therefore, this model system offers a unique opportunity to study the effects of different conditions on both proliferation and apoptosis.

DD conditions brought about an extension of the lag phase of the growth curve of murine haemopoietic cells when cultured in the presence of IL-3. DD conditions also decreased the rate of recovery of the cytoplasmic pH of the cells from acid load, an indicator of the activity of the Na⁺/H⁺ antiport. Moreover, DD conditions increased the rate of apoptotic cell death in the IL-3-deprived samples, with no effect on cell viability in the normal, IL-3-supplied population.

The results indicate that DD conditions a/ interfere with the onset of cell proliferation by extending the period during which the cells enter the phase of intense divisions, b/ modulate the activity of the Na⁺/H⁺ antiport, and c/ promote apoptosis after being induced by a physiological inducer. The implications of these findings will be discussed in the light of the two distinct signalling pathways employed by IL-3 with respect to the two cellular decisions: the Shc-Ras-MAPK pathway to induce proliferation and the PI3-P-Akt-Bax-P cascade to suppress apoptosis.

The authors wish to express their thanks to Professor T.M. Dexter and Dr. D. Allan (Paterson Institute for Cancer Research, Manchester, U.K.) for making it possible to conduct the study.

Keywords: deuterium, deuterium depletion, proliferation, apoptosis, hematopoietic cells, Na⁺/H⁺ antiport, signalling pathways

Anti-aging effects of deuterium depletion on Mn-induced toxicity in a *C. elegans* model

Daiana Silva Ávila^[a], Gábor Somlyai^[b], Ildikó Somlyai^[b] and Michael Aschner^[a]

^[a]Vanderbilt Medical Center, Nashville TN, USA, E-mail: michael.aschner@vanderbilt.edu

^[b]HYD LLC for Cancer Research and Drug Development, Budapest, HUNGARY

Sub natural concentrations of deuterium (D) in water have been shown to have several health effects. Herein, we tested the hypothesis that deuterium-depleted water (DDW) can reverse the effects of manganese in a *Caenorhabditis elegans* (*C. elegans*) experimental model. A synchronous population of N2(wild type) worms was treated with 35mM MnCl₂ for 30 minutes followed by 48 h treatment with 150, 120 or 90 ppm of DDW. Mn reduced DAF-16 (a transcription factor strongly associated with life-span regulation) levels in the worms and this effect was restored by 90 ppm DDW treatment. Superoxide dismutase (SOD) and AKT, downstream and upstream proteins in the DAF-16 pathway, respectively, were altered by Mn exposure, and their expression was also restored by DDW treatment. These findings demonstrate that DDW may play a protective role against Mn toxicity and aging, likely by attenuating Mn-induced reactive oxygen species (ROS) generation. The effect of DDW is likely mediated by the DAF-16 pathway, as a transcriptional factor that increases the expression of antioxidants proteins and increase in lifespan in *C. elegans*. Additional studies are necessary in order to clarify the precise molecular mechanisms of the anti-aging activity of DDW.

Keywords: sub-natural deuterium, *Caenorhabditis elegans*, life-span, manganese, DAF-16, SOD-3, anti-aging effect

Deuteronation and ATP Synthase: A Stochastic Mechanism of Aging

Abdullah Olgun

Biogerontology Laboratory, ARGE-1 Binası Kat: 2 No:1, Teknokent, Akdeniz University, TURKEY, E-mail: aolgun@yahoo.com

Although the ratio of deuterium to hydrogen is ~1/6600 in nature, deuterium/proton ratio is ~1/15000 due to the lower ionization of deuterium that has a twofold mass of hydrogen. Therefore in any biological molecular reaction/interaction where proton is involved, there is a ~1/15000 chance of deuteronation.

Chemical bond formed by deuterium is stronger, shorter and have a different angle than hydrogen bond. The same conditions apply for the F₀ part of ATP synthase also where deuteriation increases the pK_a of its Asp61 by 0.35. This increase can make difficult the dissociation of deuterium from Asp61 by stator subunit's Arg210 and likely causes the rotation of F₀ in both directions in a futile manner that stops ATP synthesis at least transiently. Each second, one of ~15 ATP synthases is likely transiently deuteriated at Asp61 site. If a critical percentage of ATP synthases is stochastically deuteriated at a certain time point in a mitochondrion, this can lead to local ATP deficiency with reversible or irreversible consequences in maintenance and repair. As exemplified by ATP synthase, the role –if any- of deuteriation in the mechanisms of aging and age related pathologies needs and deserves to be clarified.

Keywords: deuterium, deuteriation, ATP synthase, aging

Deuterium-depleted water inhibits human lung carcinoma cell growth by apoptosis

Fengsong Cong

School of Life Sciences and Biotechnology, Shanghai Jiaotong University, Shanghai, CHINA, E-mail: fscong@sjtu.edu.cn

Objective: To explore the *in vivo* and *in vitro* inhibitory effects of deuterium-depleted water (DDW) on human lung cancer, and to explore the possible mechanisms.

Methods: The inhibitory effect of DDW on the proliferation of human lung carcinoma A549 cells and human embryonic lung fibroblast HLF-1 cells was examined by MTT assay; apoptosis of A549 cells was examined by TUNEL; and cell cycle was analyzed by flow cytometry. Mouse model of lung carcinoma was established by inoculating human lung carcinoma H460 cells into BALB/c nude mice, and the growth of implanted tumors was observed after DDW treatment for 60 days.

Results: Compared with control group, A549 cells treated with DDW containing 25, 50 or 105 ppm deuterium DDW showed significantly decreased proliferation at 10 h ($P < 0.01$). Then the inhibitory effects of DDW gradually disappeared, but re-appeared 48 h later, becoming significant at 72 h ($P < 0.05$). DDW showed no inhibition on the proliferation of HLF-1 cells ($P < 0.05$). TUNEL assay verified DDW-induced apoptosis in A549 cells, which was significantly higher than that of the control group ($[45.30 \pm 4.21]\%$ vs $[(22.25 \pm 0.30)\%, P < 0.01$). Cells in S phase were significantly increased in DDW-treated A549 cells compared with those in the control group ($P < 0.05$). Life quality of H460 cell-inoculated nude mice treated with

DDW was greatly improved, with a tumor inhibition rate of 30.08%. **Conclusions:** DDW inhibits the proliferation of lung cancer cells at a wide dosing range, but with a fluctuation pattern; its mechanism might be associated with induction of apoptosis and S-phase cell cycle arrest in tumor cells.

Keywords: deuterium, deuterium-depleted water, A549 human lung carcinoma cells, apoptosis, tumor inhibition

The effect of DDW on the kinetics of tumor clone in *in vitro* experiments

S. A. Roumyantsev,^[a] E. Yu. Osipova,^[a] O. V. Kozlitina,^[a] T. V. Shamanskaya,^[a] A. A. Timakov^[b]

^[a]Federal Scientific Clinical Center for Children's Hematology, Oncology and Immunology, Ministry of Health of the Russian Federation, Moscow, RUSSIA; E-mail: s.roumyantsev@mail.ru

^[b]Medical-Technological Complex "Iceberg" Ltd., Moscow, RUSSIA

Acute leukemia represents a group of heterogeneous malignant blood disorders the key role in the development of which is played by the disbalance between proliferation and differentiation of hematopoiesis progenitor cells. Recent studies have shown that deuterium depleted water (DDW) can affect both the proliferation and apoptosis of the malignant cells. DDW may become a potentially perspective drug in the prevention of cancer and blood disorders.

In this study we investigated the effect of DDW on the rate of spontaneous apoptosis by incubating leukemic cells in culture media with deuterium concentration of 10 or 50 ppm. The leukemic cells were extracted from bone marrow of patients with first diagnosed leukemia. In all experiments, the number of viable cells before incubation was 95%. The cells were incubated in RPMI-1640 medium, based on bi-distilled DDW with deuterium concentration 10 or 50 ppm, for 24, 48 and 72 hours. Control cells were incubated in a medium with 143 ppm deuterium concentration. After incubation, the cells were washed in phosphate-buffered saline in the centrifuge at 1000 rpm for 5 minutes at 18°C. The pellet was resuspended in 200 ml saline, and the cell suspension was put into 2 test tubes. To one, 15 µL of annexin V/FITC and 10 µL of propidium iodide was added. Unstained cells were used as negative control and for determining growth rate. The samples were shaken on a vortex and incubated in the dark for 15 minutes at room temperature. After that, 400 µL phosphate-buffered saline was added to the samples, and these were analyzed by means of a FACScan cytofluorimeter (Becton Dickinson, USA) with fluorescence excitation in channel FL1 (525 nm) and red range excitation in FL2 channel (525 nm). Evaluation was done with the CELLQuest program

according to the characteristics viable cells, early apoptotic cells, late apoptotic cells, and necrotic cells.

Cells of acute leukemia patients (M1 subtype in the FAB classification; marrow, blast cells 95%), cells of patients with acute lymphoblastic leukemia (marrow, blast cells 98%) and mononuclear cells of a healthy donor were investigated. The sensibility of the analyzed cells to the decrease of deuterium concentration in the medium and its rate was different for all periods of incubation. For example, after incubating the M1 cells at 10 ppm deuterium level for 24 hours, the number of viable cells was not significantly different from the control (46.8 vs. 46.7%), while in the medium with 50 ppm deuterium the number of viable cells was 10% lower than in control. Cells of acute lymphoblastic leukemia were, in contrast, more sensitive to decreased deuterium concentration (10 ppm). Prolongation of the incubation period regularly led to decrease of cell viability and increase of the number of cells in different apoptosis stages.

Mononuclear cells of the healthy donor were also sensitive to the deuterium concentration. At the beginning of culturing the cells, the difference vs. control was significant and reached 20%.

DDW affected the viability of leukemic cells in *in vitro* experiments. The reaction of the cells on decreased deuterium concentration in the medium depended on the cell type, deuterium level, and length of cultivation.

Keywords: deuterium, deuterium-depleted water, cell culture, leukemic cells

Lung cancer patients, who consume deuterium depleted water, have extended survival

Zoltán Gyöngyi,^[a] Ferenc Budán,^[a] István Szabó^[a] István Ember,^[a] István Kiss,^[a] Krisztina Krempels,^[b] Ildikó Somlyai^[b] and Gábor Somlyai^[b]

^[a]Department of Public Health, Medical School, University of Pécs, Pécs, Hungary, E-mail: zoltan.gyongyi@aok.pte.hu.

^[b]HYD LLC for Cancer Research and Drug Development, Budapest, HUNGARY

Lung cancer is the leading cause of cancer mortality. In Hungary, the median survival time (MST) of lung cancer patients is 7.5 months for men and 11.3 months for women, based on the data obtained between 2002 and 2005.

While smoking is the primary risk factor of lung cancer, environmental pollution and genetic factors can also promote formation of lung cancer in non-smoker population, too. Moreover, regular lung cancer therapy is less effective

than patients and physicians wish. Deuterium depletion slows cell division and suppresses tumour-related genes and longer survival of breast and prostate cancer patients is observed respectively. We followed more than 3 hundred patients with diagnosed lung cancer. These Hungarian patients voluntary consumed deuterium depleted water (DDW) beside regular chemo and radiotherapy. The calculated MST was dependent mainly on gender and histological subtype but it was significantly, 2-7 times longer in the group of patients, who drank DDW than it was calculated in the entire Hungarian lung cancer population. Tissue samples were not obtained from patients, because DDW consumption was beginning after surgery, but in an animal model we could measure diminished expression of several cancer-related genes in the lung tissues of DDW-drinking animals. We assume being correlation of silenced expression of those genes and extended cancer survival of DDW-drinking patients having lung cancer at the beginning of follow-up.

Keywords: Deuterium depletion, lung cancer, median survival time, MST

A retrospective study of survival in breast cancer patients undergoing deuterium-depletion in addition to the conventional therapies

Krisztina Krempels, Ildikó Somlyai, Krisztina Balog and Gábor Somlyai

HYD LLC for Cancer Research and Drug Development, Budapest, HUNGARY, E-mail: krempels@hyd.hu

Breast cancer is among the most prevalent forms of malignancies worldwide. It ranks as the second most common fatal cancers in women. Although population screening by mammography and rapidly developing new therapies (i.e.: surgery, radiotherapy, hormonal therapy, chemotherapy and targeted drugs) improve early diagnosis and multidisciplinary treatment options, morbidities for breast cancer remain relatively high.

The possible role of naturally occurring deuterium (D) and the impact of its shortage on cell proliferation have already been established for numerous biological systems. Anticancer effects of D-depletion have been demonstrated in *in vitro* cell growth studies and in animal models of tumor xenografts. Deuterium depleted water (DDW) in a human phase II clinical trial of prostate cancer and retrospective evaluations all showed anticancer- and preventive effects as a novel treatment modality.

The aim of the present study was to investigate the impact of deuterium depletion (D-depletion) on breast cancer outcome. The daily water intake of patients was replaced with DDW (105-25 ppm D) at least for 91 days, without restrictions for the continued conventional treatment regimen. The DDW treatment started with 105 ppm D, which was gradually decreased to preparations with 85 ppm, 65 ppm and 45 ppm, (i.e.: 20 ppm lower D contents than the

starting preparation) every 1 to 3 month, reaching a total of 6 to 10 months treatment periods. DDW treatments are discontinued with 2 to 3 month intervals, and then repeated several times for 4 to 6 months periods.

The data base of 232 breast cancer patients (median age: 50 years) was retrospectively evaluated, the median follow up time was 49.7 months. Patients were continuously enrolled between February 1993 and April 2011. Patients consumed DDW for a median time period of 14.1 months. Median survival time (MST) from the diagnosis was 148 months (12.3 years) for the population of the DDW treated cohort. According to the staging at initial diagnosis, patients with primary breast cancer achieved 217 months (18.1 years) MST, which was 52 months (4.3 years) in patients with advanced cancer. Since the median time from the initial diagnosis to the start of DDW treatment reached 13.2 months (1.1 years), MST was also calculated from the initiation of DDW treatment. Most patients underwent conventional therapies before entering the trial; therefore a new study arm was created for restaging at the time of inclusion in the study. Due to the extremely long survival of patients already in remission at the start of DDW treatment MST calculations are still pending: one patient out of the 48 patients died during the cumulative total follow-up of 289 years (median: 47.8 months). Patients with primary breast cancer achieved 89 months (7.4 years) MST, while in advanced breast cancer MST is achieving 39 months (3.3 years).

In comparison with published data DDW treatment in combination with, or as an extension of, conventional therapies noticeably prolonged MST in subgroups of breast cancer patients. The method proved to be safe, and D-depletion may act as a highly effective therapy both in preventing the recurrence of breast cancer and for the treatment of primary or advanced breast cancers. We conclude that D-depletion offers additional benefits to standard treatment regimens in breast cancer.

Keywords: Deuterium depletion, breast cancer, median survival time, MST, retrospective study

Effect of reduced deuterium (D) content of drinking water in STZ-induced diabetic rats and in humans with altered glucose metabolism

Miklós Molnár,^{[a]*} K. Horváth,^[a] T. Dankó^[a] and G. Somlyai^[b]

^[a]Semmelweis University, Institute of Pathophysiology, Budapest, HUNGARY, E-mail: molmik@xenia.sote.hu

^[b]HYD LLC. for Cancer Research and Drug Development, Budapest, HUNGARY, E-mail: gsomlyai@hyd.hu

Deuterium, a stable heavy isotope of hydrogen, binds to oxygen to form D₂O. D₂O exist in the environment at 1/6700 of H₂O (150 ppm) and is expected to have biological effects. Several lines of evidences suggest that D₂O inhibits

insulin release from pancreatic islets. Very little or no data is available on the complex actions of lowering D₂O content of the cellular environment. Some experimental and clinical observations suggest that depletion of D₂O has anti-mitotic effect in various tumor cells. Some clinical observations also suggest that depletion of D₂O interferes with glucose metabolism in diabetic patients. In our experiments we wanted to test the effect of removal of D₂O on glucose metabolism in streptozotocin (STZ)-induced diabetic rat model. After 2 weeks, animals were randomly distributed in to several groups to test the effect of D₂O (25-150ppm) on glucose metabolism in diabetic animals with or without 2x1U/day insulin treatment. Our results indicate that STZ treatment significantly increased serum glucose, fructoseamine, HbA_{1c} and TBARS concentrations. Depletion of D₂O did not influence any of the measured parameters in animals not receiving insulin. However the measured parameters were significantly lower in those animals that received lower D₂O containing drinking water and insulin treatment. Membrane associated GLUT-4 was significantly higher in the soleus muscle of these animals. These observations suggest that D₂O depletion enhances insulin effect on GLUT-4 translocation and potentiate glucose uptake in diabetic animals. The mode of action of D₂O depletion is not fully understood and needs further experiments to be elucidated in insulin-requiring Type1 diabetes.

To investigate the effect of DDW in humans on metabolic diseases a 90 day-long open label study was completed using a) the hyperinsulinemic euglycemic clamp technique, b) the homeostasis model assessment methods (HOMA-IR) and c) HOMA-B% and S%. The study was approved by the Regional and Institutional Ethical Committee before prospective patients were enrolled and screened. A total of 30 patients with established insulin resistance and/or with glucose intolerance (IFG or IGT) were selected for inclusion in this study, screened within two weeks prior to the first drug administration. Male and female patients, between age 18-60 years consumed 1.5 liters DDW per day with 110 ± 5 ppm. Before and after the treatment period blood samples were collected and stored at -80°C to determine HbA_{1c}, FFA, triglycerid, lipidfractions, leptin, adiponectin, osteocalcin, kathepsin, sRANKL, osteoprotegerin, IL6, IL1β, TNFalpha, usCRP, ApoA, Apo B, vitamin D₃, oestradiol, tesztosteron, FSH. Serum D-concentration decreased from 148 ppm (146-150 ppm) to 134 ppm (125-143 ppm) during the treatment. The average body mass increased from 85.55 kg to 86.71 kg (p=0.0071).

Insulin resistance decreased in 11 volunteers (36.6%), total body glucose uptake increased with 0.2 to 4.2 mg/bwkg/min. The possible cause-effect relationship will be discussed based on volunteer IFG, IGT, type 2 DM status, insulin concentrations, body weight, fasting glucose levels and HDL concentrations. The results clearly show that consumption of DDW reduces fasting glucose levels, increase HDL concentrations, and, in early disease stages, reduce insulin resistance.

Keywords: deuterium, deuterium depletion, GLUT-4, insulin resistance, diabetes, HDL